UNIVERSIDADE FEDERAL DO PARANÁ

THAÍS MARZALEK BLASI

NEW APPROACHES TO DISTRIBUTED ENERGY RESOURCES AND MICROGRID INTEGRATION INTO ACTIVE DISTRIBUTION SYSTEMS

CURITIBA

2024

THAÍS MARZALEK BLASI

NEW APPROACHES TO DISTRIBUTED ENERGY RESOURCES AND MICROGRID INTEGRATION INTO ACTIVE DISTRIBUTION SYSTEMS

Documento apresentado ao Programa de Pós-Graduação em Engenharia Elétrica, do Setor de Tecnologia da Universidade Federal do Paraná, como requisito para obtenção do título de Doutora em Engenharia Elétrica.

Orientador: Prof. Dr. Alexandre Rasi Aoki
Coorientadora: Profª. Drª. Thelma Solange Piazza Fernandes

CURITIBA
2024

DADOS INTERNACIONAIS DE CATALOGAÇÃO NA PUBLICAÇÃO (CIP)
UNIVERSIDADE FEDERAL DO PARANÁ
SISTEMA DE BIBLIOTECAS – BIBLIOTECA DE CIÊNCIA E TECNOLOGIA

Blasi, Thaís Marzalek
New approaches to distributed energy resources and microgrid integration into active distribution systems / Thaís Marzalek Blasi. – Curitiba, 2024.
1 recurso on-line : PDF.

Tese (Doutorado) - Universidade Federal do Paraná, Setor de Tecnologia, Programa de Pós-Graduação em Engenharia Elétrica.

Orientador: Alexandre Rasi Aoki
Coorientador: Thelma Solange Piazza Fernandes

1. Recursos energéticos distribuídos. 2. Microrredes. 3. Eletrônica de Potência. I. Universidade Federal do Paraná. II. Programa de Pós-Graduação em Engenharia Elétrica. III. Aoki, Alexandre Rasi. IV. Fernandes, Thelma Solange Piazza. V. Título.

Bibliotecário: Leticia Priscila Azevedo de Sousa CRB-9/2029

ATA Nº39

ATA DE SESSÃO PÚBLICA DE DEFESA DE DOUTORADO PARA A OBTENÇÃO DO GRAU DE DOUTORA EM ENGENHARIA ELÉTRICA

No dia vinte e seis de fevereiro de dois mil e vinte e quatro às 14:00 horas, na sala https://teams.microsoft.com/l/meetup-join/19%3ameeting_MTE3M2Y5ZTAtY2JjOS00MGJlLWE4YzMtMzA2ZjU4ODBkNjZi%40thread.v2/0?context=%7b%22Tid%22%3a%22c37b37a3-e9e2-42f9-bc67-4b9b738e1df0%22%2c%22Oid%22%3a%2206155d56-b4a7-4755-9bd6-1c4fda326e73%22%7d, Microsoft Teams, foram instaladas as atividades pertinentes ao rito de defesa de tese da doutoranda **THAÍS MARZALEK BLASI**, intitulada**: NEW APPROACHES TO DISTRIBUTED ENERGY RESOURCES AND MICROGRID INTEGRATION INTO ACTIVE DISTRIBUTION SYSTEMS**, sob orientação do Prof. Dr. ALEXANDRE RASI AOKI. A Banca Examinadora, designada pelo Colegiado do Programa de Pós-Graduação ENGENHARIA ELÉTRICA da Universidade Federal do Paraná, foi constituída pelos seguintes Membros: ALEXANDRE RASI AOKI (UNIVERSIDADE FEDERAL DO PARANÁ), WALMIR DE FREITAS FILHO (UNIVERSIDADE ESTADUAL DE CAMPINAS), ODILON LUIS TORTELLI (UNIVERSIDADE FEDERAL DO PARANÁ), ANDREA LUCIA COSTA (UNIVERSIDADE TECNOLÓGICA FEDERAL DO PARANÁ). A presidência iniciou os ritos definidos pelo Colegiado do Programa e, após exarados os pareceres dos membros do comitê examinador e da respectiva contra argumentação, ocorreu a leitura do parecer final da banca examinadora, que decidiu pela APROVAÇÃO. Este resultado deverá ser homologado pelo Colegiado do programa, mediante o atendimento de todas as indicações e correções solicitadas pela banca dentro dos prazos regimentais definidos pelo programa. A outorga de título de doutora está condicionada ao atendimento de todos os requisitos e prazos determinados no regimento do Programa de Pós-Graduação. Nada mais havendo a tratar a presidência deu por encerrada a sessão, da qual eu, ALEXANDRE RASI AOKI, lavrei a presente ata, que vai assinada por mim e pelos demais membros da Comissão Examinadora.

Curitiba, 26 de Fevereiro de 2024.

Assinatura Eletrônica
28/02/2024 08:03:27.0
ALEXANDRE RASI AOKI
Presidente da Banca Examinadora

Assinatura Eletrônica
28/02/2024 13:59:43.0
WALMIR DE FREITAS FILHO
Avaliador Externo (UNIVERSIDADE ESTADUAL DE CAMPINAS)

Assinatura Eletrônica
28/02/2024 09:47:42.0
ODILON LUIS TORTELLI
Avaliador Interno (UNIVERSIDADE FEDERAL DO PARANÁ)

Assinatura Eletrônica
28/02/2024 11:22:37.0
ANDREA LUCIA COSTA
Avaliador Externo (UNIVERSIDADE TECNOLÓGICA FEDERAL DO PARANÁ)

MINISTÉRIO DA EDUCAÇÃO
SETOR DE TECNOLOGIA
UNIVERSIDADE FEDERAL DO PARANÁ
PRÓ-REITORIA DE PESQUISA E PÓS-GRADUAÇÃO
PROGRAMA DE PÓS-GRADUAÇÃO ENGENHARIA ELÉTRICA - 40001016043P4

TERMO DE APROVAÇÃO

Os membros da Banca Examinadora designada pelo Colegiado do Programa de Pós-Graduação ENGENHARIA ELÉTRICA da Universidade Federal do Paraná foram convocados para realizar a arguição da tese de Doutorado de **THAÍS MARZALEK BLASI** intitulada: **NEW APPROACHES TO DISTRIBUTED ENERGY RESOURCES AND MICROGRID INTEGRATION INTO ACTIVE DISTRIBUTION SYSTEMS**, sob orientação do Prof. Dr. ALEXANDRE RASI AOKI, que após terem inquirido a aluna e realizada a avaliação do trabalho, são de parecer pela sua APROVAÇÃO no rito de defesa.

A outorga do título de doutora está sujeita à homologação pelo colegiado, ao atendimento de todas as indicações e correções solicitadas pela banca e ao pleno atendimento das demandas regimentais do Programa de Pós-Graduação.

Curitiba, 26 de Fevereiro de 2024.

Assinatura Eletrônica
28/02/2024 08:03:27.0
ALEXANDRE RASI AOKI
Presidente da Banca Examinadora

Assinatura Eletrônica
28/02/2024 13:59:43.0
WALMIR DE FREITAS FILHO
Avaliador Externo (UNIVERSIDADE ESTADUAL DE CAMPINAS)

Assinatura Eletrônica
28/02/2024 09:47:42.0
ODILON LUIS TORTELLI
Avaliador Interno (UNIVERSIDADE FEDERAL DO PARANÁ)

Assinatura Eletrônica
28/02/2024 11:22:37.0
ANDREA LUCIA COSTA
Avaliador Externo (UNIVERSIDADE TECNOLÓGICA FEDERAL DO PARANÁ)

I dedicate this dissertation to my mother, Marília and to my brother Raphael that are my best friends and are who always supported and encouraged me.

ACKNOWLEDGMENT

First, I thank God for the gift of life, for always show me the paths that I should follow and give me the opportunity to do this research.

I would like to thank my family, my mother Marília Marzalek Blasi, my brother Raphael Marzalek Blasi and my father Paulo Küster Blasi for all the love, affection, dedication, support, and incentive during all my life and for encouraging me to follow my dreams.

I would like to thank my professor supervisor Dr. Alexandre Rasi Aoki for the friendship and for all his dedication, patience, support and for always giving me opportunities to learn more and more.

I would like to thank my professor auxiliary supervisor, Dra. Thelma Solange Piazza Fernandes, for the friendship and for all her support, dedication, patience and for always encouraging me to develop this work.

I would like to thank all my colleagues from OPAL-RT, especially Marcela Trindade and Victor Hirata for the friendship, support and incentive to develop this work.

I would like to thank Companhia Paranaense de Energia—COPEL for the funding from the research and technological development (RTD) program, through the PD-02866-0511/2019 project, entitled “Programação diária de microgrids e redes ativas de distribuição considerando o gerenciamento pelo lado da demanda” realized from 2020 to 2022.

“The wisdom of men is proportional not to their experience, but to their ability to acquire experience.”

George Bernard Shaw

RESUMO

Com o avanço da modernização das redes de distribuição, tem se tornado um desafio cada vez maior para as distribuidoras a realização da operação segura e eficaz da rede. Esse desafio justifica-se pela inclusão dos recursos energéticos distribuídos (DER), em uma rede que foi concebida com o objetivo de entregar energia ao consumidor final, sendo um elemento passivo e que agora passa a se tornar ativo. Uma forma de minimizar os impactos desses novos agentes na rede consiste no provisionamento de serviços ancilares, passando a contribuir para a qualidade da operação da rede. O fluxo de potência ótimo é um método de otimização utilizado para planejar a operação da rede de distribuição, no qual, os recursos energéticos distribuídos podem ser modelados e o provisionamento de serviços ancilares pode ser considerado. Dessa forma o objetivo do trabalho consiste em compreender as alterações que vem ocorrendo nas redes de distribuição com a entrada dos DERs, avaliando seus impactos, bem como a proposição da realização de serviços ancilares. Ademais, objetiva-se avaliar a entrada de novas tecnologias na rede de distribuição, em consonância com os elementos tradicionais já existentes. Além do provisionamento de serviços ancilares, busca-se também otimização da operação desse novo cenário de operação, considerando um Fluxo de Potência Ótimo Multiperíodo (MPOPF) com a inserção de geração distribuída, sistemas de armazenamento de energia, microrredes e veículos elétricos na rede de distribuição. Este MPOPF inclui a prestação de serviços auxiliares pelos inversores associados aos equipamentos ligados à rede principal, realizando por exemplo o despacho de reativos para suporte de tensão. Na formulação, toda a rede é modelada, considerando a colocação de equipamentos clássicos como regulador de tensão e bancos de capacitores, além de tecnologias modernas como equipamentos com eletrônica de potência, além de inversores de quatro quadrantes. O MPOPF foi simulado para diversos cenários considerando um alimentador de teste de 90 barras e uma rede de distribuição real de Curitiba – Brasil contendo uma microrrede no parque Barigui. A partir dos resultados, o MPOPF mostrou-se altamente robusto, sendo capaz de simular a rede com todos os equipamentos conectados simultaneamente, realizando o despacho ótimo de potência ativa e reativa, além de permitir a operação de serviços ancilares como suporte de tensão, peak-shaving e gestão do lado da demanda. Ademais foi desenvolvida uma metodologia hierárquica para integração do despacho ótimo da microrrede com o cálculo do despacho ótimo da rede como um todo. Nesse processo a abordagem mestre-escravo é considerada com uma realimentação entre as metodologias até que se atinja a operação ótima da rede considerando a integração de múltiplos DERs. Por fim, visando avaliar a aplicabilidade de metodologia hierárquica, uma abordagem de um gêmeo-digital da microrrede do parque Barigui foi realizada com simulação em tempo-real. Nessa abordagem, além da simulação da operação da microrrede considerando diferentes cenários, foi modelada também a comunicação com o SCADA da distribuidora, usando o protocolo de comunicação IEC 60870-5-104. Cada uma das abordagens utilizadas apresenta características próprias de modo que representam diferentes pontos de vista para o planejamento e operação das redes ativas de distribuição.

Palavras-Chave: Redes Ativas de Distribuição, Serviços Ancilares, Eletrônica de Potência, Recursos Energéticos Distribuídos, Microrredes, Fluxo de Potência Ótimo Multiperíodo, Modelo Hierárquico, Gêmeo-Digital, Simulação em Tempo-Real.

ABSTRACT

With the advancement of modernization in distribution networks, it has become an increasingly challenging task for distributors to ensure the safe and efficient operation of the grid. This challenge is justified by the integration of Distributed Energy Resources (DERs) into a network that was originally designed to deliver energy to the end consumer as a passive element, now transitioning to an active one. One way to minimize the impacts of these new agents on the grid is through the provision of ancillary services, thus contributing to the quality of grid operation. Optimal power flow is an optimization method used to plan the operation of the distribution network, where distributed energy resources can be modeled, and the provision of ancillary services can be considered. Therefore, the objective of this work is to understand the changes occurring in distribution networks with the introduction of DERs, assessing their impacts, and proposing the provision of ancillary services. Additionally, the aim is to evaluate the integration of new technologies into the distribution network in line with existing traditional elements. In addition to the provision of ancillary services, the optimization of this new operational scenario is also sought, considering a Multiperiod Optimal Power Flow (MPOPF) with the integration of distributed generation, energy storage systems, microgrids, and electric vehicles into the distribution network. This MPOPF includes the provision of ancillary services by inverters associated with equipment connected to the main grid, performing tasks such as reactive power dispatch for voltage support. In the formulation, the entire network is modeled, considering the placement of classical equipment such as voltage regulators and capacitor banks, as well as modern technologies such as power electronics equipment and four-quadrant inverters. The MPOPF was simulated for various scenarios considering a 90-bus test feeder and a real distribution network in Curitiba, Brazil, containing a microgrid in the Barigui Park. From the results, the MPOPF proved to be highly robust, capable of simulating the network with all connected equipment simultaneously, optimizing active and reactive power dispatch, and allowing the operation of ancillary services such as voltage support, peak-shaving, and demand-side management. Furthermore, a hierarchical methodology was developed for integrating the optimal dispatch of the microgrid with the overall grid dispatch calculation. In this process, the master-slave approach is considered with feedback between the methodologies until optimal grid operation considering the integration of multiple DERs is achieved. Finally, to assess the applicability of the hierarchical methodology, a digital-twin approach of the Barigui Park microgrid was performed with real-time simulation. In this approach, in addition to simulating the microgrid operation considering different scenarios, communication with the utility's SCADA system was also modeled using the IEC 60870-5-104 communication protocol. Each of the approaches used presents its own characteristics, representing different perspectives for the planning and operation of active distribution networks.

Keywords: Active Distribution Networks, Ancillary Services, Custom Power, Distributed Energy Resources, Microgrids, Multiperiod Optimum Power Flow, Hierarchical Model, Digital-Twin, Real-Time Simulation.

LIST OF ILLUSTRATIONS

FIGURE 1 - PV BY SEGMENT CAPACITY, IN WORLD, 2000-2025, IN GW 24
FIGURE 2 - 5-YEAR CAPACITY GROWTH, PV DISTRIBUTED AND UTILITY-SCALE SYSTEMS, WORLD 24
FIGURE 3 – PV COST REDUCTION OVER THE LAST DECADE ($/W). 26
FIGURE 4 - NUMBER OF DG SYSTEMS OF ALL SOURCES IN BRAZIL FROM 2013-2023 28
FIGURE 5 – CUMULATIVE INSTALLED POWER OF DG SYSTEMS OF MULTIPLE SOURCES IN BRAZIL FROM 2013-2023 28
FIGURE 6 - ANNUAL GENERATION ESTIMATE BY ENERGY SOURCE FOR MINI AND MICRO DISTRIBUTED GENERATION IN BRAZIL 29
FIGURE 7 – YEARLY ELECTRICITY GENERATION ESTIMATE FROM MINI AND MICRO DISTRIBUTED GENERATION IN BRAZIL 29
FIGURE 8 - INCREASING OF LITHIUN-ION IN ANNUAL BATTERY STORAGE CAPACITY ADDITIONS GLOBALLY 31
FIGURE 9 – SCENARIOS OF STATIONARY BATTERY CAPACITY GROWTH UP TO 2030, WORLDWIDE 32
FIGURE 10 – INNOVATIONS FOR FUTURE POWER SYSTEMS 41
FIGURE 11 - BENEFITS PROVIDED BY DEMAND RESPONSE TO POWER SYSTEM OPERATION. 48
FIGURE 12 - BRAZILLIAN WHITE TARIFF VALUES AND BEHAVIOR. 82
FIGURE 13 - SOLAR IRRADIATION PROFILE 83
FIGURE 14 - TEST DISTRIBUTION FEEDER WITH 90 BUSES 84
FIGURE 15 - LOAD ACTIVE AND REACTIVE POWER PROFILE FOR 90 BUS TEST FEEDER. 85
FIGURE 16 - EV DAILY AND NIGHT CHARGING BEHAVIORS. 86
FIGURE 17 - ACTIVE POWER BALANCE AT THE SUBSTATION BUS FOR 90 BUSES TEST FEEDER BASE CASE 89
FIGURE 18 - REACTIVE POWER BALANCE AT THE SUBSTATION BUS FOR 90 BUS TEST FEEDER BASE CASE 89
FIGURE 19 - VOLTAGE BEHAVIOR FOR ALL 90 BUSES IN THE BASE CASE SCENARIO 90

FIGURE 20 - VOLTAGE REGULATOR TAP CHANGES FOR 90 BUSES BASE CASE SCENARIO...90
FIGURE 21 - BUSES WITH REVERSE POWER INJECTION FOR 90 BUSES TEST CASE WITH DG AT 12H. 92
FIGURE 22 - PV SYSTEMS REACTIVE POWER DISPATCH. 92
FIGURE 23 - VOLTAGE BEHAVIOR FOR ALL 90 BUSES WITH 70% OF DISTRIBUTED GENERATION PENETRATION AND REACTIVE POWER DISPATCH. 93
FIGURE 24 - SUBSTATION BUS VOLTAGE BEHAVIOR FOR 100% PENETRATION WITH NO D-SVC AND NO REACTIVE DISPATCH. 94
FIGURE 25 - VOLTAGE BEHAVIOR FOR ALL BUSES FOR 90 BUSES TEST FEEDER WITH 100% PV PENETRATION WITH NO D-SVC AND NO REACTIVE DISPATCH. 95
FIGURE 26 - VOLTAGE REGULATOR TAP CHANGES FOR 90 BUSES TEST FEEDER WITH 100% OF PV PENETRATION AND NO D-SVC AND NO REACTIVE DISPATCH 95
FIGURE 27 - SUBSTATION BUS VOLTAGE BEHAVIOR FOR 100% PV PENETRATION WITH D-SVC AND NO REACTIVE DISPATCH. 96
FIGURE 28 - D-SVC BEHAVIOR AT 90 BUSES TESTS FEEDER WITH 100% OF PV PENETRATION WITHOUT REACTIVE DISPATCH. 96
FIGURE 29 - PV SYSTEMS REACTIVE POWER DISPATCH WITH 100% PENETRATION...97
FIGURE 30 - D-SVC BEHAVIOR AT 90 BUSES TEST FEEDER WITH 100% OF PV PENETRATION WITH REACTIVE DISPATCH. 97
FIGURE 31 - VOLTAGE BEHAVIOR FOR ALL 90 BUSES WITH 100% OF DISTRIBUTED GENERATION PENETRATION AND REACTIVE DISPATCH. 98
FIGURE 32 - BUSES WITH REVERSE POWER FLOW FOR 90 BUSES TEST FEEDER WITH 100% OF PV PENETRATION AT 12H. 99
FIGURE 33 - REACTIVE POWER BALANCE AT THE SUBSTATION BUS FOR 90 BUSES TEST FEEDER WITH PV, EV CHARGING AT DAYTIME, AND D-SVC....100
FIGURE 34 - BESS ACTIVE POWER BEHAVIOR WHEN CONNECTED AT THE SUBSTATION BUS 101
FIGURE 35 - BESS STATE-OF-CHARGE (SOC) WHEN CONNECTED AT THE SUBSTATION BUS 101

FIGURE 36 - DIFFERENCE BETWEEN ESTIMATED AND REALIZED LOAD PROFILES AT BUS 64 WITH DSM. 103
FIGURE 37 - ESTIMATED AND REALIZED LOAD PROFILES FOR THE MICROGRID PLACED AT BUS 64 104
FIGURE 38 - ESTIMATED AND REALIZED LOAD PROFILES FOR THE MICROGRID PLACED AT BUS 64 AFTER THE MPOPF LOAD SHEDDING, RESULTING IN A PROPOSITION OF A NEW MG PROFILE (YELLOW) 104
FIGURE 39 - ACTIVE POWER BALANCE AT THE SUBSTATION BUS FOR 90 BUSES TEST FEEDER AT SCENARIO 7 106
FIGURE 40 - REACTIVE POWER BALANCE AT THE SUBSTATION BUS FOR 90 BUSES TEST FEEDER AT SCENARIO 7 106
FIGURE 41 - D-SVC BEHAVIOR AT SCENARIO 7 107
FIGURE 42 - VOLTAGE BEHAVIOR FOR ALL 90 BUSES AT SCENARIO 7 107
FIGURE 43 - ESTIMATED AND REALIZED LOAD PROFILES FOR THE MICROGRID PLACED AT BUS 64 AT SCENARIO 7 108
FIGURE 44 - REAL DISTRIBUTION FEEDER. 109
FIGURE 45 - ACTIVE POWER PROFILE FOR REAL DISTRIBUTION FEEDER FOR SUMMER, BEING THE FILLED LINE THE MEAN AND THE DASHED LINE THE STANDARD DEVIATION AROUND THE MEAN. 110
FIGURE 46 - ACTIVE POWER PROFILE FOR REAL DISTRIBUTION FEEDER FOR WINTER, BEING THE FILLED LINE THE MEAN AND THE DASHED LINE THE STANDARD DEVIATION AROUND THE MEAN. 110
FIGURE 47 - TYPICAL ACTIVE POWER SCHEDULE FOR THE MG IN SUMMER. 112
FIGURE 48 - TYPICAL ACTIVE POWER SCHEDULE FOR THE MG IN WINTER. 112
FIGURE 49 - FLOWCHART OF NEW STRATEGY OF MPOPF DIVIDED INTO PRE-PROCESSING AND OPTIMIZATION PROCESS 113
FIGURE 50 - ACTIVE POWER BALANCE FOR REAL DISTRIBUTION FEEDER ON BASE CASE SCENARIO FOR SUMMER (SE IS THE SUBSTATION BUS). 114
FIGURE 51 - ACTIVE POWER BALANCE FOR REAL DISTRIBUTION FEEDER ON BASE CASE SCENARIO FOR WINTER. 115
FIGURE 52 - VOLTAGE BEHAVIOR FOR ALL BUSES IN REAL FEEDER BASE CASE FOR SUMMER LOAD PROFILE 115

FIGURE 53 - VOLTAGE BEHAVIOR FOR ALL BUSES IN REAL FEEDER BASE CASE FOR WINTER LOAD PROFILE 116
FIGURE 54 - ACTIVE POWER BALANCE FOR REAL DISTRIBUTION FEEDER WITH THE CONNECTION OF THE MICROGRID FOR WINTER. 117
FIGURE 55 - VOLTAGE BEHAVIOR FOR ALL BUSES IN REAL FEEDER FOR WINTER LOAD PROFILE WITH MICROGRID AND 30% OF PV PENETRATION. HIGHLIGHT FOR THE PERIOD WITH VOLTAGE INCREASE 118
FIGURE 56 - BESS POWER AND ENERGY BEHAVIOR WHEN CONNECTED TO THE REAL FEEDER WITH WINTER LOAD PROFILE AND 30% OF PV PENETRATION. 119
FIGURE 57 - VOLTAGE BEHAVIOR FOR ALL BUSES IN REAL FEEDER FOR WINTER LOAD PROFILE WITH MICROGRID, 30% OF PV PENETRATION AND BESS. 120
FIGURE 58 - HIERARCHICAL MASTER-SLAVE MODELING PROPOSED WITH POWER GRID AND MICROGRID OPTIMIZATION. 130
FIGURE 59 – BARIGUI MICROGRID SCHEMATIC DIAGRAM............................ 132
FIGURE 60 - PROPOSED DISPATCH BY THE MGOM FOR THE PILOT MICROGRID, FOR SCENARIO 1 OF THE HIERARCHICAL MODEL ANALYSIS. 133
FIGURE 61 – MICROGRID DISPATCH FROM THE MAIN GRID POINT OF VIEW, FOR SCENARIO 1 OF THE HIERARCHICAL MODEL ANALYSIS 134
FIGURE 62 – VOLTAGE BEHAVIOR FOR ALL BUSES OF THE FEEDER, FOR SCENARIO 1 OF THE HIERARCHICAL MODEL ANALYSIS 135
FIGURE 63 - PROPOSED DISPATCH BY THE MGOM FOR THE PILOT MICROGRID, FOR SCENARIO 1 OF THE HIERARCHICAL MODEL ANALYSIS. 135
FIGURE 64 - MICROGRID DISPATCH FROM THE MAIN GRID POINT OF VIEW, FOR SCENARIO 2 OF THE HIERARCHICAL MODEL ANALYSIS 136
FIGURE 65 - PROPOSED DISPATCH FROM THE MGOM FOR THE MICROGRID BEFORE THE FEEDBACK PROCESS.. 137
FIGURE 66 - PROPOSED DISPATCH FROM THE MPOPF FOR THE MICROGRID BEFORE THE FEEDBACK PROCESS.. 138
FIGURE 67 - PROPOSED DISPATCH FROM THE MGOM FOR THE MICROGRID AFTER THE FIRST INTERACTION ON THE FEEDBACK PROCESS.................. 138
FIGURE 68 - PROPOSED DISPATCH FROM THE MPOPF FOR THE MICROGRID AFTER THE FIRST INTERACTION ON THE FEEDBACK PROCESS.................. 139

FIGURE 69 - PROPOSED DISPATCH FROM THE MGOM FOR THE MICROGRID AFTER THE THIRD INTERACTION ON THE FEEDBACK PROCESS 139
FIGURE 70 - PROPOSED DISPATCH FROM THE MPOPF FOR THE MICROGRID AFTER THE THIRD INTERACTION ON THE FEEDBACK PROCESS 140
FIGURE 71 - PROPOSED DISPATCH FOR THE MICROGRID AT THE END OF THE HIERARCHICAL PROCESS 140
FIGURE 72 - VOLTAGE PROFILE OF ALL BUSES OF THE FEEDER AFTER THE HIERARCHICAL PROCESS FOR THE MG DISPATCH. 141
FIGURE 73 - MICROGRID'S DISPATCH FROM MGOM IN THE SCENARIO OF AN ACTIVE NETWORK WITH INCREASE LOAD 142
FIGURE 74 - MICROGRID'S DISPATCH FROM MFOP POINT OF VIEW IN THE SCENARIO OF AN ACTIVE NETWORK WITH INCREASE LOAD.........................143
FIGURE 75 - BEHAVIOR OF THE BATTERY FOR THE ACTIVE DISTRIBUTION NETWORK SCENARIO WITH INCREASE CHARGE...144
FIGURE 76 - BEHAVIOR OF VOLTAGE AT ALL BUSES FOR THE SCENARIO OF ACTIVE DISTRIBUTION AND LOAD INCREASE~NETWORK 144
FIGURE 77 - ILUSTRATION OF FIXED TIME STEP USAGE ON A REAL-TIME SIMULATION 148
FIGURE 78 – TYPICAL SIMULATION TIME-STEP BY APPLICATION..................148
FIGURE 79 - REAL-TIME APPLICATIONS..150
FIGURE 80 - MICROGRID MODEL IMPLEMENTED IN THE HYPERSIM TOOL, HIGHLIGHTING EACH OF THE MODELED PLOTS 154
FIGURE 81 - SIMULATION SETUP 155
FIGURE 82 - RESULTS FROM THE EV CONNECTION TO CHARGE AT THE CARPORT DURING THE DAY – PART 1 156
FIGURE 83 - RESULTS FROM THE EV CONNECTION TO CHARGE AT THE CARPORT DURING THE DAY – PART 2...157
FIGURE 84 – BEHAVIOR OF THE AVERAGE POWER AT THE PCC AND THE EV ENTRY POINT WHEN THERE IS NO SOLAR GENERATION – NIGHT. 158
FIGURE 85 - IEC 104 COMMUNICATION PROTOCOL IN HYPERSIM AND COMMUNICATION WITH FREYRSCADA IEC 60870-5-104 CLIENT/MASTER SIMULATOR DURING THE MG MODEL SIMULATION. 158
FIGURE 86 - PCC LOCATION AT THE BARIGUI PARK (AERIAL VIEW) AND ITS REPRESENTATION AT THE MODEL 159

FIGURE 87 - BEHAVIOR AT THE PCC, BEFORE, DURING AND AFTER THE ISLANDING..160
FIGURE 88 - BEHAVIOR AT PV SYSTEMS AND UNCONTROLLABLE LOADS BEFORE, DURING AND AFTER THE ISLANDING. 160
FIGURE 89 – BEHAVIOR OF THE MG BESS SYSTEM DURING AND AFTER THE ISLANDING, IN A SCENARIO WITH NO SOLAR GENERATION. 161
FIGURE 90 - HIGHLIGHT OF FAULT LOCATION AT THE MG MODEL................161
FIGURE 91 - TOP: VOLTAGE ON BUS 5 BEFORE AND DURING THE FAULT. BOTTOM: THREE-PHASE FAULT CURRENT...162
FIGURE 92 - AVERAGE POWER BEHAVIOR ON DIFFERENT ELEMENTS OF THE MG DURING THE FAULT SCENARIO AND ACTUATION OF CB2 163

LIST OF TABLES

TABLE 1 - ACTIVE DISTRIBUTION NETWORK FEATURES 40
TABLE 2 – INTERNATIONAL EXPERIENCE WITH DER INCREASE AT DISTRIBUTION GRIDS..43
TABLE 3 - CLASSIFICATION OF VOLTAGE LEVELS 81
TABLE 4 - NORMALIZED VALUES OF OBJECTIVE FUNCTION WEIGHTS FOR 90 BUS TEST FEEDER 88
TABLE 4 - RESULTS AFTER THE ALLOCATION OF PV SYSTEMS 99
TABLE 5 - RESULTS AFTER THE ALLOCATION OF THE BESS AT BUS 8.........102
TABLE 6 - RESULTS FROM DIFFERENT SCENARIOS AFTER GRADUALLY EQUIPMENT CONNECTION. 105
TABLE 7 - SUBSTATION VOLTAGE VALUES ACCORDING TO LOAD LEVELS .111
TABLE 8 - NORMALIZED VALUES OF OBJECTIVE FUNCTION WEIGHTS 113
TABLE 9 - RESULTS FROM THE REAL FEEDER WITH MICROGRID CONNECTION FOR DIFFERENT LOAD AND MICROGRID PROFILES 116
TABLE 10 - RESULTS FROM REAL FEEDER WITH MICROGRID CONNECTION FOR 30% OF PV PENETRATION AT SUMMER AND WINTER SCENARIOS 117
TABLE 11 - RESULTS FROM THE REAL FEEDER WITH MICROGRID CONNECTION, 30% OF PV PENETRATION, AND BESS 119
TABLE 12 - OPTIMIZATION TIMES FOR DIFFERENT SIMULATION SCENARIOS WITH REAL DISTRIBUTION FEEDER WITH INITIALIZATION BASED ON PREVIOUS SIMULATIONS...121

LIST OF ABBREVIATIONS AND ACRONYMS

ADMS	Advanced Distribution Management System
ADN	Active Distribution Network
ANEEL	Brazillian National Electric Energy Agency
BESS	Battery Energy Storage Systems
BRL	Brazilian Reais
BTM	Behind-the-meter
DER	Distributed Energy Resources
DERMS	Distribute Energy Resources Management System
D-FACTS	Distribution-Flexible AC Transmission System
DG	Distributed Generation
DMS	Distribution Management System
DoD	Depth-of-Discharge
DRMS	Demand Response Management System
DSM	Demand-side Management
DSO	Distribution System Operator
D-SVC	Distributed Static Var Compensator
EPE	Brazilian Energy Research Office
ESS	Energy Storage Systems
FACTS	Flexible AC Transmission Systems
FIT	Feed-in tariff
FPGA	Field-Programmable Gate Array
FTM	In-front of the meter
GW	Giga-Watts
HIL	Hardware-in-the-loop
IEA	International Energy Agency
IMG	Independent Microgrid
IOT	internet-of-things
IPOPT	Interior Point Optimizer
IRENA	International Renewable Energy Agency
LV	Low Voltage
MGOM	Microgrid Optimization Model

MIL	Model-in-the-loop
MMG	Multiple Microgrid
MPOPF	Multiperiod Optimum Power Flow
MV	Medium Voltage
NI	Number of interactions
NR	Normative Resolution
NREL	U.S. National Renewable Energy Laboratory’s
OF	Objective Function
OLTC	On-load tap changers
OPF	Optimum Power Flow
PCC	Point of Common Coupling
pf	Power factor
PHIL	Power-Hardware-in-the-loop
PLL	Phase-locked loop
PV	Photovoltaic
PVGD	Photovoltaic Distributed Generation
RCP	Rapid-Control-Prototype
R&D	Research and Development
RD	Reactive Dispatch
RF	Real Feeder
SCADA	Supervisory Control and Data Acquisition
SIL	Software-in-the-loop
SSVR	Series Static Voltage Restores
UMG	Unified Microgrids
USD	American Dollar
V1G	Vehicle-on-Grid
V2B	Vehicle-to-Build
V2G	Vehicle-to-Grid
V2H	Vehicle-to-Home
VR	Voltage Regulators

LIST OF SYMBOLS

a_j^k	taps position of voltage regulator at line *j* and period *k*
$a_{max}{}^k_j$ and $a_{min}{}^k_j$	maximum and minimum limit of the voltage regulator taps of line *j* and period *k*, respectively
A_t^c	amount of energy stored (charged) in the microgrid battery in a period t
A_t^d	amount of energy discharged from the microgrid battery in a period t
Bsh_i^k	the susceptance capacitive of capacitor banks at bus *i* and period *k*
Bst_i^k	represents the maximum limit of susceptance capacitive of D-SVC at bus *i* and period *k*
$\mathrm{c}(\boldsymbol{Pbat})$	cost function based on linear cost function $cost_{deg}$
$\mathrm{c}(\boldsymbol{Pg})$	energy cost function related to power provided by substation and other generation systems belonging to the power utility
Cb_t	cost of battery degradation in the period t
$cost_{BB}$	cost of battery bank
$cost_{deg}$	battery degradation cost
e_i^k	real component of the voltage V_i^k
Earrive	energy stored in BESS at the start of dispatch period
$Ebat$	energy storage capacity
$Ebat_{max}{}^k_{\mathrm{i}}$ and $Ebat_{min}{}^k_{\mathrm{i}}$	maximum and minimum limits of energy stored capacity of BESS at bus *i* and period *k;* respectively
eff_{bat}	battery energy efficiency
$Er1_t$	energy balance that cannot be supplied by the microgrid battery in a period t
$Er2_t$	energy balance that can be supplied by the microgrid battery in a period t
f_i^k	imaginary component of the voltage V_i^k

$fcost_{bat}$	battery degradation costs criterion of the objective function
$f_{flexible}$	load flexibility management criterion of the objective function
$flosses$	power losses criterion of the objective function
$foper$	operational cost criterion of the objective function
${F_{max}}_j^k$	maximum limit of active power flow through the *j* and period *k*
FPd_i^k	ideal flexible active power demanded at bus *i* and period *k*
FQd_i^k	ideal flexible reactive power demanded at bus *i* and period *k*
$gamma_{nb}^{nper}$	factor to cut each flexible load (***FPd***) at bus *i* and period *k*
G_{pv}	generation from the microgrid photovoltaic system in a period t
$Grid_t$	power consumption (positive values) or injection (negative values) of the microgrid into the power grid in the period t
hfp	off-peak hours of the white-tariff
hp	peak hours of the white-tariff
hpp	pre- and post-peak hours of the white-tariff
i	bus defined within the set of buses of the electric system
j	line defined within the set of lines of the electric system
k	period defined within the total time interval defined for analysis
L_t^{NP}	non-controllable critical load in a period t
L_t^P	non-controllable priority load in a period t
L_t^{CP}	load from the carport system from the microgrid in a period t
L_t^{CONT}	controllable load of the microgrid in a period t

$LS1_t$	load shedding without microgrid batteries in a period t, being limited by $0 \leq LS1_t \leq L_t^{NP}$
$LS2_t$	load shedding with microgrid batteries in a period t, being limited by $0 \leq LS2_t \leq L_t^{P}$
LS_t	load shedding in the period t
N	total number of periods calculated, being in this case 24, since is considered the dispatch of a day-ahead
η	auxiliary variable that represents the energy cost
nb	number of buses
nl	number of lines
nper	number of periods
n_cycles	expected number of cycles for the battery system over the lifetime
$Pbat_i^k$	power active of BESS injected at bus *i* and period *k*
${Pbat_{max}}_i^{nper}$ and ${Pbat_{min}}_i^{nper}$	maximum and minimum limits of the active power of BESS at bus *i* and period *k*; respectively
Pd_i^k	represents the inflexible active power demanded at bus *i* and period *k*
$Pd_{ideal,t}$	ideal active power flow between the MG and the distribution grid in the period t
$Pd_{realized,t}$	realized active power flow between the MG and the distribution grid in the period t
Pgh_i^k	active power injected at bus *i* and period *k*
${Pg_{max}}_1^k$ and ${Qg_{max}}_1^k$	maximum limits of the active and reactive power injected by the substation at bus 1 and period *k*, respectively
$Pgsun_i^k$	active photovoltaic power injected at bus *i* and period *k*
$Qbat_i^k$	reactive battery power injected at bus *i* and period *k*
Qd_i^k	represents the inflexible reactive power demanded at bus *i* and period *k*
Qgh_i^k	reactive power injected at bus *i* and period *k*

$Qgsun_i^k$	reactive photovoltaic power injected at bus *i* and period *k*
$Sbat_i^k$	BESS apparent power injected at bus *i* and period *k*
$Ssun_i^k$	apparent photovoltaic power injected at bus *i* and period *k*
Δt	time interval between two consecutive periods
T	represents that the vector is transposed
t	period that is being evaluated
Tls_t	load shedding cost in the period t
T_{pen}	penalty pricing for the difference between the ideal and the realized power flow between the MG and the main power grid
T_t	energy price at the period t
$\boldsymbol{u}$	unit vector with size (*nb.nper* x 1)
V_i^k	voltage phasors at bus *i* and period *k*
$vmax_i^k$ and $vmin_i^k$	maximum and minimum limits of the voltage magnitude at bus *i* and period *k*; respectively
$wbat$	weight relative to the importance of battery degradation costs criterion
wc	weight relative to the importance of the operational costs criterion
wgd	weight relative to the importance of load flexibility management
$wload$	weight relative to the importance of BESS load maximization
wp	weight relative to the importance of the loss criterion
$w_{targetload}$	weight relative to the criterion that forces that the total expected load must be supplied
$\mathbf{x}$	corresponds to the vector that stores the real and imaginary components of all the bus voltages with dimension (2.*nb.nper* x 1)

SUMMARY

1 INTRODUCTION....23
1.1 CONTEXT....23
1.2 JUSTIFICATION....33
1.3 RESEARCH PROBLEM DEFINITION AND SCIENTIFIC QUESTION....36
1.4 OBJECTIVES....36
1.5 SCIENTIFIC CONTRIBUTION....37
1.6 DOCUMENT STRUCTURE....38
2 ACTIVE DISTRIBUTION NETWORKS....39
2.1 CONCEPT....39
2.2 DISTRIBUTED ENERGY RESOURCES....42
2.3 ANCILLARY SERVICES....45
2.3.1 Voltage Support and Reactive Power Control....45
2.3.2 Demand Response....47
2.3.3 Contingency and Emergency Frequency Response....49
2.3.4 Grid Resiliency and Black Start....50
2.3.5 Islanded Operation....51
2.3.6 Grid Flexibility....52
2.4 MICROGRIDS....53
2.5 FINAL CONSIDERATIONS....55
3 MULTIPERIOD OPTIMUM POWER FLOW FOR ACTIVE DISTRIBUTION NETWORKS....57
3.1 OPTIMUM POWER FLOW LITERATURE REVIEW....57
3.2 BASIC CONCEPTS OF THE PROPOSED MULTIPERIOD OPTIMUM POWER FLOW62
3.3 INPUT VARIABLES....64
3.4 CONTROL AND DEPENDENT VARIABLES....72
3.5 OBJECTIVE FUNCTION....75
3.6 OPERATIONAL CONTRAINTS....77
3.6.1 Equality Constraints....77

3.6.2 Inequality Constraints 78

4 STUDY CASES FOR THE MULTIPERIOD OPTIMUM POWER FLOW PROPOSED FOR ACTIVE DISTRIBUTION NETWORK, MICROGRID AND ANCILLARY SERVICES 81

4.2 TEST FEEDER DESCRIPTION 83

4.3 TEST FEEDER RESULTS 88

4.3.1 90 Bus Test Feeder – Base Case 88

4.3.2 Changing Voltage Support Equipment 91

4.3.3 Including Distributed Generation 91

4.3.4 Inserting Electric Vehicles 99

4.3.5 Inserting Battery Energy Storage Systems 100

4.3.6 Inserting Flexible Loads 102

4.3.7 Inserting Microgrids 103

4.4 REAL DISTRIBUTION GRID APPLICATION 108

4.4.1 REAL DISTRIBUTION GRID DESCRIPTION 108

4.4.2 REAL DISTRIBUTION GRID RESULTS 113

4.4.2.1 Real Feeder – Base Case 114

4.4.2.2 Real Feeder with the Connection of the Pilot Microgrid 116

4.4.2.3 Real Feeder as Active Distribution Network 117

4.4.2.4 Computational Performance 120

4.5 FINAL CONSIDERATIONS ABOUT SIMULATION RESULTS 121

5 HIERARCHICAL MODEL 123

5.1 HIERARCHICAL MODEL BASIC CONCEPTS 123

5.2 MODELING 125

5.2.1 Modeling the Master Problem 126

5.2.2 Modeling the Slave Problem 127

5.2.3 Modeling the Hierarchical Problem 129

5.3 HIERARCHICAL MODEL SIMULATION 131

5.3.1 Scenarios definition for the Hierarchical Model Simulations 131

5.3.2 Hierarchical Model Simulations Results 133

5.3.2.1 Scenario 1: original load for the feeder and the Barigui microgrid ..133

5.3.2.2 Scenario 2: condition of programmed microgrid isolation (schedule islanding) 135

5.3.2.3 Scenario 3: feeder and microgrid with increased load 136

5.3.2.4 Scenario 4: consideration of the most complex grid scenario, with the presence of distributed generation and batteries, as well as the microgrid, with load increased 142

5.4 FINAL CONSIDERATIONS ABOUT THE HIERARCHICAL MODEL............144

6 REAL-TIME SIMULATION AND DIGITAL-TWIN..147

6.1 REAL-TIME SIMULATION CONCEPTS..147

6.2 DIGITAL-TWIN BASIC CONCEPTS...151

6.3 DIGITAL-TWIN OF A REAL MICROGRID MODELING 152

6.4 MICROGRID DIGITAL-TWIN REAL-TIME SIMULATION............................155

6.4.1 EV connection for loading at the carport 156

6.4.2 MG islanding 159

6.4.3 Fault application on the MG 161

6.5 FINAL CONSIDERATIONS ABOUT THE DIGITAL-TWIN...........................164

7 CONCLUSIONS AND FUTURE WORKS 165

REFERENCES…………………………………………………………………………172

1 INTRODUCTION

In the last years distribution grids have been facing transformations guided by the digitalization of the process, as well as the introduction of new elements as distributed energy resources (DER). Driven by concern on climate change, the increase of new energy solutions is being encouraged worldwide, with new equipment, markets, and solutions, that can push a more sustainable energy system. Part of this process is known as 3Ds of energy transformation, corresponding to: Decarbonization, Digitalization and Decentralization. Moreover, some authors consider a fourth D, that corresponds to system Democratization, which means, changes on energy systems with consumers actuating more actively on it.

1.1 CONTEXT

There are different concepts for distributed generation (DG) worldwide, but in general it can be defined as electric power sources connected to distribution grid, close to consumers, presenting flexibility in terms of installation and network connection, being placed behind-the-meter (DE CASTRO; DANTAS, 2017). The DG can be connected to the power utility distribution lines, integrating the distribution system, or can be part of a microgrid, which will be defined in detail later.

In the beginning of the 20th century, generation sources located close to the consumers corresponded to the main electricity source, once customers could share the small generation at a time when there were no large power generation units. At that time, small hydro units and diesel sources were used for electricity generation.

With the growth of electricity demand, the necessity of large power generation capacity requires the installation of large generation plants, being those located far from the consumers centers. This corresponds to the “traditional power system” that works worldwide during most of 20th century.

Recently, power generation units are again being placed close to consumers, this being driven by the energy matrix transition, aiming to reduce the dependency of fossil fuels to power generation. In this way, some countries have been provided incentives for the introduction of DG based on renewable sources, such as solar photovoltaic, small wind generation, and biomass.

The most used technology consists in solar photovoltaic (PV) generation, mainly due to its easy installation and low costs in comparison with other renewable systems. According to the International Energy Agency (IEA), the growth of PV systems worldwide increased after the first decade of the 21st century, as can be seen at FIGURE 1. The insertion of PV systems is happening not only with residential and commercial systems, but also with large systems (utility-scale), as presented at FIGURE 2.The graphics present not only the growth from the last years, as well as a forecast for the next years, where a more expressive growth is expected.

FIGURE 1 - PV BY SEGMENT CAPACITY, IN WORLD, 2000-2025, IN GW.

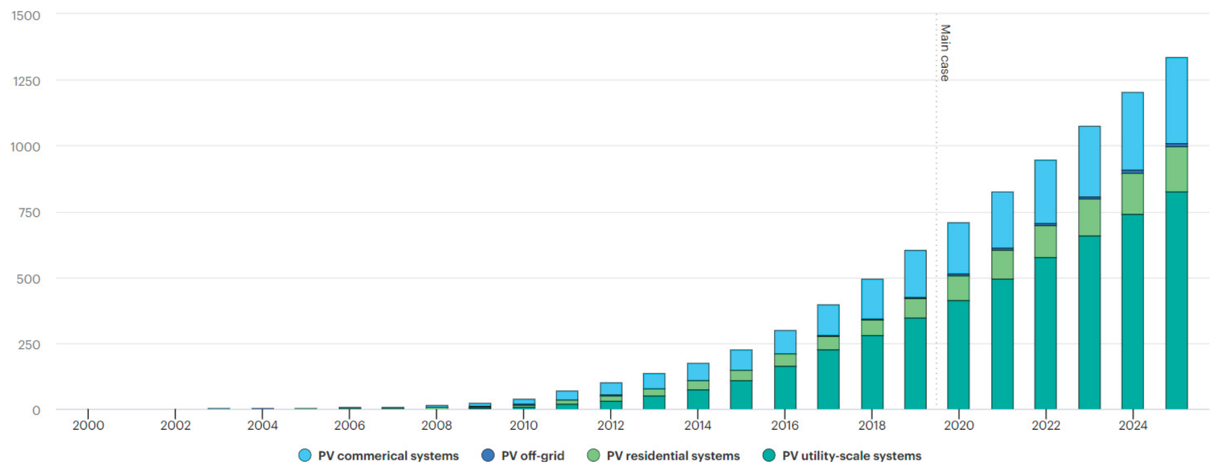

Source: IEA, 2020.

FIGURE 2 - 5-YEAR CAPACITY GROWTH, PV DISTRIBUTED AND UTILITY-SCALE SYSTEMS, WORLD

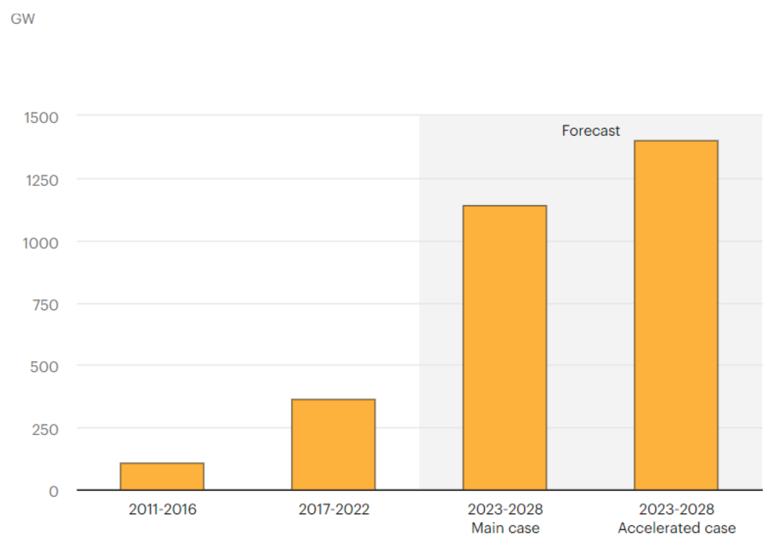

(a) PV distributed systems

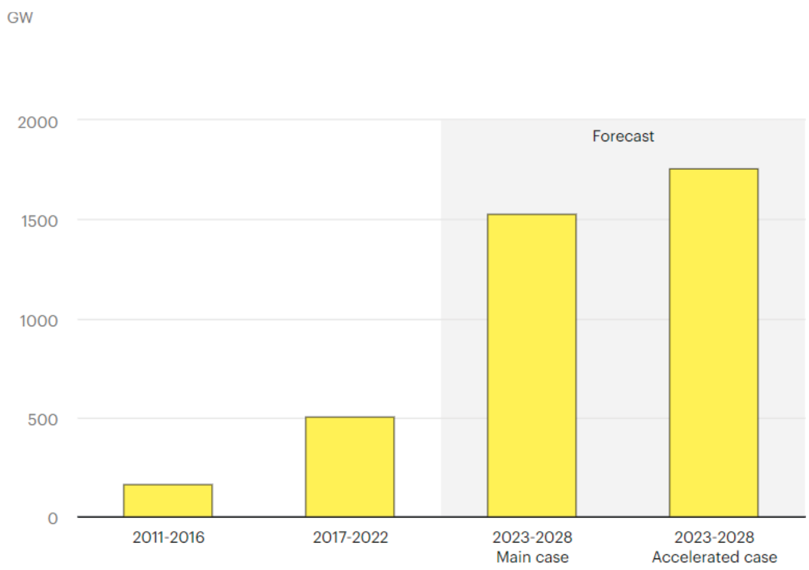

(b) PV utility scale systems

Source: IEA, 2024.

According to a survey realized by the U.S. National Renewable Energy Laboratory's (NREL), the costs of PV systems has been reducing over the last decade, and this effect is seen in PV systems of all sizes, from residential applications to utility-scale, as presented at FIGURE 3 (NREL, 2021).

The graphics also present the price composition for the PV systems, being the highest amount related to modules prices and other costs, with the biggest reduction over the years being linked to the decrease in module prices largely driven by market growth and technological development. Additionally, the hardware and inverter costs have also been reduced significantly over the last decade. Considering the total costs, since 2010 the reduction was 64%, 69% and 82% for residential, commercial-rooftop and utility-scale systems, respectively. According to some manufactures, in the last years, the prices are for PV distributed generation (PVDG) systems are remaining stable, and the financing available for the end-user customers are becoming even more common (GREENER, 2021).

FIGURE 3 – PV COST REDUCTION OVER THE LAST DECADE ($/W).

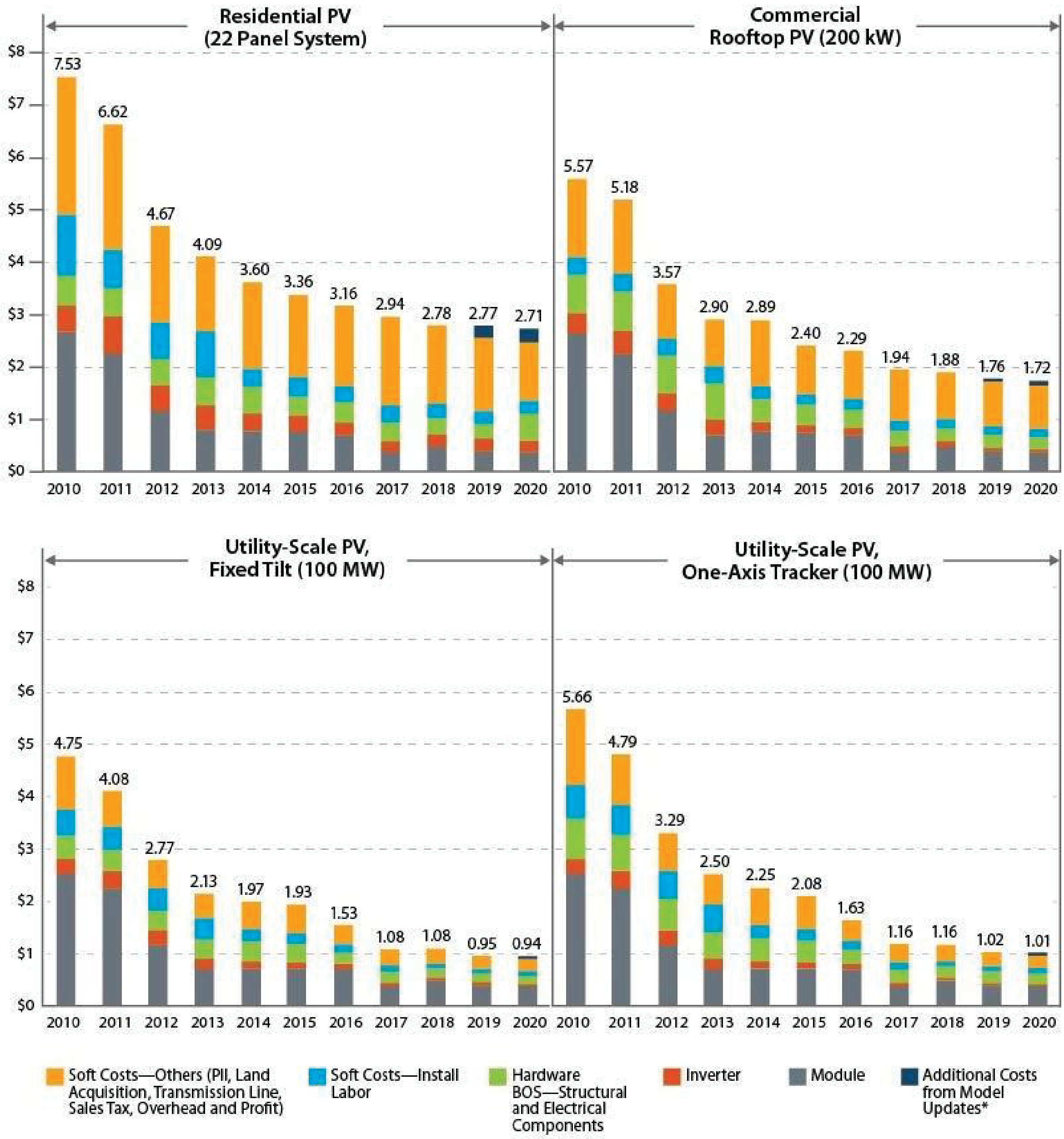

Source: NREL (2021).

In the Brazilian scenario is also possible to note the PV Systems growth trend. Even though the energy matrix is mostly composed of renewable sources of energy, solar photovoltaic generation has been increasingly over the years. In 2021, according to the Brazilian National Electric Energy Agency (ANEEL) Generation Information System, the solar generation corresponds to 2,22% of the energy matrix share, with 4,409 solar generation power plants (ANEEL, 2021a). In the first two months of 2024, in the Brazilian power systems were added more than 2GW of installed power from PVDG, corresponding to 20% of the growth expected for the year. In total, at the end of February 2024, the country presents more than 26.8 GW of installed power coming from PVDG (TAPIA, 2024).

According to the ANEEL Normative Resolution (NR) 482/2012, for Brazilian net metering the distributed generation can be defined in two groups: the micro-generation which corresponds to systems with up to 75 kW of installed power, while mini-generation comprises systems above 75 kW up to 3 GW for hydro sources, or up to 5 GW for other sources (ANEEL, 2012).

The distributed generation scenario in Brazil, is presenting an exponential growth mainly in the last decade, increasing from 14 systems in 2011, to more than six hundred thousand systems in 2021, and more than 2.5 million in 2023. This growth is also seen at the total installed power which increases from 178.22 kW in the end of 2011 to more than 25 GW in 2023. Both scenarios of DGs growing in Brazil are presented in FIGURE 4 and FIGURE 5.

Even with the pandemic of Covid-19 in 2020 and 2021, both years presented an increase on DG new connections in Brazil, presenting 212,891 and 398,495[1] new systems respectively (ANEEL, 2021b). The growth in 2021 happened following the trend of the previous years, being additionally driven by the increase in the electricity tariff, resulting from the application of higher rates due to the water crisis in the country, compromising hydroelectric generation and requiring an increase in thermoelectric generation.

Considering the different sources of micro and mini DG in Brazil it is possible to see that it corresponds mostly to Photovoltaic generation, specially in the last years, as presented at FIGURE 6. Also, it is possible to see that the amount of energy injected into the power grid is also growing due to the increase of generation systems, according to the EPE estimation presented at FIGURE 7.

[1] Up to December 31st, 2021.

FIGURE 4 - NUMBER OF DG SYSTEMS OF ALL SOURCES IN BRAZIL FROM 2013-2023.

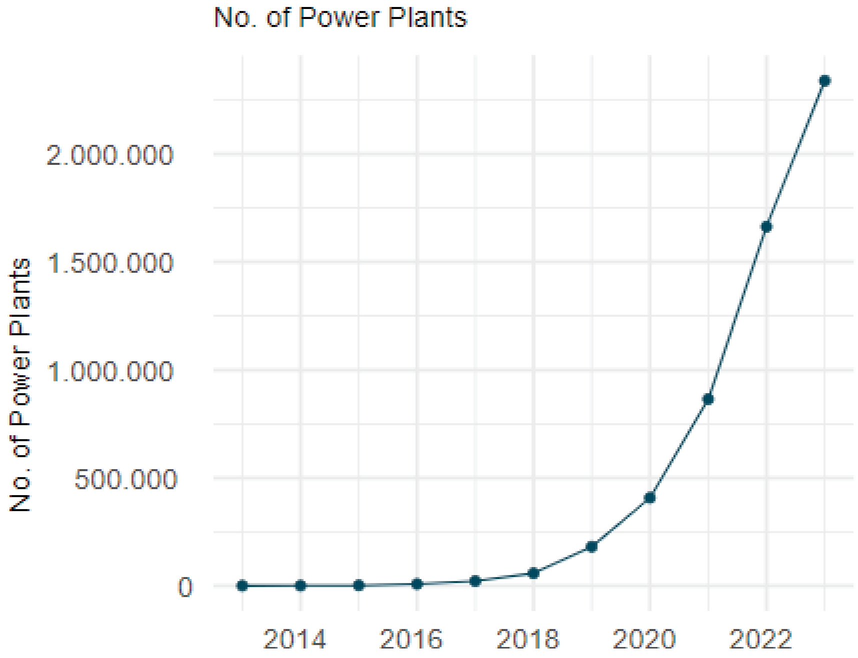

Source: EPE (2024).

FIGURE 5 – CUMULATIVE INSTALLED POWER OF DG SYSTEMS OF MULTIPLE SOURCES IN BRAZIL FROM 2013-2023.

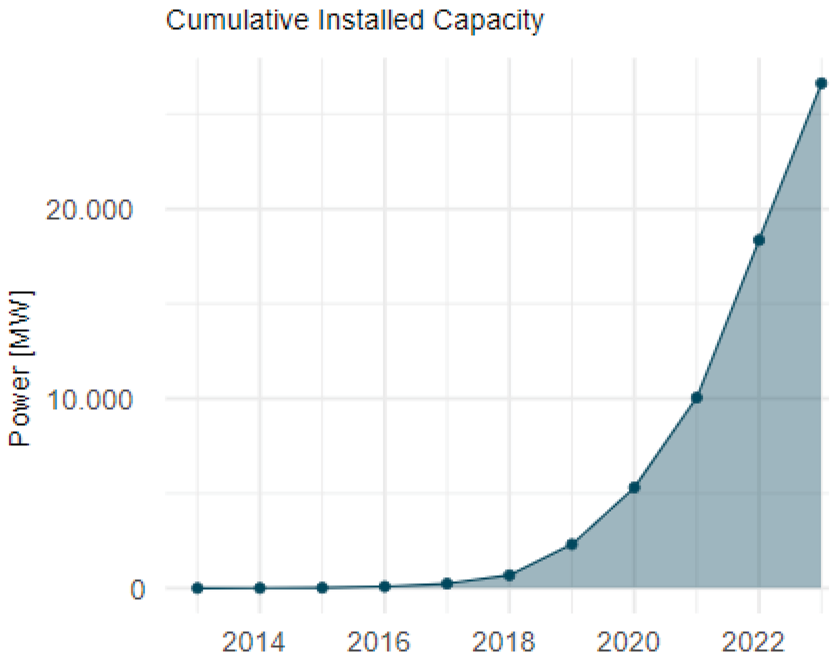

Source: EPE (2024).

FIGURE 6 - ANNUAL GENERATION ESTIMATE BY ENERGY SOURCE FOR MINI AND MICRO DISTRIBUTED GENERATION IN BRAZIL.

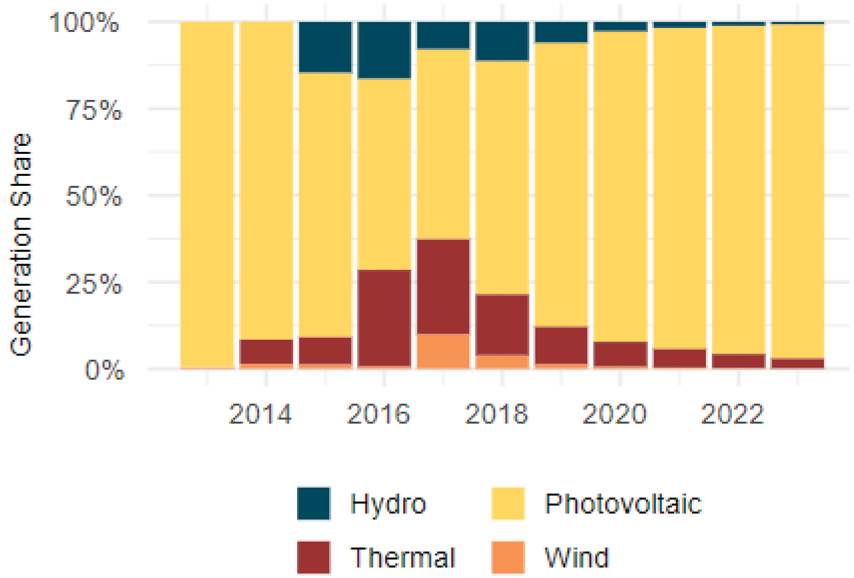

Source: EPE (2024).

FIGURE 7 – YEARLY ELECTRICITY GENERATION ESTIMATE FROM MINI AND MICRO DISTRIBUTED GENERATION IN BRAZIL.

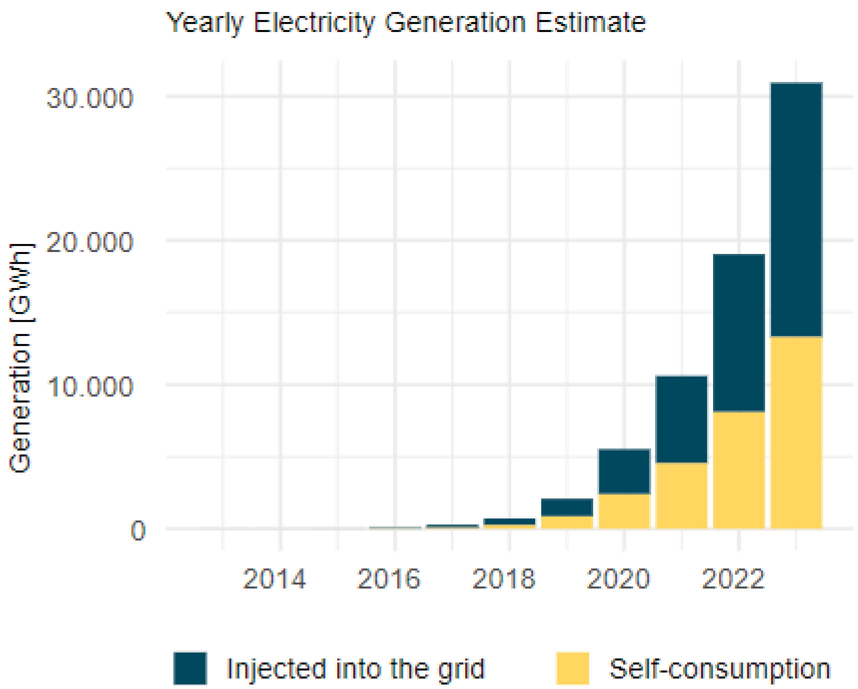

Source: EPE (2024).

Each country presents a specific regulatory framework and policies for DG connection. In terms of market, the most used strategy is the feed-in tariff (FIT), which consists in the payment for the active power injection into the distribution grid, being an incentive for people to install generation systems and be paid for their generation. There are also other market strategies, as the energy compensation system, in which credits are generated from the power injected into the grid that will be compensated in the future on the consumer's energy bill. This market strategy is the one implemented in Brazil, by the NR 482/2012.

All this growth of DG brings a lot of challenges for distribution power utilities operation, since the distribution grids were not prepared for the insertion of generation units and their effects as reverse power flow and overvoltage. In this way, distribution power utilities are searching for new equipment and solutions that can contribute to a safety and reliable operation.

One of the solutions that are being used are the energy storage systems (ESS), mainly battery energy storage systems (BESS), due to their easy implementation and sizing flexibility. The BESS placement in distribution system can provide several services for power grid such as voltage support, load following, peak-shaving, and black start. In these cases, the applications are usually in front of the meter (FTM). In small applications, usually placed close to consumers with DG, they are located behind the meter (BTM) and are used to reduce electricity bills, maximizing the benefits of the DG, as well as can realize demand-side management (IRENA, 2019a).

According to Sufyan et al. (2019) energy storage systems can bring different benefits to the power system operation, since it can be used for different applications such as: peak shaving, home energy management, load leveling, transmission and distribution update deferral, frequency regulation, voltage control, loss minimization, reliability improvement, demand response and reserve application. The application desired will define the system size in terms of power and energy, as well as its location.

In 2018, the largest yearly growth of energy storage happened in South Korea, corresponding to one-third of the total energy storage installed worldwide in that year. Regarding BTM applications, in 2018 Japan has become a global market leader reaching over 200 MW of energy storage BTM capacity, being this growth driven by the FIT implemented in the country for PV systems owners (IEA, 2019a).

According to IEA (2019), only in 2019, 2.9 GW of storage capacity were added to power electricity system worldwide. The largest amount corresponds to battery systems; however, there are still brand-new applications and technologies, which brings some concern and insecurity. In this way, the growth of batteries applications is heavily dependent on policy support.

In Brazil, for example, the utility scale application was encouraged by the ANEEL Strategic Research and Development (R&D) Call 21/2016, "Technical and Commercial Arrangements for the Insertion of Energy Storage Systems in the Brazilian Electric Sector", launched in 2016, aimed at proposing technical and commercial arrangements for the evaluation and insertion of energy storage systems in the Brazilian electric sector, being approved 23 different projects.

Different technologies of batteries are being tested. Nowadays, the largest number of new batteries power system applications are being done with lithium-ion (Li-ion) technologies. At FIGURE 8 is presented the increase of Li-ion share in annual battery energy storage, corresponding, since 2013, to more than 50% of the total. The graphic also presents the growth of stationary storage systems over the years in the trend line (IRENA, 2019a).

FIGURE 8 - INCREASING OF LITHIUN-ION IN ANNUAL BATTERY STORAGE CAPACITY ADDITIONS GLOBALLY.

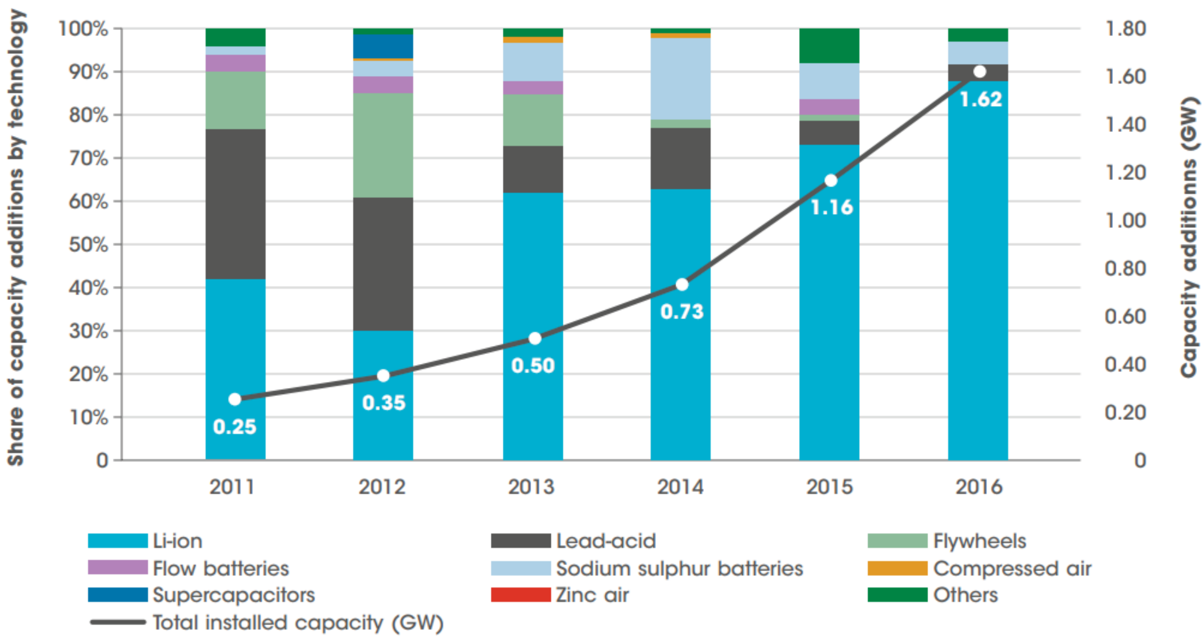

Source: IRENA (2019).

As forementioned, the growth of storage systems, especially batteries, is largely associated with the growth of DG and renewable energy penetration. According to IRENA (2019) it is possible to consider two different scenarios of growth up to 2030, which results are presented at FIGURE 9. The low and high scenarios consider the range of the forecast, considering 2017 as the reference scenario. For 2030 values there are two options for each scenario, being the reference considering the amount of DG and renewables existing in 2017, that the doubling scenario considers the double of DG and renewable systems. For all scenarios it is possible to notice that utility-scale systems will correspond to 44% of the BESS, whereas 56% corresponds to BTM applications distributed along the power systems.

FIGURE 9 – SCENARIOS OF STATIONARY BATTERY CAPACITY GROWTH UP TO 2030, WORLDWIDE.

Source: IRENA (2019).

With the predicted growth of storage systems in both FTM and BTM applications new businesses and services may emerge. One of the possibilities corresponds to the provision of ancillary services by both systems by the provisioning of active and/or reactive power according to power grid necessity, regarding the market and regulations. There is also the possibility of BESS operation BTM providing services for its owner, mainly related to energy back-up, demand flexibility and demand peak reduction, resulting in benefits mainly related to the reduction of the electric energy bill, been this kind of operation already seen in some applications in Brazil, as seen at MICROPOWER (2021).

Another possibility is the development of microgrids or energy communities, based on the existence of energy generation systems simultaneous to storage systems and management devices.

Microgrids can be defined as part of the power grid that can be disconnected from the main grid and operate autonomously. Thus, for a microgrid to be possible, it is necessary to have distributed energy resources such as distributed generation and storage systems that allow the load to be supplied in periods when it is disconnected from the main grid.

Microgrids have brought new paradigms, since several applications can be realized, e.g.: residential/commercial microgrids, with customers acting actively in the energy market; microgrids providing ancillary services to the distribution grid, acting together with the distributor, for example, for voltage support and load shifting; or the microgrids can be constituted to serve isolated localities, in places where there is no electrical grid.

In Brazil there are already several microgrids for isolated systems, as is the case of the island of Fernando de Noronha, served by diesel and solar photovoltaic generation systems, with the recent installation of a storage system with lithium batteries. In addition, there are microgrid applications to serve communities in remote locations such as the Islands of Lençóis and Ilha Grande, both in the state of Maranhão, as well as to serve the populations living in the Pantanal Sul-Matogrossense region.

For applications of microgrids connected to the distribution network, in September 2021, ANEEL approved the implementation of a pilot project for the Public Call of the Companhia Paranaense de Energia (Copel) for the acquisition of energy from distributed generation through the formation of a microgrid. The pilot project will last five years, since ANEEL's authorization is configured as a “regulatory sandbox” in which some rules can be relaxed and/or changed, with duration and conditions previously delimited so that the agents in the sector can carry out innovations (ANEEL, 2021c; COPEL, 2021).

1.2 JUSTIFICATION

Considering the increase of the new elements in power distribution grids, it is necessary to take actions aiming a better understand of the grid and their players.

From the consumer side, it is necessary to understand how to be more active in the distribution grid maximizing his own profits. For this, it is necessary to better understand his possibilities, which can consist in more than only provide active power to the system. The prosumer[2] will have more options as much the technology, policies, regulation and market allow. Besides the microgrid formation, the prosumer can provide ancillary services for distribution grids, as voltage support, peak shaving, load shifting, and black start, by the reactive dispatch of his generation/storage system or by the load flexibility that can be provided by this power system. In this way, the power system regulations need to allow the disconnection and the islanded operation, as well the reactive power injection.

From the Distribution System Operator (DSO) side the power grid transformation brings innovation and new challenges to be faced, since the power reliability and quality levels must be kept. In this way, it is necessary to better understand the grid operation with a high penetration of DG, storage systems, microgrids, as well electric vehicles, and flexible loads. This can impact on voltage levels, protection studies and the operation of switching equipment's as voltage regulators and capacitor banks. Moreover, investments in communication and control systems will be required, allowing to get accurate information from the grid to communicate with the DERs from the power utility as well with the prosumers allowed to provide services to the grid.

One of the new systems of the DSOs thinking in the future of power grids is the Advanced Distribution Management System (ADMS), which is connected to many other systems as SCADA (Supervisory Control and Data Acquisition) and the Distributed Energy Resources Management System (DERMS), increasing system management and optimization. Some functions of the ADMS are: automate outage isolation and restoration, volt-watt and volt-volt-ampere optimization, voltage control, peak demand management, operational support for microgrids, as many others (DOE, 2015). This is one more new technology that can contribute to the future of the distribution grids.

One of the strategies for DSOs to better understand grid behavior, is the usage of an optimum power flow approaches, which can consider the DERs models inclusion and optimize the entire grid operation. This approach will be considered in the present

[2] Prosumer: consumer that presents some kind of generation system.

thesis, in which the distribution grid will be modeled considering the previously existing equipment as capacitor banks and voltage regulator, and the addition of DERs equipment. Furthermore, ancillary services provisioning will be allowed to the main grid. The grid optimization will be done using a multiperiod optimum power flow overture solved using interior-points method.

In and EPRI research, Smith (2014) evaluate the mean concerns of USA DSOs considering the increase of DERs penetration, and what are considered the main solutions to avoid their impacts. According to the search the most cited mitigation measures are the voltage regulation devices placement; implementation of volt-var control in inverters or on grid equipment, as capacitor banks; installation of new equipment as D-FACTS (Distribution-Flexible AC Transmission System); and investments in control and communication technologies. These solutions will also be considered in the proposed formulation of this work.

Moreover, the integration of microgrids in the distribution grid will be considered in the multiperiod optimum power flow, first in an approach where the MG corresponds to a bus of the feeder where it is possible to absorb or provide power. Another approach can be considered, based on the microgrid connection with the main grid, where the internal optimization of the MG will propose a pre-dispatch, which should be informed to the DSO in order to update the behavior proposed by the MG, which will directly affect the feeder dispatch.

For this integration between both dispatches, a hierarchical model can be proposed, where the “master” dispatch will be realized by the entire grid optimization, and the “slave” corresponds to the internal dispatch realized in the MG, considering its own structure and resources available. This process will also be presented in this thesis and represents a better integration between the MG and the distribution feeder, where the main goal is to improve the power grid operation.

Besides the pre-dispatch for the power grid operation, considering the increase of the complexity on power grid operation, it is necessary to have as much information from the grid as possible, feeding the optimization systems which will support the system operator on the decisions to be taken. In this way, the development and implementation of monitoring and supervisory systems are growing, as aforementioned.

Another approach in this way is the development of digital-twins on the grid or part of it, where the digital-twin corresponds to a model from the grid which will be feeds with information from the real grid and will simulate the grid behavior with the same time response of the real grid. This allows the power system operator to better understand the dynamics of the system, as well as reproduce it when necessary, allowing to get a better understanding of the grid operation.

In this way, the digital-twin approach is also considered in this thesis, also reproducing the communication layer between the digital-twin and the SCADA from the power utility.

1.3 RESEARCH PROBLEM DEFINITION AND SCIENTIFIC QUESTION

The distribution systems are significantly changing in the last years, mainly due to the introduction of multiple DERs technologies. Based on this future scenario, the power grid and equipment modeled on this work consider the integration of multiple DERs simultaneously on the power grid, as well as that the power grid has technologies that allow the different scenarios proposed, like: the on-load tap changers transformers; the possibility of custom power devices [3]usage on distribution grids; four-quadrant inverters for photovoltaic and battery systems; the demand side management being carried out by mutual agreement between the power utility and the customer; the communication link between the power utility and a microgrid to receive and send information to the microgrid control in real-time.

This thesis contributes or some of the following questions: How will be the operation of distribution grids in a scenario with multiple distributed energy resources operating simultaneously and with more active consumers? Which are the ancillary services that can be interested in a distribution grid with multiple distributed energy resources? How to integrate a microgrid on the distribution grid dispatch, considering the grid and the microgrid optimization simultaneously? How to integrate the operation of a microgrid on the distribution grid, considering a real-time operation?

1.4 OBJECTIVES

The main objective of the current work is to propose different approaches for the distribution grid operation analysis, considering a scenario of an AND with DERs

[3] Custom power devices corresponds to Distribution-Flexible AC Transmission System (D-FACTS) devices used on distribution grids.

and microgrid integration, into a day-ahead planning and a rea-time operation scenario.

In addition to evaluate the impacts arising from the increased penetration of DERs, the provisioning of ancillary services and the insertion of new equipment technologies in distribution networks will also be considered.

To reach the main objective, some specific objectives are defined:

- Analyze the smart grid enabling technologies of distributed energy resources and management systems;
- Evaluate the main ancillary services that can be provided by the distributed energy resources and microgrids to the distribution grid;
- Proposition of new approaches of distributed energy resources and microgrids integration, by the development of optimization techniques with Optimum Power Flow (OPF) considering a day ahead approach;
- Integration of a hierarchical model between the microgrid and the distribution grid optimization, using the OPF approach;
- Real-Time microgrid operation based on a digital-twin model, evaluating the microgrid behavior under different scenarios and the communication between the microgrid and the main grid.

1.5 SCIENTIFIC CONTRIBUTION

The main expected scientific contribution is related to the proposition of techniques that allowed the operation and integration of different scenarios of active distribution networks, and the provision of ancillary services by the distributed energy resources and new grid equipment.

For the multi-period optimum power flow analysis, the contribution is also related to the entire grid modeling and the integration of DERs in the optimization considering a multi-objective approach. In addition, the reactive power dispatch proposed contributes as a new approach for this problem, as well as the custom power addition in distribution grids scenarios.

Regarding the hierarchical model proposed for the integration of multiple microgrids in the distribution grid, this approach considers the integration of the multi-period optimum power flow of the entire grid with the local optimization of the microgrid, both considering a day-ahead scenario. This integration between both optimizations also consists in a important scientific contribution of the current work.

Additionally, the real-time simulation approach brings another optic for the work, contributing to the development of digital-twin concepts applied to power systems.

1.6 DOCUMENT STRUCTURE

This document is organized as follow: Chapter 1 presents the context and the main objectives of the thesis; Chapter 2 describe the main concepts of active distribution networks, ancillary services, and microgrids; Chapter 3 presents the optimum power flow approach and its proposed formulation; Chapter 4 brings the multiperiod optimum power flow study cases; Chapter 5 define the hierarchical model methodology and brings its simulation results; Chapter 6 presents real-time and digital-twin concepts, its modeling and simulation results; Chapter 7 summarizes the main conclusions of this thesis and suggests future works to be developed.

2 ACTIVE DISTRIBUTION NETWORKS

2.1 CONCEPT

Distribution grids were designed to be the part of the power system which is responsible to deliver power to the end user consumers connected in medium or low voltage levels. However, over the years, they started to face some changes as the consumers started to produce electricity, being no longer a passive system.

The introduction of DG was only the first step in this transition from passive to active distribution networks. Additionally, other resources as energy storage, electric vehicles, microgrids and smart meters were being aggregated to the system increasing the planning and operation challenges for the distribution system operators.

In the Technical Brochure 457 – Development and Operation of Active Distribution Networks, from CIGRE (2011), there are multiple ways to define an Active Distribution Network (ADN). However, in general, it is possible to define an ADN as a grid that enables the DSO to interact with the consumers, managing the power flow, coordinating, and controlling the distributed energy resources integration and operation.

Some features related to ADN are presented at TABLE 1. One of the keys for ADNs is the management system, this being responsible for coordinating the system operation. Thus, this system requires plenty of measurements and data information that could support the decisions. For this reason, many investments are made in information and communication infrastructure. Additionally, new sensors and control systems are being installed in the grid, as well the replacement of old technologies for the ones that present communication and allowed interoperability, such as the substitution of electromechanical devices by electronic ones (VANDARI, 2020).

TABLE 1 - ACTIVE DISTRIBUTION NETWORK FEATURES

Functionalities	Specifications	Driver/Benefit
• DG, ESS, Demand Side Management • Fast and Autonomous Grid Reconfiguration • Ancillary Services • Power Flow Congestion Management • Improve Grid Flexibility • Data Collection and Management	• Integration Between Multiple Systems • Communication • Protection • Flexible Network Topology • Smart Metering Technologies	• Improve Reliability • Improve Grid Flexibility • Improve Asset Usage • Improve Access to DG and other DERs • Alternative to Grid Reinforcements • Improve Network Efficiency

Source: Adapted from CIGRE (2011) and D'Adamo et al. (2009).

Additionally, advanced management systems are being developed, to improve the ADN operation and contribute to keeping the grid operation in the optimum and safe status, both for DSO and for the prosumer/consumer. Some of these systems are listed in the sequency (AOKI et al., 2020):

- SCADA (Supervisory Control and Data Acquisition): monitors and controls network elements, however it is not specifically designed to optimize the use of Distributed Energy Resources. It is the monitoring and control system employed in most distribution utilities today.
- DMS (Distribution Management System): responsible for controlling and optimizing the assets of the utilities such as reclosers, circuit breakers, switches, transformers, capacitor banks and regulators.
- DRMS (Demand Response Management System): controls the load to meet the requirements of the network or the market.
- DERMS (Distribute Energy Resources Management System): is the system responsible for controlling and managing the existing DERs in the network, as well as being the system responsible for iteracting with these resources.
- ADMS (Active Distribution Management System): is the system that encompasses the entire distribution network and is responsible for integrating the other platforms. Among the functionalities of ADMS is possible to list: location and fault isolation, and restoration services; volt and volt-ampere

optimization; voltage control; peak demand management; as well support for DERs (VANDARI, 2020).

According to IRENA (2019b) the future of electrical grids requires a set of new technologies and approaches basically divided into four major dimensions: enabling technologies, business models, market design, and system operation. Some of the key elements are presented at FIGURE 10. It can be noted that about enabling technologies, not only those capable of acting in terms of power are needed, but also technologies associated with communication and control. In terms of business models, new approaches are emerging with aggregators, which are responsible for managing distributed energy resources in the grid, interfacing between prosumers and the DSO, as well as new market models focused mainly on the concept of energy as a service.

This same concept is maintained in the market design, mainly based on the decentralization of control and service provision. Finally, the operation of the system foresees greater synergy between the operation of transmission and distribution as well as the need for more advanced systems of supervision and control.

FIGURE 10 – INNOVATIONS FOR FUTURE POWER SYSTEMS.

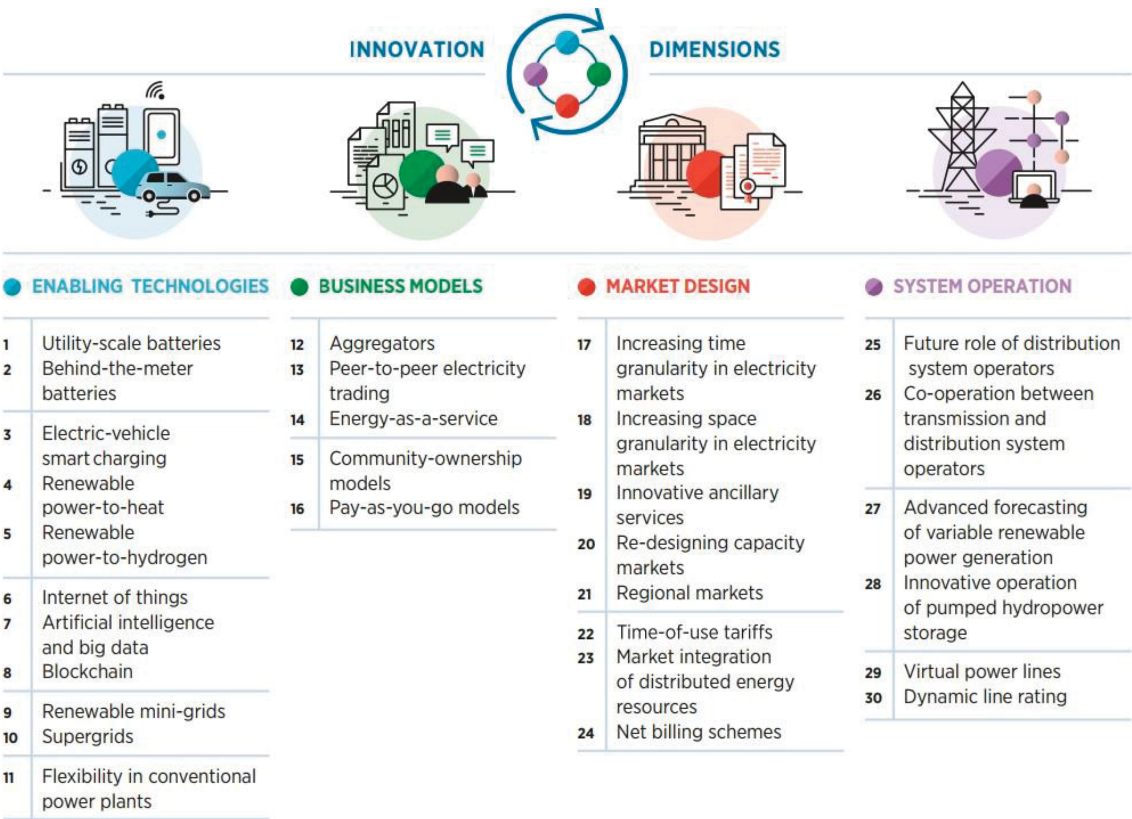

Source: IRENA (2019b).

2.2 DISTRIBUTED ENERGY RESOURCES

With the changes in the distribution network, it was necessary to define the concept of distributed energy resources (DER), encompassing not only distributed generation, but a series of equipment and resources that started to integrate the distribution system, changing its operation and planning.

According to the Brazilian Energy Research Office (EPE), DER can be defined as the electricity generation and/or storage technologies, usually connected behind-the-meter (in the consumer units), being located within the boundary of the power utility. Additionally, EPE considers that DERs contemplates: distributed generation; energy storage; electric vehicles and recharge infrastructure; energy efficiency; and, demand side management (EPE, 2018).

Following the same approach, the Australian Renewable Energy Agency defines DERs as the source of decentralized and community-generated energy, including renewable and non-renewable generation, energy storage, inverter base technologies, electric vehicles, and controllable loads, all of them associated with smart meters and data services (ARENA, 2018).

As reported in the EPE discussion note, DERs can pose several challenges for grid operation and planning, at the same time which they can provide some benefits, as reduce network costs and improve grid reliability (EPE, 2018). TABLE 2 shows a survey from different countries about the positive and negative points in the network seen by the utilities with the increasing insertion of DERs. It is seen that grid reliability improvement is a common positive impact, while network congestion is frequently seen as a negative impact in the power grid.

The updated scenario of DERs in the world and in Brazil have been previously shown, in the first chapter of this document. In the sequence, more details regarding grid integration and technologies will be presented.

Regarding distributed generation systems, the amount of system has increased significantly over the years, largely due to reduced equipment costs. Considering the photovoltaic generation (PV) connection on distribution grids, Smith (2014) prepared a technical report with the main concerns of 21 power utilities in United States related to PV Systems connection.

TABLE 2 – INTERNATIONAL EXPERIENCE WITH DER INCREASE AT DISTRIBUTION GRIDS.

COUNTRY / REGION	POSITIVE IMPACT ON THE GRID	NEGATIVE IMPACT ON THE GRID
Germany	• Reliability Improvement • Flexibility Improvement	• Network Congestions
United kingdom	• Reliability Improvement	• Not reported
United States (California)	• Reliability Improvement • Increased Resilience	• Unpredictability And Complexity for the Control System due to the Characteristic of the Load Curve
United States (New York)	• Increased Resilience • Reduction of Peak Demand	• Not reported
Australia	• Reliability Improvement • Increased Resilience	• Voltage Increase
Chile	• Not reported	• Need of Power Generation Curtailments
Italy	• Not reported	• Network Congestions • Grid Instability
Mexico	• Reliability Improvement • Reduction of Power Losses	• Not reported
Colombia	• Increased Resilience	• Not reported
India	• Reliability Improvement	• Network Congestions

Source: Adapted from Castro (2021).

The main concerns are related to voltage regulation, especially overvoltage; increase of voltage regulator demand of operation; increased capacitor switching; protection system coordination; unintentional islanding; inverter trips due to line transients; reactive power control; multiple inverter stability; variability due to clouds, especially for large system or high penetration; balancing resources and demand response; and reverse power flow, especially for large system or high penetration.

According to CIGRE (2011) other effects that can be caused by the increase of DG penetration on distribution networks are the increase of short circuit levels above designed values, needing new protection studies with eventual exchange of equipment, to ensure reliability and safety of the operation.

For inverter-based technologies, such as photovoltaic and battery storage systems, it is possible to realize four-quadrant operation, that is, dispatching and consuming active and reactive power to the grid by the power factor control. However, for this to be possible, in addition to the technology it is necessary that the regulation allows this type of action by the owner of the system, and that there is communication between the operation of the system and the DSO, as well as the need for a market that remunerates the dispatch of both active and reactive energy to the grid.

Regarding the battery energy storage systems (BESS), their application at distribution grid can be done in utility-scale (large system), or in small applications, which could be associated with distributed generation, in behind-the-meter systems. For the utility-owned systems, dispatch is done according to the needs of the grid and can contribute in different ways to the operation of the grid, such as peak shaving, peak-shifting, or voltage support. For systems connected to prosumers the dispatch is done to guarantee, most of the time, the best financial return, dispatching in periods of higher tariffs or even contributing to the interruptible of the energy supply. Other applications of storage systems can be observed when these are integrated with microgrids, as will be detailed further on.

Another DER consists of electric vehicles (EV) and charging structures. Electric vehicles are currently only considered as loads for the distribution system. In scenarios of fleet increase, thus, there will be an increase in electricity demand, and the grid must accommodate this new load.

In the work of Salah et al.(2015) the impact of the EV fleet increase in Switzerland for the coming years is analyzed. With a presence of 50% of the market with EVs, it would result in two overloaded substations. For higher penetration scenarios more substations are overloaded, resulting in impacts not only in the medium voltage, but already impacting the high voltage. Other works such as Dogan et al. (2015), Marmaras, Xydas and Cipcigan (2017) and Lillebo et al. (2019) present other impacts that the increase in electric vehicle fleet can cause on the distribution network such as increased feeder peak demand, overload on distribution transformers, congestion on lines, increased losses and voltage drop.

To mitigate the impacts of the increase in the EV fleet it is considered the association with distributed generation systems, such as carport structures, or intelligent charging systems such as the V1G (Vehicle-on-Grid) technology, which signals to the user the most interesting periods for charging, according to the DSO definitions, contributing to the distribution of charging in less critical periods for the feeder operation.

Other technologies are being tested and are envisioned for the future with the implementation of V2G (vehicle-to-grid), V2B (vehicle-to-build), or V2H (vehicle-to-home), in which it is possible to discharge the vehicle's battery while delivering power to the grid. In this case it is possible not only to minimize the impact of the vehicles on the grid, but also to use them for ancillary services, as in the case of stationary batteries.

Demand response, or demand-side management, can be considered a DER or an ancillary service, since it can be performed by intelligent loads that have a management and control system, responding to market characteristics defined by the DSO, increasing grid flexibility. More details on demand response will be presented in the section about ancillary services.

2.3 ANCILLARY SERVICES

Aiming to improve power system security and quality, DSOs are investing in a wide array of ancillary services. Ancillary service was a concept applied only at transmission levels, but with the transformation of the distribution grids, it started to be requested in this part of the power grids also (CIGRE, 2010). These services can improve frequency response, voltage levels, network loading, and system restart.

2.3.1 Voltage Support and Reactive Power Control

Voltage quality is one of the most important characteristics of a power grid. It is given for each network node and depends on the circuit impedance and the voltage drops on these impedances. Voltage instability is one of the main causes of power system blackouts (IORGULESCU; URSU, 2017).

Voltage variation on the distribution grid happens with changes in active power demand. When the demand is higher, there is more active power flowing through the system and the voltage decreases. When demand is lower, voltage tends to increase.

Voltage control aims to reduce voltage violations on the power grid. This control can be divided into three levels. Primary voltage control is local automatic control that autonomously controls voltage in each bus. It is commonly performed by automatic voltage regulators or static voltage generators. Secondary control is centralized automatic control that co-ordinates actions of local regulators and reactive power sources in defined voltage zones. Tertiary voltage control is the optimization of active power in the power system (IORGULESCU; URSU, 2017).

Distribution grids traditionally use equipment such as transformers with off-load tap changers in secondary substations, capacitor banks, and altering network topology in specific periods to manage voltage performance. Increasingly on-load tap changers (OLTC) in secondary substations transformers are being used to complement these methods, or even power electronic devices as D-FACTS (Distribution - Flexible AC Transmission System).

Additionally, any power electronic equipment that includes a four-quadrant way converter can provide this service as well by managing active and reactive power interaction with the main grid. Importantly many sorts of distributed generation like PV systems, BESS and EV charging stations are connected to the power grid using inverters and/or converters that allow this kind of operation. However, currently there are few market strategies to monetize reactive power from distributed generators. This reduces the incentive for DER to provide these services.

A high penetration of distributed PV may suggest a different use, displacing the charging periods to look for a high degree of coincidence with PV generation during the day. This helps to solve the overvoltage problems in grids with high penetration of PV, including preventing generation curtailment. In Germany, voltage regulation services are being implemented through control of power generated by PV facilities connected to the distribution grid (GOODENERGY, 2023).

Although there are countries like Denmark whose regulatory grid codes consider the provision of reactive power to the grids, the main problem is that voltage support through reactive power still has no market mechanisms (POLIMP, 2015).

Regulators should encourage new designs for charging equipment to be capable of providing reactive power. In this sense, services related to active power are easier to implement since the markets are more mature. Some countries are testing voltage support services in regulatory sandboxes, on the path to implementation. These sandboxes may create marketplaces and specific contracts with aggregators beyond regulatory rules. Services acquired by the DSO should always be backed up by a rigorous previous cost-benefit analysis of alternatives to the service, including conventional network reinforcement investments (KNEZOVIĆ; MARINELLI, 2016).

2.3.2 Demand Response

Demand response is an ancillary service that can be performed by the loads, to alleviate line congestion and equipment overload, as well as to avoid violations in power quality limits, such as over and undervoltage.

According to IEA (2021), demand response is the key to increasing grid capacity, and is one of the most relevant ancillary services. Also, according to the agency, several countries have invested in regulations and markets that allow the performance of demand response, integrating this service to the smart grid scenario.

Just like other ancillary services, demand response contributes to increasing the grid's operational flexibility, however, to be possible, besides the communication and control infrastructure, it is necessary that the regulation and the market are favorable to this type of service.

Australia, for example, has approved a wholesale demand response mechanism, opening the market to consumers and aggregators starting in October 2021 (IEA, 2021). The main goal is to attract large industrial customers and aggregators capable of reducing demand. Belgium, meanwhile, has adopted a capacity remuneration mechanism that allows demand response operators to participate on the demand side and aims to ensure security of supply, especially during the phase-out of nuclear capacity scheduled for 2025. In the United States, the Federal Energy Regulatory Commission have been required to remove barriers to participation for distributed energy resources of more than 100 kW, including demand response, renewables, EVs and energy efficiency, beginning in August 2021.

According to the International Renewable Energy Agency (IRENA, 2019b) the enabling technologies for demand-side management are internet of things (IOT), connecting the devices; behind-the-meter batteries, bringing electricity flexibility; EV smart charging; artificial intelligence for energy management, and big data.

Regarding market strategies, price signals are needed to increase the energy efficiency of the smart consumers as well as to provide flexibility according to DSO necessities. Time-of-use tariffs could be designed to incentivize consumers to shift loads during specific time intervals to support the system. Other possibility is the net billing mechanisms, in which the balance is determined not based on the number of kWh, but on the value of the kWh consumed or injected into the grid, being the invoice calculated by the difference between consumed and injected power. For the future other business models are being prospected bearing in mind the concept of energy as a service (IRENA, 2019b).

Considering the increase on grid flexibility provided by the demand-side management (DSM), several benefits can be reached, as illustrated at FIGURE 11. Peak Clipping (or Peak Shaving) corresponds to the reduction of peak load during peak hours. It is very useful for large consumers, as industries, and contributes to reduce the peak load of the power system. Valley Filling corresponds to an increase in the load demand in periods of lower load, by the connection of the loads outside of the load peak, instead of in high-peak hours. Load shifting consists in the shifting of the load from peak periods to off-peak periods. Strategic Conservation is not always considered a demand response but consists in reducing the energy demand by the usage of more energy efficiency appliances. Strategic Load Growth corresponds to the valley filling with the increase of the total load, it can be useful to avoid overvoltage in the power grid. Finally, Flexible Load Shape consists in grid flexibility to increase and reduce the power load by providing incentive to consumers aiming to reach the reliability constraints (AIN; IQBAL; JAVAID, 2019).

FIGURE 11 - BENEFITS PROVIDED BY DEMAND RESPONSE TO POWER SYSTEM OPERATION.

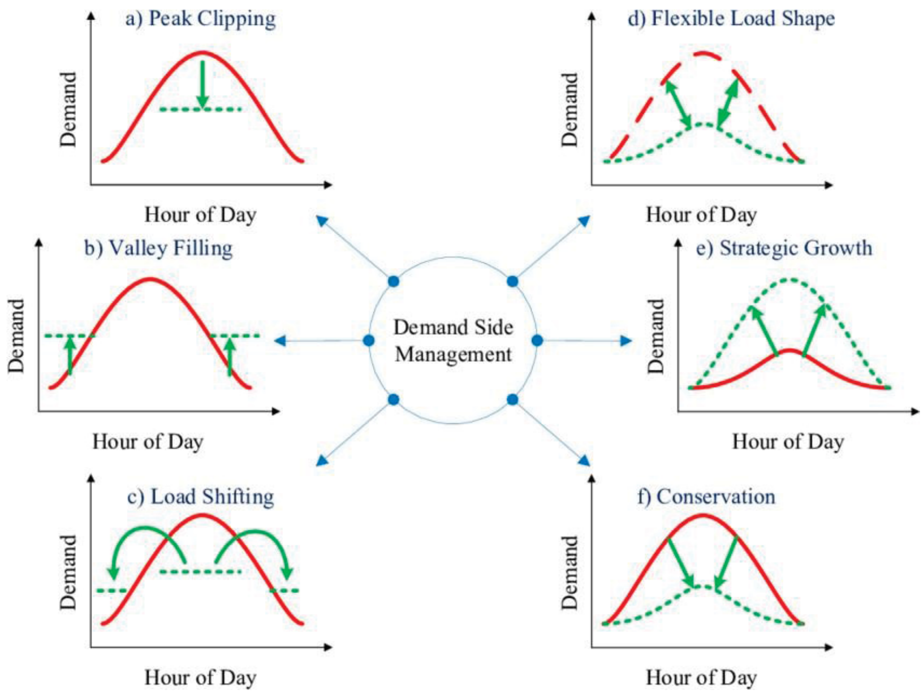

Source: Ain, Iqbal, and Javaid (2019).

Increasingly, in regions with high levels of distributed generation, there is a demand for services to integrate this generation. This may include voltage management or demand increase. For example, South Australian Power Networks have recently launched new pricing products that aim to absorb excess generation from rooftop PV (SOUTH AUSTRALIAN POWER NETWORKS, 2020).

Demand response services are usually required at times of peak power flow on the network. This can be in response to peak demand or generation. On the demand side, this would usually be on hot summer or cold winter days, depending on the region. These services are usually required in the morning or afternoon and would be serviced by reducing demand or increasing generation. On the generation side this would usually be at times of low demand and high generation (for example, mild, sunny spring/autumn days for PV).

2.3.3 Contingency and Emergency Frequency Response

Frequency control is required when the load or generation varies in a power system. This imbalance between generation and demand results in a frequency deviation. If the demand is higher than the generation, the frequency will decrease, and in the opposite, when demand is lower than a generation, the frequency will increase.

Contingency frequency response is primarily about managing the power system after loss of generation or load. These are managed economically and technically in a power system with two key services: inertia services that act to slow the rate of change of frequency; and contingency services that manage faults or day-to-day load variation.

The rise of asynchronous generators such as wind (with power electronic converters, like double fed asynchronous units) and solar (with only power electronic converters) has increased the challenge in managing frequency. Increasingly these services are provided by power electronic devices, using two key types of control: controls based on the absolute frequency and provide contingency services, and controls based on the rate of change of frequency and provide inertia type services.

Frequency control is a very interesting application for DSOs as it contributes significantly to system operation, reducing costs and increasing system reliability (AEMO, 2021).

Ortega and Milano (2018) present a primary frequency control for DSO being developed by DERs as wind generators, photovoltaic systems, and energy storage. As the DERs considered are non-synchronous the frequency control can be estimated based on voltage/current phasors at the point of connection with power grid, using a phase-locked loop (PLL) device. For the control strategy, the authors proposed a decentralized control, with a PLL for each DER; and a centralized control in which a common PLL is installed in the frequency monitoring point and communicates with the DERs. From the results centralized control presents an overall best result, however with communication delays, which do not occur on decentralized control, being more prone to be deteriorated in case of measurement losses.

2.3.4 Grid Resiliency and Black Start

Grid resilience describes the ability of the energy system to manage major disturbances like faults or natural disasters. As the grid decarbonizes and the impacts of climate change increase, resilience will become a more important issue. A resilient system recognizes that outages can occur, prepares to deal with them, minimizes their impact, and can restore service promptly.

A resilient grid can take in collapses to prevent interruptions, manage disturbances as they happen, and respond to normal operations quickly. To be resilient, the grid must have the ability to (1) anticipate, (2) absorb, (3) adapt to, and (4) quickly recover from disrupting events (ELECTRICITY ADVISORY COMMITTEE - DOE, 2018). The U.S. Federal Energy Regulatory Commission (FERC) defines grid resilience as the capacity of the bulk power system to resist or overcome disruptive incidents (FERC, 2018).

Grid resilience can be tested by natural disasters such as hurricanes, wildfires, earthquakes, thunderstorms, and flooding. Similarly manmade problems as cyberattacks may cause similar power system impacts. Resilience includes responses to non-traditional hazards, large-scale catastrophic events, cascading failures, and extensive outages.

Outages are not only disruptive but are also expensive to repair damage and restore power. To avoid this situation, DSOs had traditionally invested in redundancy, preventive measures, infrastructure reinforcements, and restoration measures

(NATIONAL ASSOCIATION OF REGULATORY UTILITY COMMISSIONERS - NARUC, 2020).

Distributed energy resources can contribute to improving grid resilience. To provide these services the capacity must be dispatchable, or able to respond at any time; islanded, or able to operate without grid connection in outages; be located at critical points of the grid; quick ramping; and able to provide other grid services like voltage and frequency support. Decentralization provides this capacity closer to points of need.

For emergency backup, islanding and black start services, stationary batteries and EVs with V2G capability can contribute providing power reserve to the individual customer or community grid.

In 2011, Nissan make available 66 electric cars model Nissan LEAF to help to provide power for heating and other purposes to hospitals and evacuation centers after an earthquake and a tsunami on the northeastern coast of Japan. Nowadays, the Nissan Leaf version with a 62 kWh battery can provide enough power for an average Japanese house for four days. This is especially relevant for countries with a high incidence of natural disasters, like bushfires.

In 2019, Nissan Leafs were again used in a similar way when typhoon Faxai caused many outages in the Chiba province in Japan. This typhoon resulted in over 340,000 households with no electricity. In the aftermath of this typhoon Nissan LEAFs provided power to community centers (NISSAN MOTOR CORPOTARION, 2019).

Power grid restoration after a total system collapse is called Black Start. Nowadays there are multiple ways to do it, considering the classical techniques and the traditional equipment. However, in the new energy scenario, it is possible to consider the Black Start provisioning by batteries and EVs, considering the V2G application.

2.3.5 Islanded Operation

A grid capable of islanded operation is one that can run without a connection to the main grid, either for a period or permanently. These microgrids include local generation and storage systems and ways of connection and disconnection from the main grid, as forementioned.

When connected to the main grid, microgrids can provide voltage and frequency control, congestion management, reduction of power losses, and power quality improvements, all of them by injecting/absorbing active and/or reactive power. Similarly, microgrids can also provide reserves to the power system such as frequency responsive spinning reserves, supplemental reserves, and backup supply in the open market, thus contributing to the real-time energy balance (IEA, 2019b).

When disconnected from the distribution grid, microgrids need to manage the internal operation of the system, optimizing the generation and demand, while simultaneously managing voltage and frequency levels. In cases of widespread energy outages, microgrids can sell power for grid black start and can reduce costs associated with system interruption, since consumers belonging to the microgrid continue to receive power when disconnected from the grid.

2.3.6 Grid Flexibility

Grid flexibility, according to IEA (2019b), can be defined as "the ability of a power system to reliably and cost-effectively manage the variability and uncertainty of demand and supply across all relevant timescales, from ensuring instantaneous stability of power system to supporting long-term security of supply". Increasing flexibility is connected to more reliability, resiliency, and more affordable energy.

Conventional power plants are the traditional source of flexibility services. Some strategies can increase the amount of flexibly conventional power plants can provide. These strategies can be divided into two groups: changes to operational practices for existing plants (improvements in data collection and real-time monitoring can improve latent flexibility from these plants), or flexibility retrofit investments for existing plants (retrofit options that can increase plant flexibility provisioning).

Variable renewable energy and energy storage systems can provide cost-competitive grid flexibility services. Several countries such as Australia, Ireland, Spain, and United States have already implemented market changes and regulations that make it easier for solar and wind generation to provide and be remunerated for flexibility services.

Electric vehicles can contribute to improving grid flexibility because their load can be managed based on the operation of the entire energy system. Additionally, EVs equipped with V2G capability can use their batteries to provide power to the grid.

Fully capturing the benefits of the additional system flexibility created by distributed energy resources and ensuring compatible system integration requires new actors such as aggregators. These new actors should be given room to innovate. These aggregators can pool the transferable load of all flexible consumers and/or establish real-time pricing for the end customers themselves. It will be critical for there to be real-time price-based communication between consumers, suppliers or aggregators, and grid operators (IEA, 2019b).

In the United Kingdon, in 2021 it was published a flexibility services tender round to be provided by DERs. The main objectives were:

- increase generation or decrease demand to reduce peak loads on high-voltage/medium-voltage substations (minimum of 10 kW – aggregated, payment for availability and utilization as a bid, real-time dispatch);
- increase generation or decrease demand to reduce peak loads on low voltage substations (minimum of 10 kW – aggregated, payment as a fixed pond/MW service fee, schedule dispatch);
- increase generation or decrease demand to meet a variety of network needs, for example, supplement secure and manage outages (payment for utilization at a price set by the flexibility provider, real-time dispatch).

UK Power Networks also defines the specifications for capability, connection of systems to the network, communications and metering systems, as well as details of the bidding for the provision of services (UK POWER NETWORKS, 2020).

2.4 MICROGRIDS

According to Brazilian Electricity Regulatory Agency (Aneel) microgrids correspond to "an electric power distribution network that can operate isolated from the distribution system, served directly by a distributed generation unit” (ANEEL, 2015). This definition is very similar to the one adopted by the U.S. Department of Energy (DOE): “a microgrid is a local energy grid with control capability, which means it can disconnect from the traditional grid and operate autonomously” (DOE, 2014).

Microgrids can be grid-connected or isolated systems. In the first case these can connect to the main grid operating in the load or generation condition. In the second application, the microgrids have no connection with the main grid, and should operate autonomously.

To be able to operate independently from the grid, the microgrid needs to present distributed energy resources such as generation and storage systems, allowing to supply the power demand, as well as controllable loads. According to CIGRE (2015) the main microgrid elements are: generation, energy conversion, and load control; energy storage that allow manage the intermittency and renewable energy generation, as well as tariff arbitrage and contribute to islanded operation; control and supervisory systems, to realize energy balance and implement different operational modes; protection and automation, to ensure safe and autonomous operation; and communication and remote monitoring systems, to enable collaborative effort of internal and external control.

The operation of microgrids in distribution grids can provide benefits as improvement of energy efficiency, minimization of overall energy consumption, reduced environmental impact, improvement of grid reliability, loss reduction, congestion relief, voltage control, and more cost-efficient electricity infrastructure replacement. Additionally, microgrids can be ancillary services providers, realizing voltage and frequency support, demand response, black start, and peak load support (CIGRE, 2015b; PARHIZI et al., 2015).

One of the main benefits of the microgrid for grid operation is the increased reliability, under normal operating conditions, but especially during outages, when part of the grid can be disconnected and is served by the available DERs. This benefit can be seen economically for the DSO by reducing violations of the reliability index limits and reducing the costs of unsupplied energy. Moreover, the increased resilience of the grid brings benefits to consumers, since in case of natural disasters, or even cyber-attacks, part of the network can continue operating and meeting the demand (PARHIZI et al., 2015).

The forms of operation of microgrids can be (i) with independent microgrids (IMG), in which each microgrid has autonomy and the groups have no common goal; (ii) with multiple microgrids (MMG), where the set of MMGs has at least one common and collaborative goal; or (iii) with unified microgrids (UMG), where the group of microgrids is operated as if it were a monolithic system with a single goal.

Regarding microgrid control schemes these should meet some basic requirements as: allow the operation of a microgrid in both connected and isolated modes; provide a smooth transition (no load shedding) between the two modes of operation; provide voltage and frequency amplitude within a desired range of values;

ensure voltage and frequency stability; control the power flow between the microgrid and the main grid; perform scheduled and unscheduled intentional islanding; manage controllable loads; and, manage loading and unloading of energy storage systems.

2.5 FINAL CONSIDERATIONS

This chapter presented the main transformations that are being carried out in distribution networks, where they are increasingly becoming active networks.

The growth in DERs penetration brings challenges and opportunities to the electricity system, the first arising from the unpredictability of its operation and the maturation of the technology, while opportunities for development and new markets are also emerging.

Thus, it is possible to use grid operation optimization tools to shed light on the main operation challenges to be faced, as well as to show possibilities of joint operation that result in benefits to the grid, as is the case of ancillary services.

In this way, the present work proposes the modeling of active distribution grids, considering the insertion of different distributed energy resources, such as distributed generation, storage, and demand-side management, to explore the main impacts caused by the operation of these elements in the grid.

Furthermore, microgrids and ancillary services provisioning will also be considered to explore how the optimized dispatch of active and reactive power by the equipment can contribute to the insertion of these new technologies without causing problems for the grid operation.

This approach corresponds to a problem that can be solved using the optimal power flow, where the operational limits of the grid and the equipment are described in constraints to the optimization problem and the objective function portrays the grid characteristic that is desired to be optimized.

For this it is necessary to model distributed generation systems, considering, for example, four-quadrant inverters to allow reactive dispatch, modeling storage systems with batteries taking into account the power and energy capacity available in the system to achieve the best support to the grid and the proper performance of the desired ancillary service, as well as modeling loads and equipment on the network in order to verify their operation in an active network scenario.

Moreover, different approaches can be used to evaluate the new complexity of distribution grids dispatch and operation, considering the microgrids and DERs. For the MG integration with the main grid, and hierarchical model can be considered in order to propose a better integration between the optimization problems, considering the optimum dispatch from the MG and from the entire grid, by the feeding back process in those two levels.

Additionally, the approach of a digital-twin can provide knowledge about the MG operation in real-time, corresponding to a different, but complementary approach.

With these changes in the grid, as much knowledge the system operator has about the grid, better taking decision support it will have to perform a stronger grid operation.

3 MULTIPERIOD OPTIMUM POWER FLOW FOR ACTIVE DISTRIBUTION NETWORKS

The classical objective of an OPF determines an optimal operational point for a given instant of time, aiming to establish, among other interests, the power injection in all system buses. In the proposed case, a multiperiod scenario is proposed, where the interdependency between the periods is considered for the optimization.

The formulation proposed for the present work was based on Borges, Fernandes and Almeida (2011) that minimizes the system power losses and costs in a hydrothermal pre-dispatch problem, implementing an MPOPF solved using Interior Points Method with a Primal-Dual Version.

Works developed by Blasi (2020) follow the same approach considering it for a distribution system with the insertion of distributed energy resources as distributed generation, batteries, and electric vehicles. In this work, this approach is extended, in addition of voltage regulation planning via reactive power dispatch of ADNs, and demand side response of controllable loads and microgrids.

3.1 OPTIMUM POWER FLOW LITERATURE REVIEW

Different techniques can be used to proposed optimizations to power system, being one of them the Optimum Power Flow (OPF), which consists of determining the operating state of the power grid, optimizing a given objective, considering the technical and physical constraints.

The objective function describes what is desired to be optimized, such as: minimization of losses, minimization of generation costs, minimization of load shedding, among others. The constraints determine the operational limits of the grid and are expressed through equality or inequality constraints.

When multiple numbers of periods with dependency between them are simultaneously analyzed inside a time horizon, a multiperiod approach of the OPF can be used.

The sizing of the objective function is related to the sizing of criteria and the complexity of the problem is related to the objectives that are modeled. On the other hand, the constraints are also dependent on the complexity of the variable modeling as well the sizing of the system. In a multiperiod approach, both structures are dependent on the number of periods.

As an optimization problem, the OPF can be solved by different strategies, from conventional methods, like linear and nonlinear programming, quadratic programming, Newton's method, and interior points, or even be done using artificial intelligence techniques as particle swarm, human or physics-inspired techniques, evolutionary optimization or neural networks (EBEED; KAMEL; JURADO, 2018).

Ongoing to improve DERs integration on the distribution grid, new OPF approaches have been proposed, considering different targets to be optimized and different scenarios to be analyzed.

Aiming to improve active and reactive power dispatch, the work proposes by Gabash and Li (2016) has separated the optimization problem into two sub-problems: one for active and another for reactive power. Using this approach, the authors proposed an optimum power flow to minimize power losses and improve voltage levels, considering a battery energy storage operation.

The work developed by Riffoneau et al. (2011) proposes a Multiperiod Optimum Power Flow (MPOPF) to reduce the energy costs and the aging of a battery energy storage system (BESS) considering three different time horizons: a forecast stage, a predictive optimization stage, and a local control stage.

Works developed by Gayme and Topcu (2012); Jayasekara, Masoum and Wolfs (2016); Reihani et al. (2016); Wang et al. (2017); and Zhang and Li (2013) consider the development of optimum power flow for grid optimization with the insertion of distributed energy resources, as distributed generation, in addition to optimize the dispatch of BESS placed on the system.

In Gayme and Topcu (2012) the optimization is solved by extended semi-defined program relaxations, being an equivalent process to Lagrangean dual. Wang et al. (2017) solves a MPOPF using the GAMS software (optimization solver programming language using algebraic notation). Jayasekara, Masoum and Wolfs (2016) represents the battery and power grid constraints along the simulation periods using a Fourier coefficient vector, being aggregated to the rest of the nonlinear optimization problem solved using the interior points method. The work proposed by Zhang and Li (2013) considers multiple generators and batteries on the distribution grid solving the optimization problem using an expanded Lagrangean approach with KKT (Karush-Kuhn-Tucker optimization base conditions). At least, Reihani et al. (2016) solves the optimization problem of its OPF using dynamic programming techniques, resulting in the optimum scenario of grid and battery dispatch.

Aiming to compare the performance of the OPF for one or multiple periods, Nguyen et al (2015) modeled a distribution system considering the integration of battery energy storage systems and wind generation on a distribution system with 14 buses and another model with 57 buses, considering both approaches. The authors defined the objective function to minimize the generation costs, as well as the operational costs of the battery system. Implementing both methodologies on Matlab, the mono period approach executes the calculation of each period independently, while the multiperiod considers the interdependency of the periods. Analyzing the results, the multiperiod approach presents lower costs results then the mono period, as well as the battery behavior is more accurate on this approach, charging and discharging according to the wind generation.

On the work proposed by Bukhsh, Zhang and Pinson (2016) the MPOPF model considering the integration of renewable sources, as well as the demand response. For the renewable integration, the authors used the stochastic programming approach. Additionally, the problem was separated on two steps, being the first one for the operational behavior of the conventional generation plants, and the second step is used to define the renewable energy integration into the system, considering the power load flexibility.

The work developed by Usman and Capitanescu (2021) proposes a nonlinear MPOPF for a smart grid with DERs considering the provisioning of ancillary services, regarding grid voltages and congestions issues. To solve the OPF, it was used a mixed-integer nonlinear model (MINLP) via Julia programming language. It was added the stochasticity of the wind/solar generation using an auto-regressive integrated moving average. In this paper the authors modeled a 34-bus test feeder, including the optimization of the on-line tap change (OLTC) transformer at the substation bus, two flexible loads, three energy storage systems and eight distributed generation with solar and wind. For the objective function authors aimed to minimize the costs related to active power curtailed of distributed generation (DG), energy storage usage, power demand flexibility and costs of OLTC operation. In this case the reactive dispatch is proposed only for the DG units using a power factor control strategy. From the results, it was verified that the location of the energy storage, in addition to the operation of the DGs, can contribute to minimize the load curtailment under different conditions.

In Yi et al. (2019), the authors consider the real case of a smart grid in the European inteGRIDy project, which is modeled as a microgrid for the study that aims to evaluate the impacts of DGs and the benefits from energy storage systems (ESS). The approach of the article is to develop an OPF to control the ESS itself and after integrated to an OLTC, considering a distribution grid with distributed generation systems and demand-side management. In this case, it is aimed to minimize the operational costs from generators and from ESS, as well as maximize the DG contribution. For the OPF it is considered the power constraints related to active and reactive power dispatch, being controllable by the apparent power limits. Considering different configurations, it is seen voltage levels improvement and reduction of tap changes as much reactive dispatch is considered. Additionally, the ESS contributes to the power flow management, allowing the maximization of DG power provisioning.

Besides the provisioning of ancillary services can be made by the reactive power dispatch, that could be performed by equipment with inverters and conventional equipment as capacitor banks. However, there is another possibility that can dispatch reactive power into the grid, that is the power electronic devices named FACTS (Flexible AC Transmission Systems).

On the OPF approach, some works included the usage of FACTS, however, most of them consider the transmission systems, as done in Abdel-Moamen and Paphy (2003), and Basu (2008). Recently, various manufacturers started to developed FACTS applicable to distribution systems, named D-FACTS (Distribution - Flexible AC Transmission System) since more and more the voltage control is becoming a challenge due to the transformations that are happening in this grid level. The work developed by Liu et al. (2016) proposes an OPF with the allocation of Series Static Voltage Restores (SSVR) in distribution grids with photovoltaic systems. The SSVR is modeled to allow the adjustment of line series reactance or inject/absorb power from the distribution grid, contributing to voltage levels improvement. The OPF proposed was solved using IPOPT (Interior Point Optimizer) open-source software.

Regarding the usage of D-FACTS in Active Distribution Networks, Freitas, Portelinha and Tortelli (2019) presents the main advantages of D-FACTS usage at distribution networks, focusing on the D-SVC (Distributed Static Var Compensator). This equipment is based on conventional thyristors, able to generate or absorb reactive power by the exchange of capacitive or inductive current. This behavior can be modeled as an adjustable reactance for steady-state analysis, being controllable according to power grid needs. The authors propose the entire formulation for D-SVC modeling at distribution system power flow, being implemented at Matlab and tested for a 69-bus distribution feeder. From the results, it is noticed the effectiveness of the D-SVC usage for voltage control, even when DG is considered.

The authors Abdi, Beigvand and La Scala (2016) presented a review of optimal power flow applied to studies in smart grids and microgrids. In this paper, the authors present the definition of the OPF, as well as the main variables and constraints defined for this network optimization approach. The paper also presents the mathematical formulation of some of these variables considering different approaches to the OPF, such as distributed OPF, three-phase, with linearization and approximation, among others, besides approaches considering the uncertainties of the generation sources. However, the article does not present formulations related to the multiperiod OPF, as well as does not present more detail regarding the modeling of the elements that compose the smart grid and the microgrids, such as distributed generation and storage systems.

Considering the application of the OPF in conjunction with microgrids, the authors Levron, Guerrero, and Beck (2013) developed an FPO, considering photovoltaic and wind generation, as well as the battery energy storage system connections in a microgrid. The main objective of the formulation developed was to minimize the price of energy imported from the main grid, represented as an equivalent, and to optimize the voltage profile. For this, the authors proposed an FPO that integrated storage devices, presenting the global optimization for the grid and time domain. The problem was solved using the multiperiod approach and a recursive process is performed to determine the parameters of the operating network.

The work by Dall'Anese, Zhu, and Giannakis (2013) uses FPO applied to an unbalanced microgrid with the goal of optimizing the operation of the microgrid in order to minimize losses, the energy exchange of the microgrid with the grid, and the maintenance of voltage levels. The solution of the FPO in this work was performed by means of semidefinite polynomial relaxation, in view of the unbalance found in the problem.

Based on the works found in the literature, it is possible to verify the use of the optimal power flow method for different situations, considering, for example, distributed generation systems, storage and microgrids. In this approach different objectives are defined for optimization, frequently being: minimization of costs and losses.

Furthermore, different techniques for optimization of the proposed formulations have been employed, from classical methods to those with artificial intelligence, developed in different programming languages, using or not, solvers for numerical calculation.

Regarding the analyzed circuits, the authors usually employ a network equivalent connected to the part of the circuit where they want to evaluate the insertion of DERs. Applications considering multiple DERs simultaneously usually correspond to simulations of microgrids, where the optimal dispatch of the elements internal to the microgrid is performed, consisting on a problem with a small number of nodes.

The present work proposes a Multiperiod Optimum Power Flow (MPOPF) to optimize the day-ahead planning of an ADN, which presents distributed generation, energy storage, flexible loads, and microgrids. These elements are modeled to allow the optimization of their active and/or reactive power dispatch. Additionally, the distribution grid is completely modeled, considering voltage regulators, capacitor banks, and D-FACTS, which operations are also optimized by the MPOPF proposed.

The non-linear optimization problem is modeled by the definition of a multi-objective function, that aims to minimize power losses, costs and simultaneously maximize load supply for flexible loads and microgrids. In addition, operational constraints are defined by equalities and inequalities expressions representing the operative limits of the grid and the considered equipment. The MPOPF is solved by the Interior-Points Method in a Primal-Dual version (BORGES; FERNANDES; ALMEIDA, 2011; CARVALHO, 2006; GRANVILLE; MELLO; MELLO, 1996; PAIVA, 2006). The first implementation was done in Matlab, being further developed a new version in Python language, which is currently being updated and improved. Both versions consider a completed formulation, without any solver usage.

3.2 BASIC CONCEPTS OF THE PROPOSED MULTIPERIOD OPTIMUM POWER FLOW

With the connection of the newly described equipment, ancillary services are becoming more necessary, which can be provided in different ways and by different actors.

Among ancillary services, there are voltage support, demand response, emergency frequency response, grid resiliency and flexibility, and many others.

Regarding voltage support, one of the strategies is reactive power control, which can be performed by equipment with four-quadrant inverters, or even power electronic devices as D-FACTS.

In the case of PVs with four-quadrant inverters, there is the possibility to operate providing/absorbing reactive power independently of the solar generation. However, it is important to highlight that nowadays, most parts of electricity markets do not remunerate this reactive injection, being not attractive to the system owner.

Battery systems are also connected to distribution grids by inverters, that could operate in four-quadrant mode, and can realize some ancillary services to the power grid also. In this case, as the system can control the active and reactive power injection/absorb, it is possible to realize the voltage support (by active and reactive power control), load-leveling (relieving peak load periods of the feeder and increasing load in periods of lower demand) and load peak shaving (reducing the peak demand of distribution feeder). Since BESS can be owned by power utilities, its operation can be defined to supply the biggest issues of the power grid.

The use of FACTS in distribution grids is brand new and is becoming more attractive as grids become more complex and have more DERs connected. According to some manufacturers, the main benefits of D-FACTS usage consist of fast voltage regulation, damping of active power oscillations, and increase of power flow through AC lines.

There are many equipment technologies, however for the present work a D-SVC was chosen, due to the compatibility of voltage level, sizing, and because of the possibility to inject or absorb reactive power from the grid, controlling bus voltage, and providing voltage support. According to Afzal et al. (2018) several studies have been carried out considering the insertion of D-SVCs in feeders that present distributed generation. In addition, some articles reviewed in Afzal et al. (2018) show that the allocation of D-SVCs contributed to the improvement of voltage levels and reduction of power losses.

Another ancillary service is the Demand Side Management (DSM), which consists of the managing of flexible loads, according to grid necessities, cutting these loads suppling in some periods, or shifting this demand for periods, in which the system has a low load. This kind of ancillary service requires specific load contracts as well the communication between load and Distribution System Operator (DSO).

When microgrids are connected to the grid, they operate as a flexible load, however with the possibility to provide power to the main system. In this way, it is possible to perform a DSM with microgrids proposed behavior, which arise from the internal optimization and control, and that should be informed to the DSO. With this information, DSO can evaluate the entire grid operation and, if some power quality problems are faced, a DSM can propose a new scheduled behavior for the microgrid, that will re-optimize its operation, considering the DSO recommendations.

The microgrid behavior can also provide some ancillary services to the power grid, as voltage support, peak shaving, and load leveling, depending on its periods operating as loads or generators.

In this work, all elements described in this section as ancillary service providers will be modeled on a Multiperiod Optimum Power Flow, used to plan a day ahead operation of a distribution feeder.

So, the present work proposes an MPOPF for ADN in a day-ahead, considering distributed generation, energy storage, flexible loads and microgrid, in addition to the complete grid model, which includes voltage regulator, capacitor banks, and D-FACTS.

The main contributions of this optimization problem are the modeling of an active distribution network, with multiple elements and actions being considered simultaneously: (i) active and reactive power dispatch from DERs (from PVs and BESS) via apparent power limits; D-SVC operation and optimization and (iii) Demand Side Management of controllable loads and microgrids.

MPOPF formulation is based on input and control variables. The definition of the objective function, and the power systems operation constraints are presented in the sequence.

3.3 INPUT VARIABLES

Input variables are the ones related to system structure, being expressed for each bus, line, or equipment, being previously defined and responsible for the characterization of the scenario in which the optimization will be performed.

For the active and reactive power demand of all buses (number of buses - *nb*), vectors $\mathbf{Pd}$ and $\mathbf{Qd}$ are respectively defined for each of the total numbers of periods (*nper*) considered. These vectors have information of fixed and manageable demand powers and their sizing corresponds to (*nb.nper* x 1).

$$\mathbf{Pd} = \begin{bmatrix} Pd_1^1 \\ \vdots \\ Pd_{nb}^1 \\ \vdots \\ \vdots \\ Pd_1^{nper} \\ \vdots \\ Pd_{nb}^{nper} \end{bmatrix} \qquad \mathbf{Qd} = \begin{bmatrix} Qd_1^1 \\ \vdots \\ Qd_{nb}^1 \\ \vdots \\ \vdots \\ Qd_1^{nper} \\ \vdots \\ Qd_{nb}^{nper} \end{bmatrix} \tag{1}$$

where:

Pd_i^k: represents the inflexible active power demanded at bus *i* and period *k*;

Qd_i^k: represents the inflexible reactive power demanded at bus *i* and period *k*.

The inflexible demand value of each bus and period of the day (24 hours) depicts the behavior of the loads along with the analysis.

Microgrids are seen as a flexible load from the grid MPOPF point of view. In this case, another load profile is considered at this point of connection, presenting positive values, when its behavior is of load, draining energy from the grid, negative values when it injects power in the grid, operating as a generation, and null values when considered islanded operation, being disconnected from the main grid.

The definition of the flexible loads is given in another vector, $\boldsymbol{FPd}$**,** that presents the list of foreseen flexible buses that have the possibility of demand managing for active and reactive power:

$$\boldsymbol{FPd} = \begin{bmatrix} FPd_1^1 \\ \vdots \\ FPd_{nb}^1 \\ \vdots \\ \vdots \\ FPd_1^{nper} \\ \vdots \\ FPd_{nb}^{nper} \end{bmatrix} \qquad \boldsymbol{FQd} = \begin{bmatrix} FQd_1^1 \\ \vdots \\ FQd_{nb}^1 \\ \vdots \\ \vdots \\ FQd_1^{nper} \\ \vdots \\ FQd_{nb}^{nper} \end{bmatrix} \tag{2}$$

where:

FPd_i^k: ideal flexible active power demanded at bus *i* and period *k*;

FQd_i^k: ideal flexible reactive power demanded at bus *i* and period *k*.

Regarding electric mobility, applications such as V2G (vehicle-to-grid) are not being considered and the electric vehicle charging stations in the grid are portrayed as load. In this case, the difference is due to the behavior of the load curve used, aiming to represent the power demanded to charge the vehicle at each instant of time.

Concerning the integration of photovoltaic systems (PV) as distributed generation, its active power output is considered an input variable for the MPOPF. Since it major depends on solar irradiation and considering a day-ahead scenario, its behavior can be estimated based on the weather forecast.

Nowadays, the techniques used for weather estimation are very trustworthy, resenting a reliability of 98% (INPE, 2019). With the irradiation forecasted information and knowing the installed power of the PV systems located along the feeder it is possible to calculate the solar active power ($\boldsymbol{Pgsun}$) provisioning in each bus for all the analysis periods:

$$\boldsymbol{Pgsun} = \begin{bmatrix} Pgsun_1^1 \\ \vdots \\ Pgsun_{nb}^1 \\ \vdots \\ \vdots \\ Pgsun_1^{nper} \\ \vdots \\ Pgsun_{nb}^{nper} \end{bmatrix} \tag{3}$$

where:

$Pgsun_i^k$: active photovoltaic power injected at bus *i* and period *k.*

The PV system reactive power ($\boldsymbol{Qgsun}$) can be calculated by the power factor (pf) considered for the power system inverter responsible for the connection of the generation system to the grid. In most cases of real applications, the power factor is one, which corresponds to the injection of only active power. However, the reactive power injection can be useful to improve power grid operation, as providing voltage support. In this case, the solar reactive power will be an optimized variable that depends on the limits given by the magnitude of the apparent power of the inverters ($\mathbf{Ssun}$):

$$\boldsymbol{Ssun} = \begin{bmatrix} \boldsymbol{Ssun_1^1} \\ \vdots \\ \boldsymbol{Ssun_{nb}^1} \\ \vdots \\ \vdots \\ \boldsymbol{Ssun_1^{nper}} \\ \vdots \\ \boldsymbol{Ssun_{nb}^{nper}} \end{bmatrix} \tag{4}$$

where:

$Ssun_i^k$: apparent photovoltaic power injected at bus *i* and period *k*.

Other input variables are generation units active ($\boldsymbol{Pg_{max}}$ and $\boldsymbol{Pg_{min}}$) and reactive ($\boldsymbol{Qg_{max}}$ and $\boldsymbol{Qg_{min}}$) fixed power limits, excluding distributed generation in this case. The power provisioning limits from the substation are included in those vectors, since it actuates as a power source for the distribution system, corresponding to a generation system connected to bus 1:

$$\boldsymbol{Pg_{max}} = \begin{bmatrix} Pg_{max}{}_1^1 \\ \vdots \\ 0 \\ \vdots \\ \vdots \\ Pg_{max}{}_1^{nper} \\ \vdots \\ 0 \end{bmatrix} \quad \boldsymbol{Qg_{max}} = \begin{bmatrix} Qg_{max}{}_1^1 \\ \vdots \\ 0 \\ \vdots \\ \vdots \\ Qg_{max}{}_1^{nper} \\ \vdots \\ 0 \end{bmatrix} \tag{5}$$

where:

$Pg_{max}{}_1^k$ and $Qg_{max}{}_1^k$: maximum limits of the active and reactive power injected by the substation at bus 1 and period *k*, respectively.

Voltage magnitude limits ($\boldsymbol{V_{max}}$ and $\boldsymbol{V_{min}}$) should also be provided for all buses in all periods. It is important to highlight that the voltage limits will not necessarily be the same over the whole period and nor will it be the same for all buses in the circuit, as it may depend, for example, on the grid load levels, according to the regulatory definitions:

$$\boldsymbol{V_{max}} = \begin{bmatrix} vmax_1^1 \\ \vdots \\ vmax_{nb}^1 \\ \vdots \\ \vdots \\ vmax_1^{nper} \\ \vdots \\ vmax_{nb}^{nper} \end{bmatrix} \quad \boldsymbol{V_{min}} = \begin{bmatrix} vmin_1^1 \\ \vdots \\ vmin_{nb}^1 \\ \vdots \\ \vdots \\ vmin_1^{nper} \\ \vdots \\ vmin_{nb}^{nper} \end{bmatrix} \tag{6}$$

where:

$vmax_i^k$ and $vmin_i^k$: maximum and minimum limits of the voltage magnitude at bus *i* and period *k*; respectively.

Correlated with voltage boundary, there are the limits of voltage regulator taps ($\boldsymbol{a_{max}}$ and $\boldsymbol{a_{min}}$). The voltage regulators are allocated in series with a line:

$$\boldsymbol{a_{max}} = \begin{bmatrix} a_{max}{}_1^1 \\ \vdots \\ a_{max}{}_{nl}^1 \\ \vdots \\ \vdots \\ a_{max}{}_1^{nper} \\ \vdots \\ a_{max}{}_{nl}^{nper} \end{bmatrix} \quad \boldsymbol{a_{min}} = \begin{bmatrix} a_{min}{}_1^1 \\ \vdots \\ a_{min}{}_{nl}^1 \\ \vdots \\ \vdots \\ a_{min}{}_1^{nper} \\ \vdots \\ a_{min}{}_{nl}^{nper} \end{bmatrix} \tag{7}$$

where:

$a_{max}{}_j^k$ and $a_{min}{}_j^k$: maximum and minimum limit of the voltage regulator taps of line *j* and period *k*, respectively;

nl: number of lines.

Moreover, there is the information regarding the susceptance capacitance of capacitor banks ($\boldsymbol{Bsh}$):

$$\boldsymbol{Bsh} = \begin{bmatrix} Bsh_1^1 \\ \vdots \\ Bsh_{nb}^1 \\ \vdots \\ \vdots \\ Bsh_1^{nper} \\ \vdots \\ Bsh_{nb}^{nper} \end{bmatrix} \tag{8}$$

where:

Bsh_i^k: the susceptance capacitive of capacitor banks at bus *i* and period *k*.

The $\boldsymbol{Bsh}$ vector corresponds to the static capacitor banks that are considered connected or disconnected from the main grid, without control during the optimization performance.

However, it is possible to optimize the input or output of reactive power dispatch using D-FACTS. These systems can contribute to control voltage levels, as well as improve system reliability (MORAES et al., 2012; RELIĆ et al., 2020). So, it is necessary to define the maximum value of susceptance capacitive (which will be represent the injected reactive power to the grid), $\boldsymbol{Bst_{max}}$, and the minimum value of susceptance inductive (which will be represent the absorbed reactive power from the grid), $\boldsymbol{Bst_{min}}$. These values are defined according to the sizing of the considerable D-SVC:

$$\boldsymbol{B_{st_{max}}} = \begin{bmatrix} B_{st_{max_1}}^{1} \\ \vdots \\ B_{st_{max_{nl}}}^{1} \\ \vdots \\ \vdots \\ B_{st_{max_1}}^{nper} \\ \vdots \\ B_{st_{max_{nl}}}^{nper} \end{bmatrix} \qquad \boldsymbol{B_{st_{min}}} = \begin{bmatrix} B_{st_{min_1}}^{1} \\ \vdots \\ B_{st_{min_{nl}}}^{1} \\ \vdots \\ \vdots \\ B_{st_{min_1}}^{nper} \\ \vdots \\ B_{st_{min_{nl}}}^{nper} \end{bmatrix} \tag{9}$$

where:

Bst_i^k: represents the maximum limit of susceptance capacitive of D-SVC at bus *i* and period *k*.

As a D-SVC is a shunt element, it was modeled in a similar way to the capacitor banks, however, its reactive power injection is dispatchable according to the grid needs (FREITAS; PORTELINHA; TORTELLI, 2019).

The circulating active power flow limits through the lines are given by $\boldsymbol{F_{max}}$. The minimum active power flow limit is considered as the negative of the maximum active power flow limit:

$$\mathbf{F}_{max} = \begin{bmatrix} Fmax_1^1 \\ \vdots \\ Fmax_{nl}^1 \\ \vdots \\ Fmax_1^{nper} \\ \vdots \\ Fmax_{nl}^{nper} \end{bmatrix} \tag{10}$$

where:

$F_{max}{}_j^k$: maximum limit of active power flow through the *j* and period *k*.

Considering the integration of energy storage systems into distribution grids, more specifically battery energy storage systems (BESS), its behavior and characteristics were also modeled to be part of the MPOPF formulation. Thus, the active power boundaries ($\boldsymbol{P_{bat_{max}}}$ and $\boldsymbol{P_{bat_{min}}}$) should also be defined, regarding the capacity of the storage system to absorb and provide power. Those limits are associated not only with the battery itself but with the power system inverter used to couple the BESS to the main grid. In this way, the reactive power can be defined by the operational power factor considered, as done for PV system, or even can be considered dispatched for the provisioning of the ancillary services:

$$\boldsymbol{P_{bat_{max}}} = \begin{bmatrix} P_{bat}{}_{max_1}^1 \\ \vdots \\ P_{bat}{}_{max_{nl}}^1 \\ \vdots \\ \vdots \\ P_{bat}{}_{max_1}^{nper} \\ \vdots \\ P_{bat}{}_{max_{nl}}^{nper} \end{bmatrix} \qquad \boldsymbol{P_{bat_{min}}} = \begin{bmatrix} P_{bat}{}_{min_1}^1 \\ \vdots \\ P_{bat}{}_{min_{nb}}^1 \\ \vdots \\ \vdots \\ P_{bat}{}_{min_1}^{nper} \\ \vdots \\ P_{bat}{}_{min_{nb}}^{nper} \end{bmatrix} \tag{11}$$

where:

$Pbat_{max}{}_i^{nper}$ and $Pbat_{min}{}_i^{nper}$: maximum and minimum limits of the active power of BESS at bus *i* and period *k*; respectively. It can be used $\boldsymbol{P_{bat_{min}}} = -\boldsymbol{P_{bat_{max}}}$.

Energy stored capacity should also be defined ($\boldsymbol{EBAT_{max}}$ and $\boldsymbol{EBAT_{min}}$) being the upper boundary related to system sizing (kWh) and the lower boundary dependent on the depth-of-discharge (DoD) defined by the system owner:

$$\boldsymbol{EBAT_{min}} = \begin{bmatrix} Ebat_{min_1}^{1} \\ \vdots \\ Ebat_{min_{nb}}^{1} \\ \vdots \\ \vdots \\ Ebat_{min_1}^{nper} \\ \vdots \\ Ebat_{min_{nb}}^{nper} \end{bmatrix} \quad \boldsymbol{EBAT_{max}} = \begin{bmatrix} Ebat_{max_1}^{1} \\ \vdots \\ Ebat_{max_{nb}}^{1} \\ \vdots \\ \vdots \\ Ebat_{max_1}^{nper} \\ \vdots \\ Ebat_{max_{nb}}^{nper} \end{bmatrix} \tag{12}$$

where:
$Ebat_{max_i}^{k}$ and $Ebat_{min_i}^{k}$: maximum and minimum limits of energy stored capacity of BESS at bus *i* and period *k;* respectively*.* It can be established in $EBAT_{min_i}^{nper}$*,* the desired values that the BESS must be loaded at the final of the day.

In the same way as PV reactive power, the reactive power of BESS can be useful to improve power grid operation, providing voltage support. In this case, the BESS reactive power will be an optimized variable that depends on the apparent power limits of its inverter:

$$\boldsymbol{Sbat} = \begin{bmatrix} Sbat_1^1 \\ \vdots \\ Sbat_{nb}^1 \\ \vdots \\ \vdots \\ Sbat_1^{nper} \\ \vdots \\ Sbat_{nb}^{nper} \end{bmatrix} \tag{13}$$

where:

$Sbat_i^k$: BESS apparent power injected at bus *i* and period *k*.

Besides the forementioned variables, other information can be defined as input variables, such as: power system parameters; system configurations; reference bus (swing bus); equipment locations; the energy stored in BESS at the start of dispatch period (*Earrive*), and BESS efficiency; tariff values, among others.

The vectors represented in equations (1)-(6), (8), and (11)-(13) have dimensions (*nb.nper* x 1) where *nb* is the number of buses in the grid and *nper* is the number of analyzed periods. Moreover, the vectors presented in equations (7), (9), and (10) have dimensions (*nl.nper* x 1) where *nl* is the number of lines in the grid.

3.4 CONTROL AND DEPENDENT VARIABLES

All voltage phasors are represented by the rectangular coordinates, as used in (BARAN JUNIOR; PIAZZA FERNANDES; BORBA, 2019):

$$\dot{\boldsymbol{V}} = \begin{bmatrix} \dot{V}_1^1 \\ \vdots \\ \dot{V}_{nb}^1 \\ \vdots \\ \dot{V}_1^{nper} \\ \vdots \\ \dot{V}_{nb}^{nper} \end{bmatrix} = \begin{bmatrix} e_1^1 \\ \vdots \\ e_{nb}^1 \\ \vdots \\ e_1^{nper} \\ \vdots \\ e_{nb}^{nper} \end{bmatrix} + j \begin{bmatrix} f_1^1 \\ \vdots \\ f_{nb}^1 \\ \vdots \\ f_1^{nper} \\ \vdots \\ f_{nb}^{nper} \end{bmatrix} \therefore \dot{\boldsymbol{V}} = e + jf \tag{14}$$

where:

V_i^k: voltage phasors at bus *i* and period *k*;
e_i^k: real component of the voltage V_i^k;
f_i^k : imaginary component of the voltage V_i^k.

The elements that compose the real and imaginary components of the bus voltages are grouped as $\boldsymbol{e} = [\mathrm{e}_1^1 \ \cdots \ e_{nb}^{nper}]^T$ and $f = [f_1^1 \ \cdots \ f_{nb}^{nper}]^T$ (FERNANDES, 2004).

The vector **x** is composed by voltage components of all periods:

$$\mathbf{x} = [\ \mathbf{e} \quad \boldsymbol{f} \quad]^{\boldsymbol{T}} \tag{15}$$

where:

x: corresponds to the vector that stores the real and imaginary components of all the bus voltages with dimension (2.*nb.nper* x 1);
T: represents that the vector is transposed.

The rectangular representation is used to overcome the problems of poor numerical conditioning of distribution networks due to short stretches interspersed with excessively long and predominantly radial stretches. Besides that, this rectangular representation results in quadratic active and reactive power balance equations, which facilitate the convergence of the optimization problem (GRANVILLE; MELLO; MELLO, 1996).

Voltage regulators tap positioning is a controllable variable, since it is defined during the optimization process, as (LACHOVICZ, 2018):

$$\mathbf{a} = [\, a_1^1 \quad \dots \quad a_{nb}^1 \quad \dots \quad a_1^{nper} \quad \dots \quad a_{nb}^{nper}]^{\boldsymbol{T}} \tag{16}$$

where:

a_j^k: taps position of voltage regulator at line *j* and period *k.*

Likewise, the BESS active power behavior is optimized by the MPOPF, which decides the charging ($P_{bat} > 0$) and discharging ($P_{bat} < 0$) periods:

$$\boldsymbol{Pbat} = [\, Pbat_1^1 \dots\ Pbat_{nb}^1 \ \dots\ Pbat_1^{nper} \dots\ Pbat_{nb}^{nper}]^{\boldsymbol{T}} \tag{17}$$

where:

$Pbat_i^k$: power active of BESS injected at bus *i* and period *k.*

In this work, it is assumed that ideal or predicted values of flexible loads are previously stipulated by their owners ($\boldsymbol{FPd}$ and $\boldsymbol{FQd}$). If this predicted or ideal flexible load cannot be dispatched, due to technical reasons of the grid, it must be cut off. This is done by the optimization variable, $\boldsymbol{gamma,}$ that weighs the values of $\boldsymbol{FPd}$ and $\boldsymbol{FQd,}$ multiplying them.

The management of the loads that present flexibility is carried out by the $\boldsymbol{gamma}$ variable, which represents how much of the load has been cut:

$$\boldsymbol{gamma} = [\, gamma_1^1 \dots gamma_{nb}^1 \ \dots\ gamma_1^{nper} \dots gamma_{nb}^{nper}]^{\boldsymbol{T}} \tag{18}$$

where:

$gamma_{nb}^{nper}$: factor to cut each flexible load ($\boldsymbol{FPd}$) at bus *i* and period *k.*

Related to reactive power for elements connected to the grid via inverters, such as PV systems and BESS, these will be taken as control variables if reactive dispatch is being considered. Otherwise, if the power factor is considered fixed, the reactive power injected by these systems will be a dependent variable.

So, if the reactive dispatch of PV systems and BESS are optimized by the MPOPF, the reactive power injection of PV ($\boldsymbol{Qgsun}$) and the reactive power injection of BESS ($\boldsymbol{Qbat}$) are:

$$Qgsun = \begin{matrix}[Qgsun_1^1 \ldots Qgsun_{nb}^1 \ldots \\ \ldots Qgsun_1^{nper} \ldots Qgsun_{nb}^{nper}\ ]^T\end{matrix} \tag{19}$$

$$Qbat = \begin{matrix}[Qbat_1^1 \ldots Qbat_{nb}^1 \ldots \\ \ldots Qbat_1^{nper} \ldots Qbat_{nb}^{nper}\ ]^T\end{matrix} \tag{20}$$

where:

$Qgsun_i^k$: reactive photovoltaic power injected at bus *i* and period *k* and,

$Qbat_i^k$: reactive battery power injected at bus *i* and period *k.*

Reactive dispatch of D-FACTS can also be considered a control variable and, thus, be optimized. Its operation will be based on voltage levels, actuating mainly for voltage control. Since the circuit presents different elements that can act to improve the voltage levels, in future analysis they will be considered individually in different scenarios, allowing to verify the effectiveness of each method application (voltage regulator, capacitor bank, reactive dispatch of the generation and storage systems, and the D-FACTS operation):

$$\mathbf{Bst} = [\ Bst_1^1\ \ldots\ Bst_{nb}^1\ \ldots\ Bst_1^{nper}\ \ldots\ Bst_{nb}^{nper}]^{\boldsymbol{T}} \tag{21}$$

where:

Bst_i^k: the susceptance capacitive of D-SVC bus *i* and period *k.*

Finally, the active ($\boldsymbol{Pg}$) and reactive ($\boldsymbol{Qg}$) power provided from the substation at bus 1 are:

$$\boldsymbol{Pg} = [\,Pg_1^1 \quad \dots \quad 0 \quad \dots \quad Pg_1^{nper} \quad \dots \quad 0]^{\boldsymbol{T}} \tag{22}$$

$$\boldsymbol{Qg} = [\,Qg_1^1 \quad \dots \quad 0 \quad \dots \quad Qg_1^{nper} \quad \dots \quad 0]^{\boldsymbol{T}} \tag{23}$$

where:

Pg_i^k: active power injected at bus *i* and period *k,* being *i=1* for the substation bus and,

Qg_i^k: reactive power injected at bus *i* and period *k,* being *i=1* for the substation bus.

3.5 OBJECTIVE FUNCTION

The objective function (OF) proposed for the MPOPF comprehends:

- minimization of the operational costs;
- minimization of battery degradation costs (if a battery system is considered);
- minimization of load deviation of flexible loads and microgrids from the predicted or ideal load (if flexible loads and/or microgrids are considered);
- minimization of power losses.

Operational cost criterion is defined as:

$$foper = wc.\boldsymbol{u^T}.\,\mathrm{c}(\boldsymbol{Pg}) \tag{24}$$

where:

wc: weight relative to the importance of the operational costs' criterion.

$\mathrm{c}(\boldsymbol{Pg})$: energy cost function related to power provided by substation and other generation systems belonging to the power utility. This function also depends on the tariff values considered. The vector ***aah*** with dimension (*nb.nper* x 1) indicates the tariff for each hour ($\mathrm{c}(\boldsymbol{Pg}) = \boldsymbol{aah^T}.\boldsymbol{Pg}$);

$\boldsymbol{u}$**:** unit vector with size (*nb.nper* x 1).

The next criterion is related to battery degradation costs. This should be minimized, once every time that the battery realizes a cycle (charge and discharge), part of its lifetime is lost (SUFYAN et al., 2019).

According to Tazvinga, Zhu and Xia (2015) the battery degradation cost ($cost_{deg}$) can be defined by (25). This proposed model considered the battery bank cost ($cost_{BB}$), the DoD, the expected number of cycles (n_cycles) for the battery over its lifetime, and the total energy storage capacity of the system ($Ebat$). It is important to highlight that most of these characteristics varies according to system technology, size and type of operation realized.

$$cost_{deg} = \frac{cost_{BB}}{DoD.n_{cycles}.Ebat} \quad (25)$$

With the degradation cost definition is possible to write the corresponding OF criterion in (26).

$$fcost_{bat} = wbat.\boldsymbol{u^T}.\mathrm{c}(\mathbf{Pbat}) \quad (26)$$

where:

$wbat$: weight relative to the importance of battery degradation costs criterion;

$\mathrm{c}(\boldsymbol{Pbat})$: cost function based on linear cost function $cost_{deg}$.

The minimization of load deviation of flexible loads and microgrids is defined as:

$$f_{flexible} = wgd.\boldsymbol{u^T}.[(\boldsymbol{gamma} - \mathbf{u})]^2 \quad (27)$$

where:

wgd: weight relative to the importance of load flexibility management.

The values of $\boldsymbol{gamma}$ multiply $\boldsymbol{FPd}$ and $\boldsymbol{FQd}$ to decrease the injection or absorption of the predicted load and must deviate minimally from the unit value (which corresponds to the ideal values). As the ($\boldsymbol{gamma}$ - $\mathbf{u}$) parcel is squared, the result is positive, and the difference module is always minimized.

Aiming to avoid that the values of $\boldsymbol{gamma}$ be smaller than 1, which correspond to dispatch less than the scheduled load ($\boldsymbol{FPd}$), one more optimization criterion can be included, which corresponds to maximize the adjusted values of $\boldsymbol{gamma}$. Therefore, this criterion forces that the total expected load must be supplied, and it is weighted by $w_{targetload}$ coefficient. Adding this new criterion in (27), the $f_{flexible}$ criterion is written as:

$$f_{flexible} = wgd.\ \boldsymbol{u^T}.[(\boldsymbol{gamma} - \boldsymbol{u})]^2 - w_{targetload}.\ \boldsymbol{u^T}.\boldsymbol{gamma} \quad (28)$$

At least, the criteria related to power losses minimization is given by:

$$flosses = wp.\,\boldsymbol{u^T}.\,\mathrm{c}(\boldsymbol{Pg} + \boldsymbol{Pgsun} - \boldsymbol{Pd} - \boldsymbol{gamma}.\boldsymbol{FPd} - \boldsymbol{Pbat}) \quad (29)$$

where:
wp: weight relative to the importance of the loss criterion;
$\mathrm{c}(\boldsymbol{Pg} + \boldsymbol{Pgsun} - \boldsymbol{Pd} - \boldsymbol{gamma}.\boldsymbol{FPd} - \boldsymbol{Pbat})$: energy cost function. This function depends on the tariff value that is considered according to the case of the study.

With the definition of all the parts of the objective function it is possible to compile the multiobjective function:

$$OF = foper + fcost_{bat} + f_{flexible} + f_{losses} \quad (30)$$

Regarding the values of the weights used to prioritize the parcels of the objective function, it is important to note that the sum of all of them should be equal to one, being the correspondent values decided through exhaustive analysis to choose the best values that meet the planner's interests.

The objective function is restricted to the operational constraints to get its optimum value.

3.6 OPERATIONAL CONTRAINTS

The operational constraints are divided into two groups: the equality and the inequality constraints.

3.6.1 Equality Constraints

The active and reactive power injections are represented as below (BORGES; FERNANDES; ALMEIDA, 2011):

The active and reactive power balance equations are:

$$\boldsymbol{P} = \boldsymbol{Pg} + \boldsymbol{Pgsun} - \mathbf{diag}(\boldsymbol{gamma}).\boldsymbol{FPd} - \boldsymbol{Pbat} \quad (31)$$

$$\boldsymbol{Q} = \boldsymbol{Qg} + \boldsymbol{Qgsun} - \mathbf{diag}(\boldsymbol{gamma}).\boldsymbol{FQd} - \boldsymbol{Qbat} + \\ +\mathbf{diag}\,(|\boldsymbol{V}\,|^{2})\,(\boldsymbol{Bsh} + \boldsymbol{Bst}) \tag{32}$$

where:

$|\boldsymbol{V}\,|$: magnitude of the voltage phasor.

3.6.2 Inequality Constraints

The inequality constraints consider the physical and operational limits of the system. Equations (33) to (43) represent the range defined for the variables, based on the boundary values forementioned. All the variables delimited by the intervals are optimized in the MPOPF, so the interval defines the possible values that they can assume to achieve the convergence of the problem.

$$\boldsymbol{Pg}_{\boldsymbol{min}} \leq \boldsymbol{Pg} \leq \boldsymbol{Pg}_{\boldsymbol{max}} \tag{33}$$

$$\boldsymbol{Qg}_{\boldsymbol{min}} \leq \boldsymbol{Qg} \leq \boldsymbol{Qg}_{\boldsymbol{max}} \tag{34}$$

$$\boldsymbol{V}^{2}_{\mathbf{min}} \leq |\boldsymbol{V}|^{2} \leq \boldsymbol{V}^{2}_{\mathbf{max}} \tag{35}$$

$$-\mathbf{F}_{\mathbf{max}} \leq \mathbf{F}(\mathbf{x}) \leq \mathbf{F}_{\mathbf{max}} \tag{36}$$

$$\boldsymbol{a}_{\mathbf{min}} \leq \boldsymbol{a} \leq \boldsymbol{a}_{\mathbf{max}} \tag{37}$$

$$\mathbf{0} \leq \boldsymbol{gamma} \leq \mathbf{u} \tag{38}$$

$$-\boldsymbol{Bst}_{\boldsymbol{max}} \leq \boldsymbol{Bst} \leq \boldsymbol{Bst}_{\boldsymbol{max}} \tag{39}$$

$$\boldsymbol{Pgsun}^{2} + \boldsymbol{Qgsun}^{2} \leq \boldsymbol{Ssun}^{2} \tag{40}$$

$$\boldsymbol{Pbat}^{2} + \boldsymbol{Qbat}^{2} \leq \boldsymbol{Sbat}^{2} \tag{41}$$

$$-\,\boldsymbol{Ssun} \leq \boldsymbol{Qgsun} \tag{42}$$

$$-\,\boldsymbol{Sbat} \leq \boldsymbol{Qgbat} \tag{43}$$

Equations (33) and (34) represent the substation transformer active and reactive power injection limits, respectively. (35) represent the voltage magnitude limits. (36) are related to the power flow limit through the lines. (37) are the boundaries for voltage regulator tap position. (38) are the limits of flexible load management. (39) represents the D-SVC limits. Equation (40) represents the apparent power limit of the solar inverters, and (41) the apparent power of the battery inverters. Equations (42) and (43) present the limit boundaries for the reactive power dispatch when this possibility is allowed for DERs.

For the BESS, the active power limit injection is defined by (44), whereas the energy stored in the battery is limited by (45).

$$\boldsymbol{P_{bat_{min}}} \leq \boldsymbol{Pbat} \leq \boldsymbol{P_{bat_{max}}} \tag{44}$$

$$\boldsymbol{EBAT_{min}} \leq \boldsymbol{Ebat} \leq \boldsymbol{EBAT_{max}}. \tag{45}$$

The effective amount of energy stored ($Ebat_i^t$) depends on the values of energy stored in the previous instants, considering the initial energy at t = 0 ($Earrive$), and the efficiency (eff_{bat}) of the charging and discharging process.

$$Ebat_i^t = \sum_{k=1}^{nper} [Pbat_i^k - (1 - \mathrm{eff_{bat}}).|Pbat_i^k|].\Delta\mathrm{t} + Earrive \tag{46}$$

where:

Δt: time interval between two consecutive periods.

The problem presented by the equations (30) – objective function, (31) and (32) – equality constraints and, (33) to (46) – inequality constraints, represents the MPOPF model, that is solved by the Primal-Dual version of the Interior Points Method implemented in Matlab language.

The Interior Points Method obtains the best solution, keeping the search inside the area delimited for restrictions. The inequalities are changed to equality through the introduction of slack variables. Additionally, a logarithmic barrier function is added to the objective function to guarantee the non-negativity of the slack variables. In sequence, the Karush–Kuhn–Tucker (KKT) conditions that express the first optimality conditions of the optimization problem are resolved by the application of Newton's method to obtain the solution of the nonlinear equations (Karush-Kuhn-Tucker optimization base conditions). This method was selected due to its good performance obtained to solve traditional OPF (BLASI, 2020; BORGES; FERNANDES; ALMEIDA, 2011).

4 STUDY CASES FOR THE MULTIPERIOD OPTIMUM POWER FLOW PROPOSED FOR ACTIVE DISTRIBUTION NETWORK, MICROGRID AND ANCILLARY SERVICES

For the simulations, initially, a 90-bus distribution test feeder is considered, with different scenarios of DERs placement and ancillary services provisioning. From all scenarios, the results of power losses, voltage levels, reverse power flow, and operational costs are analyzed being compared at the end to each other and the base case, corresponding this one to the conventional distribution network, with no DERs.

At least, a distribution feeder from Curitiba (Brazil) with 359 buses is simulated considering some of the scenarios proposed initially for the test feeder, allowing to analyze how does a real system would operate when it became an ADN.

In this way it is possible to evaluate the behavior of the proposed methodology when it considers a grid with greater complexity and/or dimension.

The maintenance of voltage levels inside power quality values is one of the most important characteristics of the power grid. Voltage behavior on distribution grids depends on the active power behavior. So, when the demand in the circuit increases, the voltage tends to present lower values, whereas the greater injection of power increases the voltage.

In Brazil, the procedures for Distribution of Electric Energy in the National Electric System (from Portuguese, PRODIST), define in Module 8 – Electric Energy Quality (ANEEL, 2018) the bands of voltage for distribution buses when the system is in steady-state, being these values presented at TABLE 3. The voltage levels need to be kept between 0.93 and 1.05 pu*,* for nominal voltages between 1 kV and 69 kV*,* even with the connection of DG, EVs, or BESS systems. For this purpose, equipment as voltage regulators (VR), capacitor banks, and D-FACTS are placed along the feeder, as well as the contribution of reactive dispatch from PV and BESS systems could be considered.

TABLE 3 - CLASSIFICATION OF VOLTAGE LEVELS.

$\mathbf{0.93 \le V \le 1.05\ pu}$	Adequate
$\mathbf{0.90 \le V < 0.93\ pu}$	Precarious
$\mathbf{V < 0.9\ or\ V > 1.05\ pu}$	Critical

Source: ANEEL (2018).

The provisioning of reactive power by elements connected to the grid by inverters can be considered an ancillary service since it can be requested and remunerated by the DSO if there is regulation and a defined market for it.

To calculate the operational cost for the DSO, the white tariff values were considered. In 2019, according to COPEL distribution power utility, the values for this tariff for residential consumers (COPEL, 2019) were: 0.081426 USD/kWh for off-peak hours (*hfp*), 0.111261 USD/kWh for pre-and post-peak hours (*hpp*) and 0.172793 USD/kWh for peak hours (*hp*)[4]. As these tariff values will be used to calculate the grid operation cost, the values without taxes were adopted.

The *hfp*, *hpp*, and *hp* values compose the vector ***aah*** with dimension (*nb.nper* x 1) that indicates the tariff for each hour, and this behavior is illustrated in FIGURE 12.

FIGURE 12 - BRAZILLIAN WHITE TARIFF VALUES AND BEHAVIOR.

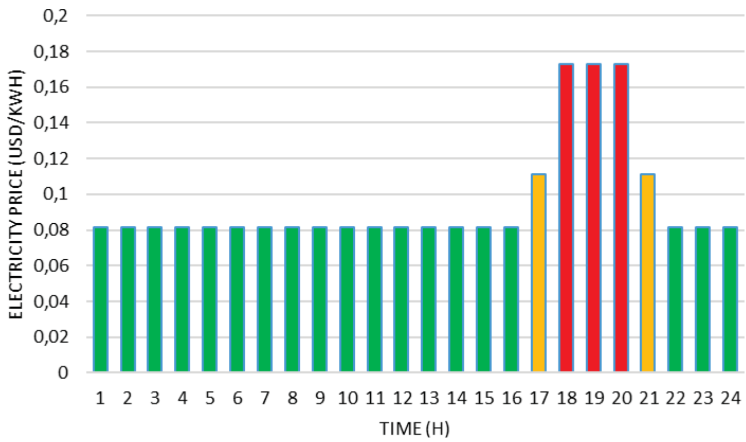

Source: Adapted from COPEL (2019).

For the distributed generation with PV systems, different radiation behaviors can be considered, however, as it is desired to study the most critical scenario, the analysis for clear sky days was prioritized, resulting in maximum solar radiation. FIGURE 13 illustrates the radiation profile that was considered, being obtained from measurements realized at Curitiba city, in Brazil (BLASI, 2017).

[4] The conversion of values from Brazilian Reais (BRL) to American Dollars (USD) was carried out based on the exchange data of April 26, 2021, according to the Brazilian Central Bank: 1USD = 5.4560 BRL.

FIGURE 13 - SOLAR IRRADIATION PROFILE

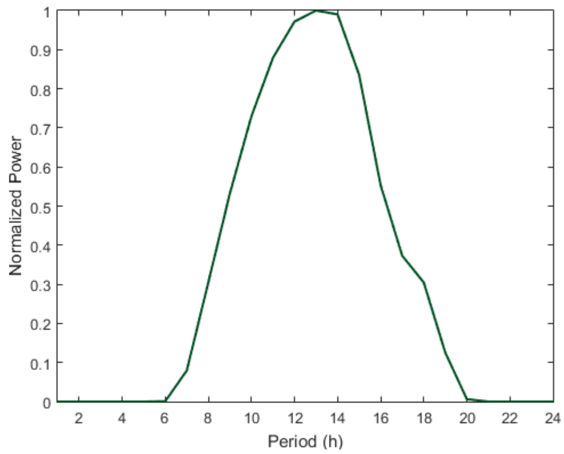

Source: The Author (2021).

4.2 TEST FEEDER DESCRIPTION

The first circuit that was analyzed was a test feeder with 90 buses adapted from Godoi; Aoki; Fernandes (2009) and Lachovicz (2018). This circuit was based on Baran and Wu (1989) system of 69 medium voltage (MV) buses, in which were added 20 low voltage (LV) buses. The schematic diagram of the distribution grid is presented at FIGURE 14.

The distribution system presents a voltage regulator placed between buses 59 and 60, since lower voltage levels are seen at LV buses 86, 87, and 88. The VR consists of an autotransformer with 32 different tap positions with +/- 10% of voltage control of total variation around the center operation value. Usually, VR placed outside of the substation bus is defined in a fit-and-forget configuration. However, as an ADN scenario is being considered, it was assumed that this equipment can present an automatic control, similar to an online tap changer voltage regulator (OLTC) and will adjust the tap positioning according to grid necessities.

There are also five fixed capacitor banks with commercial values of 100, 200, and 300 kVAr, placed at buses 13, 23, 37, 57, and 62. These capacitor banks are fixed, being considered connected or disconnected during the entire period of study, according to the ongoing analysis.

As the study considers an ADN, DERs are placed on it, as illustrated in FIGURE 14, being those characteristics described in detail in the following subsections. The study time horizon considered is 24 hours, discretized into 1h.

FIGURE 14 - TEST DISTRIBUTION FEEDER WITH 90 BUSES.

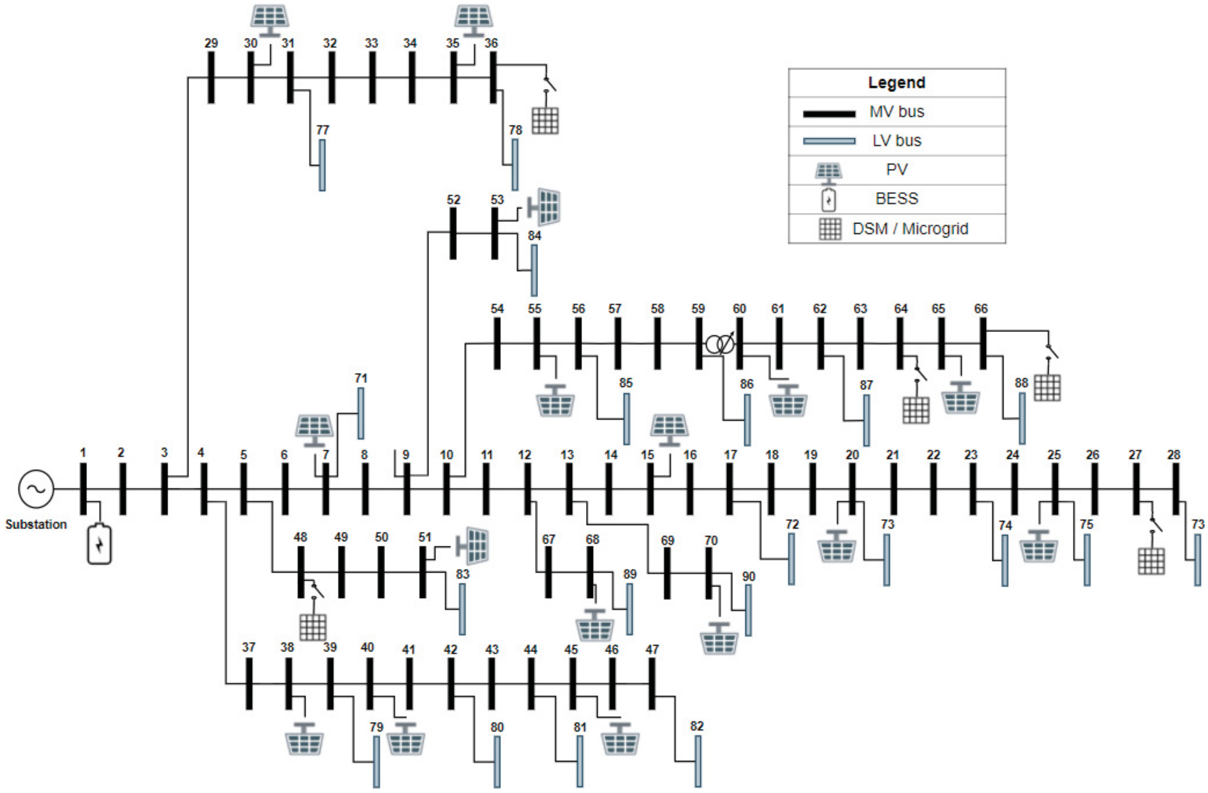

Source: The Author (2021).

Of the 90 buses, 69 are load buses that totalized 4.575 MW of installed load. Regarding the behavior of the loads, the profile sampled in FIGURE 15 was defined, which is normalized, meaning that it presents values between 0 and 1, being multiplied by the load power installed in each bus. In this way, all the load buses present the same behavior profile, but different values among themselves. FIGURE 15 shows the behavior of the active and reactive power of the loads, which present a power factor of 0.92.

Regarding PV system connection, 16 distributed generation systems were placed on it (LACHOVICZ, 2018). All systems have the same installed power and same generation profile behavior. The total installed power of the PV systems totalizes 3.2025 MW, corresponding to a penetration level of 70% concerning the total installed load (BLASI, 2020).

FIGURE 15 - LOAD ACTIVE AND REACTIVE POWER PROFILE FOR 90 BUS TEST FEEDER.

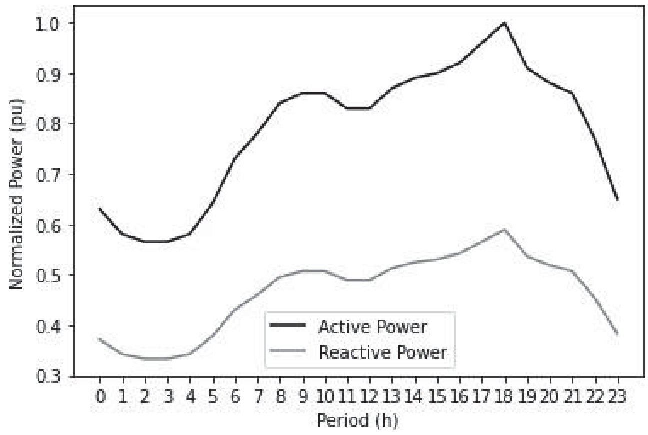

Source: The Author (2021).

For the power factor of PV system inverters, three different options were considered: unit power factor, which corresponds to injection of only active power; fixed power factor, which requires the injection of reactive power from PV systems; and the reactive power dispatch, being the power factor variable, allowing the provisioning of voltage support as an ancillary service with reactive power injection according to grid necessity.

For the electric mobility there are six electric vehicle chargers of 7.4 kW and three of 22 kW installed along with the distribution system, totalizing 110.4 kW of installed power. The EV chargers of 7.4 kW were connected to low voltage buses 72, 74, 78, 82, 88, 90, whereas the 22 kW systems were connected to medium voltage buses 51, 53, and 65.

The average energy storage capacity of the vehicles was taken as 30 kWh, and the initial state-of-charge of the battery from EVs when they arrive at the charging station was considered as 20% (corresponding to a depth-of-discharge of 80%) and resulting in a demand of 24 kWh.

According to Gerossier, Girard and Kariniotakis (2019), most of the charging of electric vehicles takes place at night, due to lower tariffs. The second most frequent charging time corresponds to the period when people are working and are not using the vehicle. Therefore, two different charging behaviors were considered: night charging (from 0:00 to 6:00) which totalizes a power demand of 662.4 kWh, being able to charge 27 vehicles with the beforementioned characteristics; or day charging (from 9:00 to 18:00), totalizing 993.6 kWh, able to charge 41 vehicles in the same conditions previously defined. The behavior of both charging strategies along the day is presented in FIGURE 16.

FIGURE 16 - EV DAILY AND NIGHT CHARGING BEHAVIORS.

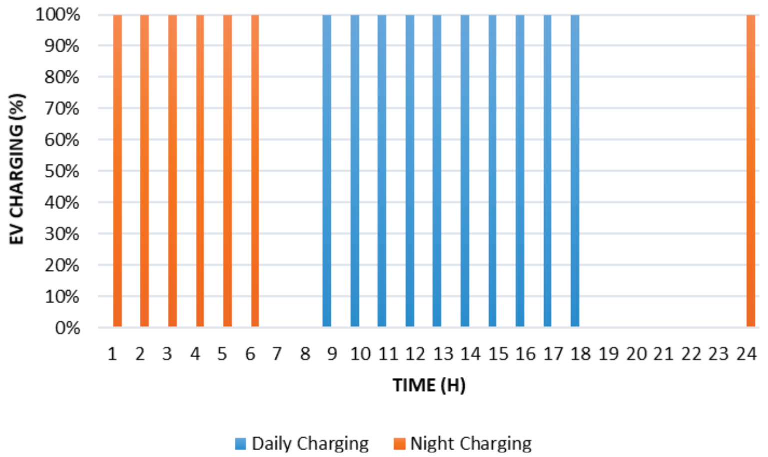

Source: The Author (2021).

The medium voltages buses that receive the EV chargers also present solar generation installed, resulting in a similar behavior of a carport system (generation and EV consumption in the same point of the system). The demand profile of EV chargers is included in vector $\boldsymbol{FPd}$ since they will operate as a load.

The stationary battery energy storage system modeled for the simulations corresponds to a utility scale lithium-ion battery with 1 MW/2 MWh. Based on market data provided by different manufacturers, in 2021, this battery would cost approximately 2.2 million dollars.

In terms of operational characteristics, the BESS will present a maximum DoD of 70%, which means approximately 4,000 cycles to failure.

Another important characteristic to be considered is the efficiency of the charging and discharging process. According to Divya and Ostergaard (2009) lithium-ion batteries present efficiency higher than 90%, low self-discharge rates, and are not affected by the memory effect as other energy storage technologies. In this way, the 90% value was considered for the efficiency of both charge and discharge processes $(\mathrm{eff_{bat}} = 0.9)$.

As forementioned, the battery is connected to the power grid using an inverter. Thus, two different scenarios were considered for the power factor, being first the fixed value of 0.92 and after allowed the reactive power dispatch, also aiming to use reactive power to improve distribution grid voltage levels.

Concerning the location of the BESS, two possibilities were also considered. As the system will be an equipment of the DSO, it can be placed at the substation bus, reducing costs related to space rental and investments in control and communication systems, however, the benefits provided by the system can be limited, as will be shown in the results section. Another possibility could be the placement outside of the substation bus. In Blasi (2020) different allocations were evaluated, and one of the best results is achieved when the BESS is connected to bus 8, since major part of the total load (66.15%) is located downstream of this point.

The D-SVC has its reactive power injection dispatchable according to the grid needs. This equipment was installed on a bus in which there was a capacitor bank (bus 57 from FIGURE 14), since at that point tends to have voltage problems. Additionally, it was desired to analyze the complementarity of voltage regulator operation and the D-FACTS. The other capacitor banks remain fixed and with the same values.

For the circuit simulated, flexible loads were considered at buses 27, 36, 48, 64, and 66. The range of load variation is defined at restriction (39), and it is considered the possibility to vary up to 15% of the demanded power. It is important to highlight that the DSM can happen only if some operational constraint is reached and is not allowed to be performed based on grid operational cost reduction.

The power grid can present not only one microgrid (MG) but multiple microgrids placed along the feeder simultaneously, resulting in different interactions with the main grid.

For the test circuit, MGs were allocated in place of flexible loads (buses 27, 36, 48, 64, and 66). Regarding the behavior of the microgrids over 24 hours, three distinct periods of operation were considered:

- 0h to 7h corresponds to load (the price of grid energy tends to be lower during this period since there is less demand);
- 8h to 17h is disconnected from the grid (taking advantage of existing generation in the MG itself for supplying internal loads);
- 18h to 21h delivers power to the grid (performing power injection in the hour of higher demand in the distribution grid);
- 22h to 23h returns to operate as load, absorbing power from the main grid.

4.3 TEST FEEDER RESULTS

For the test circuit, the gradual implementation of elements in the distribution grid was performed to verify how the insertion of the elements impacts the power system operation when MPOPF is calculated. All combinations of elements that can be allocated in the network were considered and simulated, been the most relevant ones discussed in the sequence.

The weights applied for the optimization process in the scenario of 90 bus test feeder are presented at TABLE 4, where the sum values considered were equal to 1. Some weights, like the one of target load and battery, received higher values since these portions were less expressive than the others. It is important to highlight that these values were defined after the execution of innumerous tests and combinations until the best simulation results are achieved.

TABLE 4 - NORMALIZED VALUES OF OBJECTIVE FUNCTION WEIGHTS FOR 90 BUS TEST FEEDER

Weights	Base Case	90bus+BESS	90bus+BESS+FL*
w_c	0.5	0.16	0.038
w_p	0.5	0.16	0.038
w_{bat}	-	0.68	0.17
w_{load}	-	-	-
w_{gd}	-	-	0.377
$w_{targetload}$	-	-	0.377

*FL: Flexible Load

Source: The Author (2021).

4.3.1 90 Bus Test Feeder – Base Case

The base scenario consists of the 90-bus test feeder only with load allocation, corresponding to a classic distribution circuit without any DER. In this case, the voltage regulator (VR) and the fixed capacitor banks were considered, and the total energy demand totalizes 81.27 MWh. In FIGURE 17 the active power flow balance from the substation bus is presented, being the reactive power balance illustrated in FIGURE 18.

From FIGURE 17 it is possible to visualize that all load is supplied by the substation. The same happens for reactive power in FIGURE 18, being, in this case, part of reactive power demand supplied by fixed capacitor banks and part provided by the substation.

FIGURE 17 - ACTIVE POWER BALANCE AT THE SUBSTATION BUS FOR 90 BUSES TEST FEEDER BASE CASE

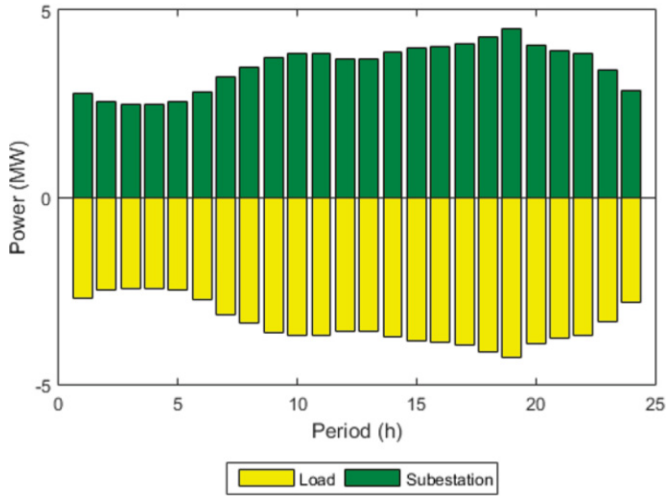

Source: The Author (2021).

FIGURE 18 - REACTIVE POWER BALANCE AT THE SUBSTATION BUS FOR 90 BUS TEST FEEDER BASE CASE

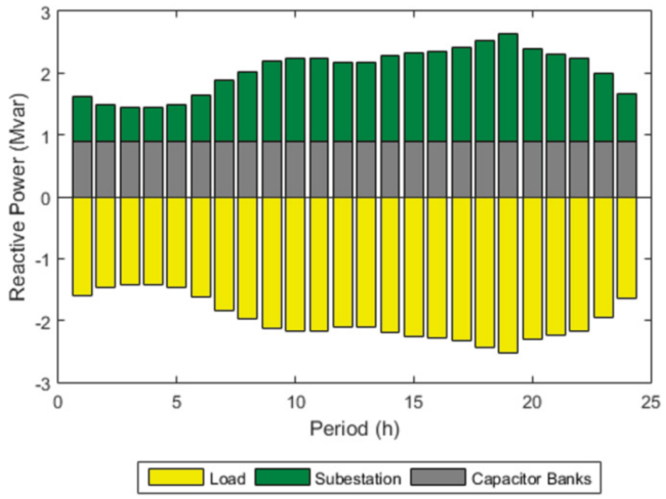

Source: The Author (2021).

In this scenario, all buses present voltage values inside of the limits to be considered adequate, as shown in FIGURE 19. The minimum voltage in this circuit is found at bus 86, however, it is not an undervoltage (it is not under 0.93 pu). In terms of maximum voltage boundary, none of the buses reached these values as well.

FIGURE 19 - VOLTAGE BEHAVIOR FOR ALL 90 BUSES IN THE BASE CASE SCENARIO.

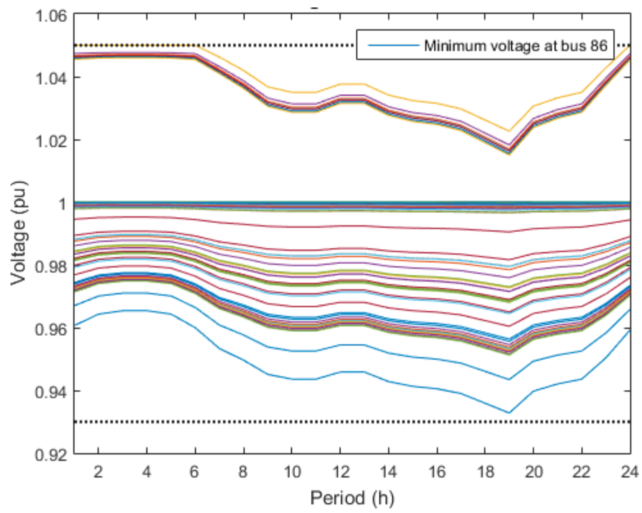

Source: The Author (2021).

For this scenario, the power losses on the circuit totalize 2.71 kWh (3,33%), arising from the circulation of power through the circuit lines. Concerning the operational cost of the DSO to supply all the load, it totals 8,122.75 USD.

Regarding the VR tap operation, the results are presented in FIGURE 20, in which it is seen that the regulator needs to change its tap position during the day to avoid undervoltage since it operates in maximum position (tap = 1.1) during most of the day.

FIGURE 20 - VOLTAGE REGULATOR TAP CHANGES FOR 90 BUSES BASE CASE SCENARIO.

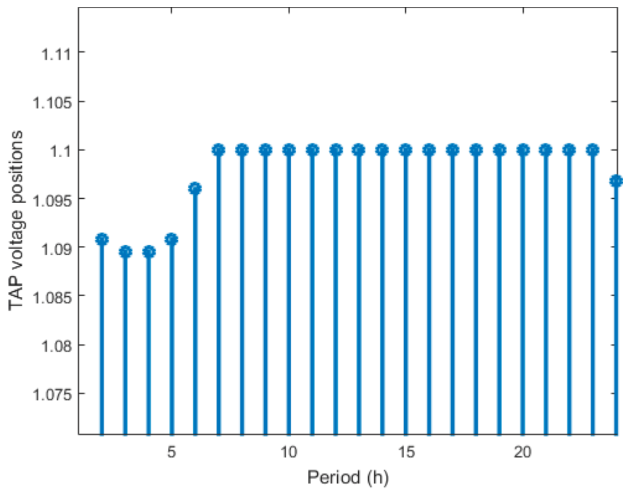

Source: The Author (2021).

4.3.2 Changing Voltage Support Equipment

In the sequence, some changes in voltage support equipment were considered. First, the VR was removed and only the capacitor banks were considered, in the sequency, the opposite was done, being removed the capacitor banks, and being considered just the VR operation. In both cases, undervoltage was found along the feeder, mainly in the branch where the VR is located, since at this branch the buses are prone to undervoltage.

In terms of power losses, for both cases, the values increased (3.45% and 3.96% respectively), being this effect reflected on prices since, with more losses, more power needs to be provided by the substation bus.

Assuming the allocation of the D-SVC at bus 57, in place of the fixed capacitor bank previously existing at this bus, the possibilities of removing either the voltage regulator or the fixed capacitor banks were considered. However, when VR is removed and it is considered only the D-FACTS and fixed capacitor banks for voltage support, the grid tends to violate the undervoltage restriction, whereas for the scenario with VR and D-SVC the grid can operate within proper voltage limits along all buses.

4.3.3 Including Distributed Generation

Considering the insertion of the distributed photovoltaic generation systems in the grid, an increase in the feeder loading level was also assumed, to evaluate the grid behavior in a higher load situation. In this way the daily demand for the feeder became 86.47 MWh.

Initially, the operation of PV systems was considered with fixed unity power factor. When this scenario is considered, there are no voltage violation problems in the grid. The power losses were reduced to 2.71% and the operating costs were reduced to 6,560.32 USD, since part of the demand is supplied by the PVs, reducing the demand for power provisioning by substation, as well as the reduction of the power flow in the lines since the DG systems are located close to the loads.

Monitoring the load flow behavior in the buses it can be observed that there is reverse flow in some regions of the feeder. This reverse power flow is absorbed by the loads located nearby and does not reach the substation bus. FIGURE 21 presented the reverse power flow values in each bus at 12h (time of the peak of solar generation).

FIGURE 21 - BUSES WITH REVERSE POWER INJECTION FOR 90 BUSES TEST CASE WITH DG AT 12H.

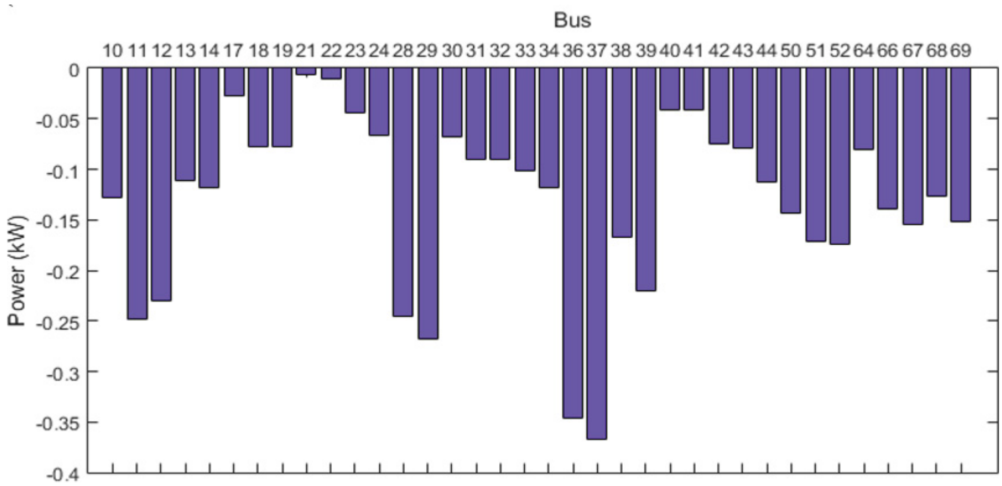

Source: The Author (2021).

In the sequence is considered the PV system inverters operation in a four-quadrant model with reactive power dispatch. In FIGURE 22 is presented the reactive power injection profile for each one of the DG systems. Some systems inject more reactive power into the system during peak load hours and perform lower injections during the period of higher active generation in the PV, since both injections are limited by the apparent power capacity of the inverter. As its reactive dispatch is affected by the reactive power balance in the region where the DG is located, as well as the voltage behavior, each DG will present its own reactive power dispatch characteristics, as presented at FIGURE 22.

FIGURE 22 - PV SYSTEMS REACTIVE POWER DISPATCH.

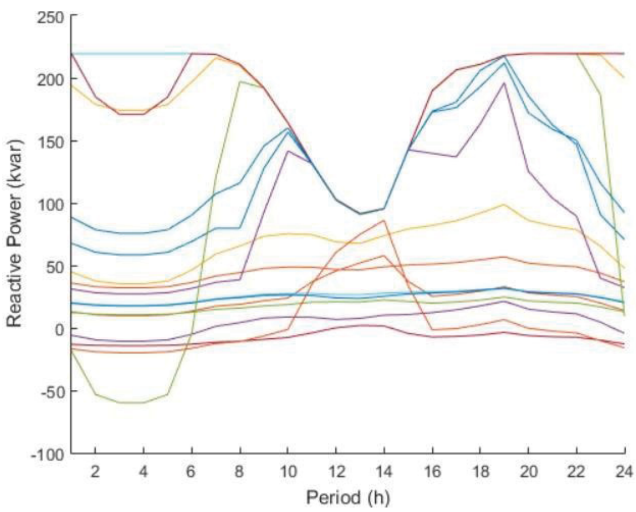

Source: The Author (2021).

When reactive dispatch happens, it is possible to operate the grid using only VR or fixed capacitor banks. However, it is important to emphasize that, in this work, PV systems owners have no benefit from contributing to the reactive dispatch of the grid.

In the scenario with reactive power dispatch, it was also obtained the reduction of power losses, being 2.26%, and a total operational cost of 6,519.98 USD (when operating in conjunction with VR and the previously existing capacitor banks in the grid).

The voltage behavior for all buses with the reactive power dispatch from the PV systems is presented in FIGURE 23. In this case is visible the increase of voltage levels during solar generation, due to the increase of active power provisioning and load supplied locally. During load peak time, there are no undervoltage in the circuit and the minimum voltage levels are higher than in the scenario without DG (FIGURE 19).

In comparison with the base case scenario, where no PV systems are considered (FIGURE 19), it is possible to see an improvement on voltage levels, especially during the solar generation period. Moreover, the minimum voltage values presented at bus 86 is higher than in the scenario without DG, however for buses close to the upper voltage level, in this scenario they get close to the volage limit during most part of the day.

FIGURE 23 - VOLTAGE BEHAVIOR FOR ALL 90 BUSES WITH 70% OF DISTRIBUTED GENERATION PENETRATION AND REACTIVE POWER DISPATCH.

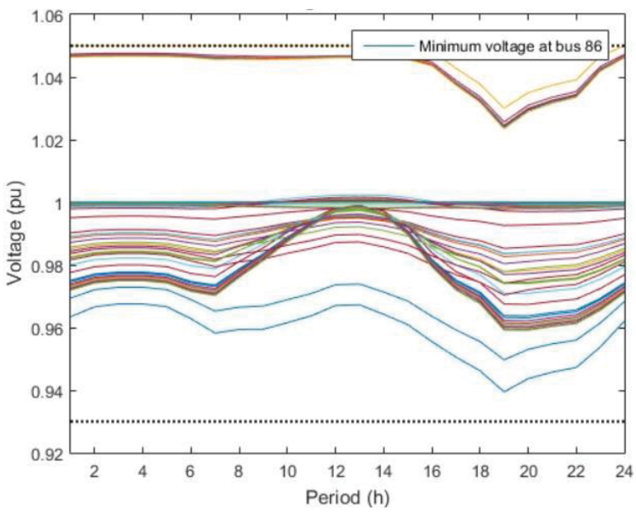

Source: The Author (2021).

If distribution grid could have 100% of DG penetration (which corresponds to the same DG and load installed power), there is a tendency to have problems with overvoltage at peak solar generation time, mainly because it does not coincide with the peak load of the feeder.

Running the simulation for this case, and do not considering the D-SVC and reactive dispatch from PVs, it is obtained the convergence of the optimization problem, however, the voltage behavior presents some problems. To keep voltage levels inside of acceptable levels, the substation bus presents 1.05 pu almost all day, and for the period with high solar generation levels, its voltage quickly changes to 0.98 pu, as shown at FIGURE 24, aiming to avoid overvoltage during the period of solar generation, since the load reduces at this point with the entrance of power generation.

With this voltage variation at the substation bus, all circuit buses present the same behavior and the entire circuit buses have high voltage changes due to the massive insertion of DG (FIGURE 25). In this case, the voltage decreases to avoid overvoltage, however, it goes close to the lower voltage limit, for the buses that don't present solar generation nearby and that usually present lower voltage profiles.

FIGURE 24 - SUBSTATION BUS VOLTAGE BEHAVIOR FOR 100% PENETRATION WITH NO D-SVC AND NO REACTIVE DISPATCH.

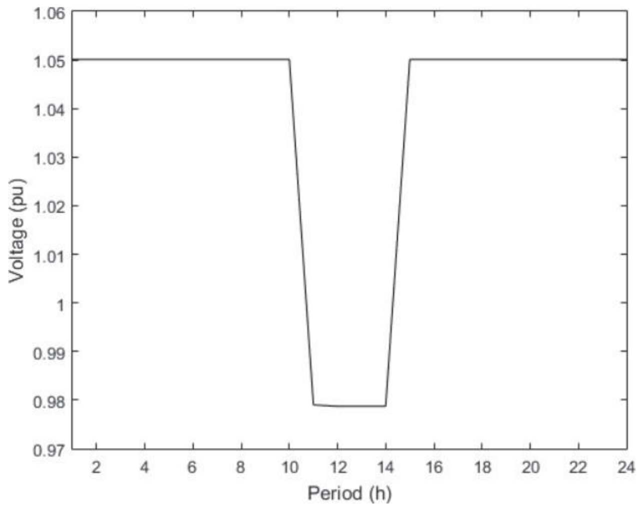

Source: The Author (2021).

FIGURE 25 - VOLTAGE BEHAVIOR FOR ALL BUSES FOR 90 BUSES TEST FEEDER WITH 100% PV PENETRATION WITH NO D-SVC AND NO REACTIVE DISPATCH.

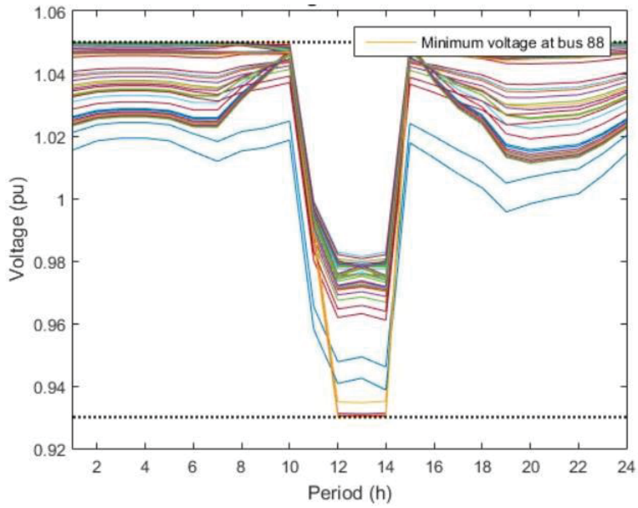

Source: The Author (2021).

In addition to the voltage variation at the substation bus, VR acts by reducing the TAP values during the solar generation period to avoid voltage problems in the downstream buses (FIGURE 26).

FIGURE 26 - VOLTAGE REGULATOR TAP CHANGES FOR 90 BUSES TEST FEEDER WITH 100% OF PV PENETRATION AND NO D-SVC AND NO REACTIVE DISPATCH

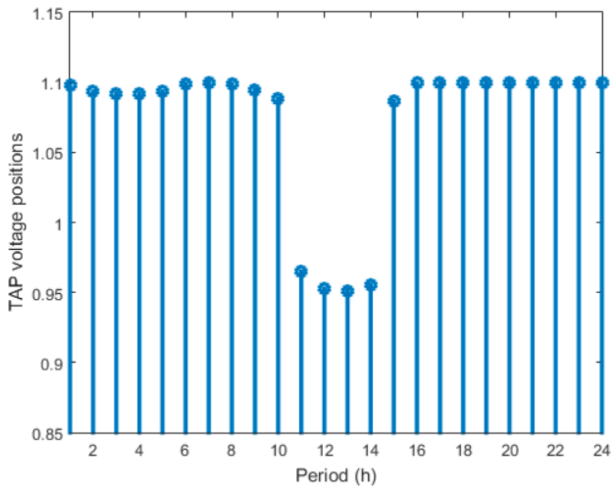

Source: The Author (2021).

Including the D-SVC operation, it is possible to consider 100% of penetration with smooth voltage changes on the circuit, keeping all voltage buses inside of the adequate range. At the substation bus behavior, presented in FIGURE 27, it is seen a lower voltage variability, being most of the day at 1pu and going to 0.98 pu during the solar generation period. In addition, the D-SVC changes its operation and starts absorbing reactive power during the period when there is an excess solar generation on the feeder (FIGURE 28).

Assuming the PV inverters with four-quadrant mode, some of these systems will start to absorb reactive power during the period of higher solar generation, as shown in FIGURE 29, contributing to mitigating possible overvoltage violations and allowing greater accommodation of DG systems on the grid. With the reactive injection/absorption from the inverters, the D-SVC operation is modified and starts to happen gradually throughout the day (FIGURE 30).

FIGURE 27 - SUBSTATION BUS VOLTAGE BEHAVIOR FOR 100% PV PENETRATION WITH D-SVC AND NO REACTIVE DISPATCH.

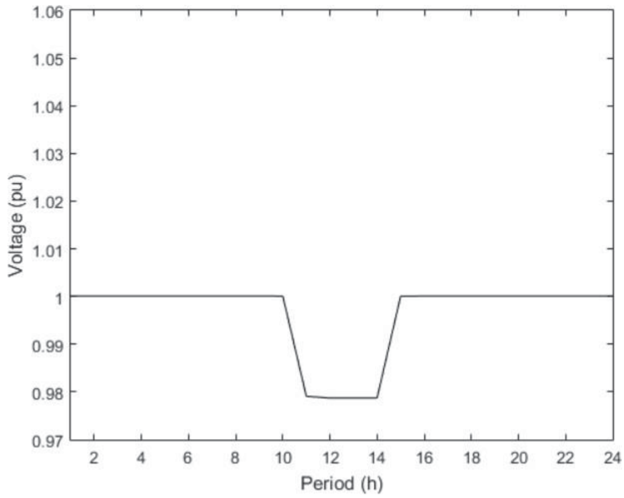

Source: The Author (2021).

FIGURE 28 - D-SVC BEHAVIOR AT 90 BUSES TESTS FEEDER WITH 100% OF PV PENETRATION WITHOUT REACTIVE DISPATCH.

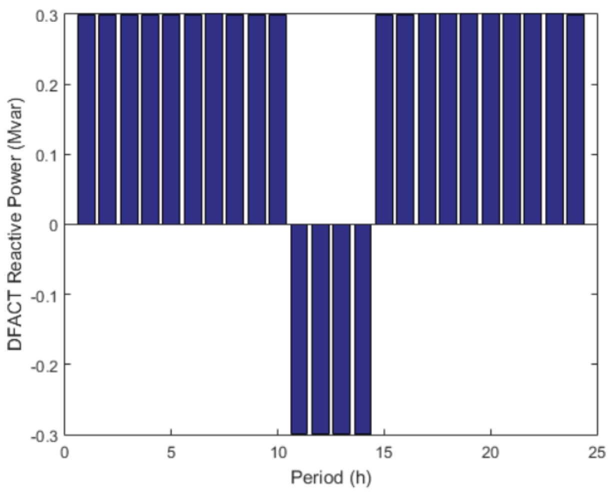

Source: The Author (2021).

FIGURE 29 - PV SYSTEMS REACTIVE POWER DISPATCH WITH 100% PENETRATION.

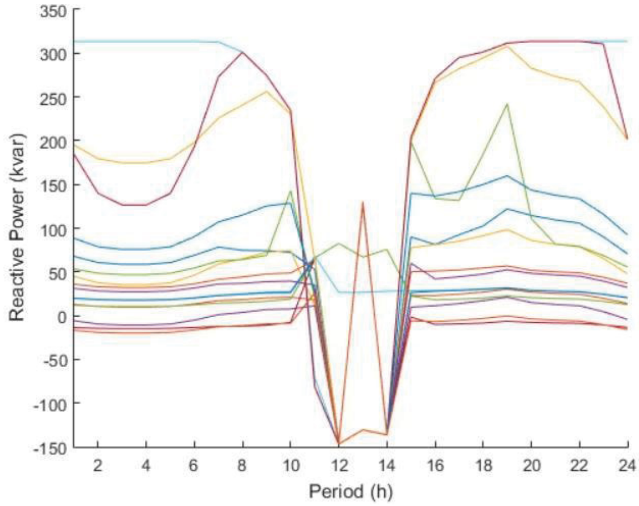

Source: The Author (2021).

FIGURE 30 - D-SVC BEHAVIOR AT 90 BUSES TEST FEEDER WITH 100% OF PV PENETRATION WITH REACTIVE DISPATCH.

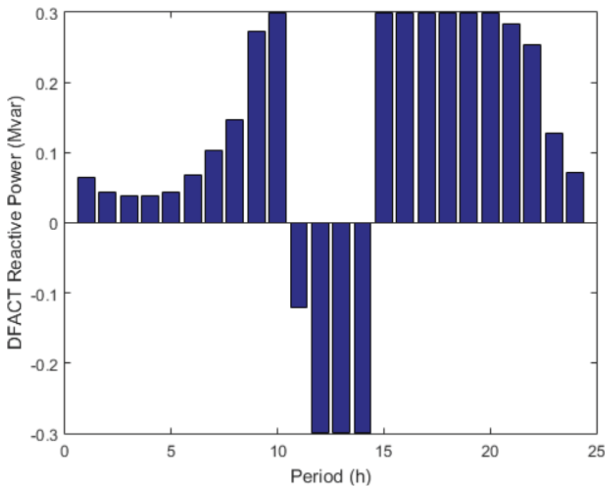

Source: The Author (2021).

For the scenario with PV generation and reactive power dispatch in addition to D-SVC operation, the voltage behavior of all buses is presented in FIGURE 31. In this case, there is still a decline in voltage levels, but not so strong as visualized in FIGURE 25 when there is no reactive power provisioning. In this case, as in the previous ones, when the maximum DG happens the voltage at the substation bus decreases to avoid overvoltages on the feeder buses. With reactive power support, the voltage reduction is not so abrupt as in the scenario without it.

FIGURE 31 - VOLTAGE BEHAVIOR FOR ALL 90 BUSES WITH 100% OF DISTRIBUTED GENERATION PENETRATION AND REACTIVE DISPATCH.

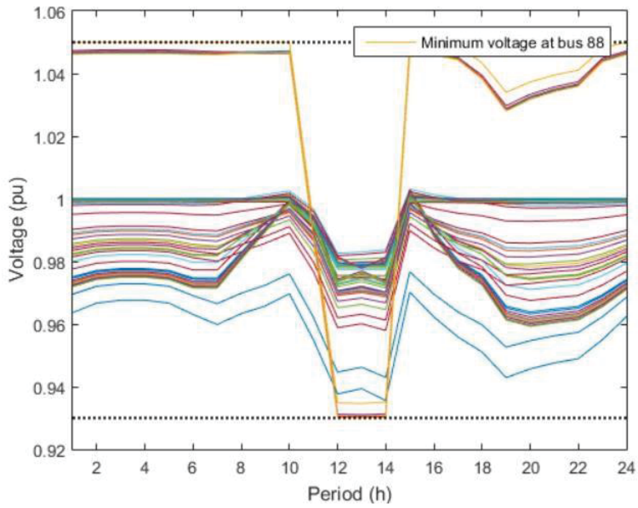

Source: The Author (2021).

TABLE 5 presents the comparison between the scenarios with PV systems integration to the distribution network. In the scenarios with 70% of penetration, as much reactive power provisioning is considered lower are the power losses, since it is possible to increase the active power generation and load supplying locally, without voltage violations, and thus reduce the power that comes from substation through the lines to the loads.

With the D-SVC operation it was possible to get even lower losses and costs, since with reactive power provisioning by the custom power device, the inverters of DGs can provide less reactive and more active power to the system, regarding the apparent power limitation. Additionally, all loads can be supplied by distributed generators during part of the day, then no power needs to be provided by the substation, which contributed to costs reduction. As the solar generation happens only in part of the day, even with 100% of penetration, the operational cost is not equals to zero, since the entire day operation is considered.

With a 100% penetration of distributed generation, there is reverse flow at the substation bus, which for real circuit applications can result in problems in the settings of control and protection equipment. FIGURE 32 shows the reverse power flow at the substation bus at 12h.

TABLE 5 - RESULTS AFTER THE ALLOCATION OF PV SYSTEMS.

Scenario	Power Losses	Operational Costs (USD)
70% PV (pf=1)	2.71%	6,560.32
70% PV (RD)	2.26%	6,519.98
70% PV (RD) + D-SVC	2.19%	6,547.70
100% PV (pf=1)	2.16%	5,640.60
100 % PV (pf=1) + D-SVC	2.07%	5,662.26
100 % PV (RD) + D-SVC	2.09%	5,654.90

* RD: Reactive Dispatch

Source: The Author (2021).

FIGURE 32 - BUSES WITH REVERSE POWER FLOW FOR 90 BUSES TEST FEEDER WITH 100% OF PV PENETRATION AT 12H.

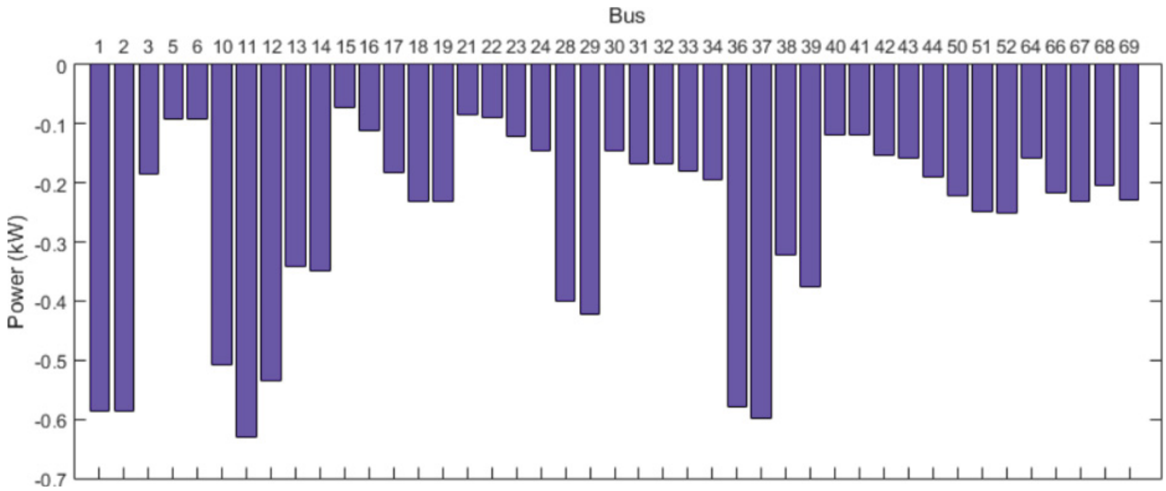

Source: The Author (2021).

For all next scenarios will be considered the distributed generators penetration level of 70%, which corresponds to high penetration, and allows the evaluation of the largest number of possible scenarios with the placement of other equipment.

4.3.4 Inserting Electric Vehicles

With the insertion of electric vehicles (EVs) chargers on the grid, when nighttime charging is considered, the impact on grid operation is lower, since the load increase happens during the feeder's light load period. In addition, it is verified that the grid operation costs are also lower due to the behavior of the applied tariff.

Yet, when daytime charging is considered, the load increase on the feeder occurs at the time of solar generation, which contributes to the reduction of reverse power flow within the feeder, also reducing losses. By comparing the grid operation costs with the entry of daytime charging of EVs there is only a 2% increase in operational costs.

When considering the reactive dispatch of the PV systems, there is a significant improvement in the voltage profile when considering the daytime charging of the EVs. If D-SVC is introduced in this scenario, the voltage profiles present higher values, with the minimum voltage value being 0.935 pu for bus 86, and no voltage values lower than 0.95 for the other buses. Regarding overvoltage, this does not occur in any case.

With the operation of D-SVC, the losses in the circuit decreased 8% in comparison with the scenario where there is only the dispatch of reactive power from the PVs. It is also observed that most of the reactive power is supplied by the PV systems throughout the day, with a reduction in the supply during solar generation, as shown in FIGURE 33, due to the apparent power limit of the inverters.

FIGURE 33 - REACTIVE POWER BALANCE AT THE SUBSTATION BUS FOR 90 BUSES TEST FEEDER WITH PV, EV CHARGING AT DAYTIME, AND D-SVC.

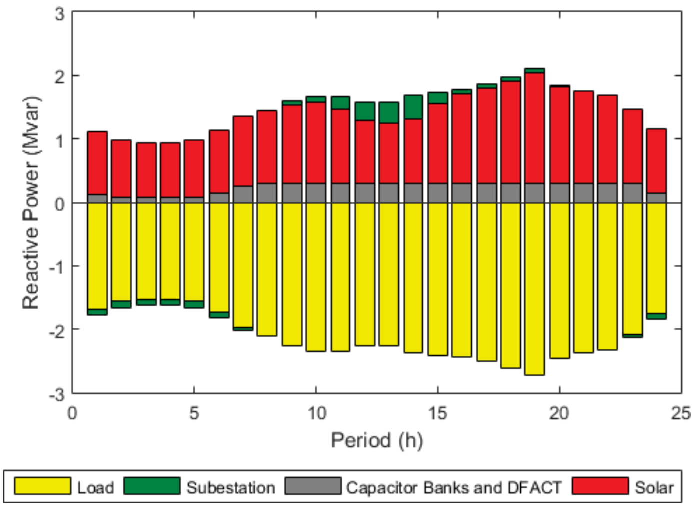

Source: The Author (2021).

4.3.5 Inserting Battery Energy Storage Systems

Returning to the grid structure with only photovoltaic systems (unit power factor), the battery storage system was included, being initially placed at the substation bus (with the power factor set at 0.92).

Considering this application, the BESS will operate in a load shedding mode, doing its charging during the period of solar generation. At this time, it has load relief at the substation bus, and the discharge occurs during the peak load period since this is the most expensive time for the system, and the one that tends to present the greatest number of problems in the operation due to the demand growth. This behavior is presented in FIGURE 34, with the power profile realized by the BESS. In FIGURE 35 the State-of-Charge (SOC) of the battery at each time is presented, being demonstrated that it charges until reaches its full capacity (100%) and discharged regarding the maximum DoD (70%).

FIGURE 34 - BESS ACTIVE POWER BEHAVIOR WHEN CONNECTED AT THE SUBSTATION BUS.

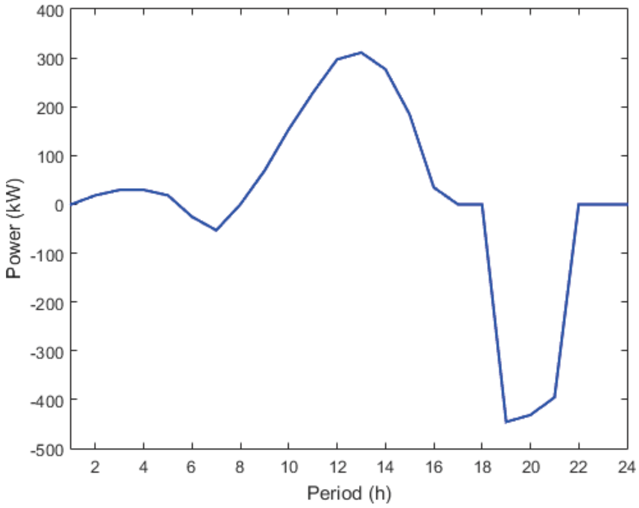

Source: The Author (2021).

FIGURE 35 - BESS STATE-OF-CHARGE (SOC) WHEN CONNECTED AT THE SUBSTATION BUS.

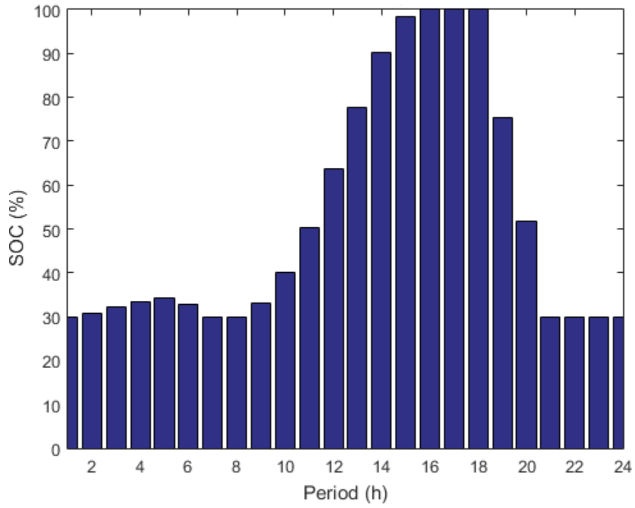

Source: The Author (2021).

For this scenario, the grid operational costs were 6,459.83 USD which are added to the depreciation costs of the storage system, which corresponds to 1,177.92 USD. As for losses, the values obtained were the same as in the scenario with the only DG with unity power factor. This happens since with the battery allocated at the substation bus there is no difference in the power flow that flows through the lines until it reaches the loads.

Considering the possibility of reactive dispatch only by the battery system, with the system allocated at the substation bus there are no operational benefits to the grid.

Changing the positioning of the BESS in the grid and allocating it at bus 8, it was possible to reduce costs and losses since the BESS is close to the loads. Besides performing the load-shedding function, the storage system also contributes to voltage regulation, especially when considering the system's reactive dispatch, being one more equipment capable of supply/absorb reactive power according to the grid needs. With the application of reactive dispatch by the battery, it is verified that, in terms of losses and costs, the D-SVC does not present significant improvements, as well as when verified the behavior of voltage levels. These results are compared in TABLE 6.

TABLE 6 - RESULTS AFTER THE ALLOCATION OF THE BESS AT BUS 8.

Scenario	Power Losses	Operational Costs (USD)	Battery Degradation Costs (USD)
PV (pf=1) + BESS (pf=0.92)	2.56%	6,454.90	1,180.17
PV (pf=1) + BESS (RD)	2.47%	6,447.02	1,179.91
PV (RD) + BESS (RD)	2.23%	6,423.85	1,179.25
PV (RD) + BESS (RD) + D-SVC	2.22%	6,424.99	1,179.25

* RD: Reactive Dispatch

Source: The Author (2021).

For the simulations with batteries, it is seen that the optimization process realized by the MPOPF needs more iterations to reach convergence, going from an average of 10 iterations for the simulations without BESS to 25 iterations with the insertion of the BESS, since it needs to optimize the charging and discharging process as well as the usage of stored energy.

4.3.6 Inserting Flexible Loads

To consider the operation of flexible loads, an increase in the feeder loading level was considered, the operational restrictions can be reached, therefore, load shedding will be necessary.

Considering the network with PV (pf = 1) and the new load, it was possible to reach the convergence of the optimization process when load shedding is performed at the buses that present this functionality. The highest demand reduction happened at bus 64 since the downstream bus 86 is the most prone to undervoltage.

Avoiding load shedding, it is possible to perform load shifting when part of the load was changed from peak time to periods with lower demand in the grid. This behavior is illustrated in FIGURE 36, where the load demand at bus 64 is changed from peak time and distributed along the day, totalizing the same daily energy consumption.

FIGURE 36 - DIFFERENCE BETWEEN ESTIMATED AND REALIZED LOAD PROFILES AT BUS 64 WITH DSM.

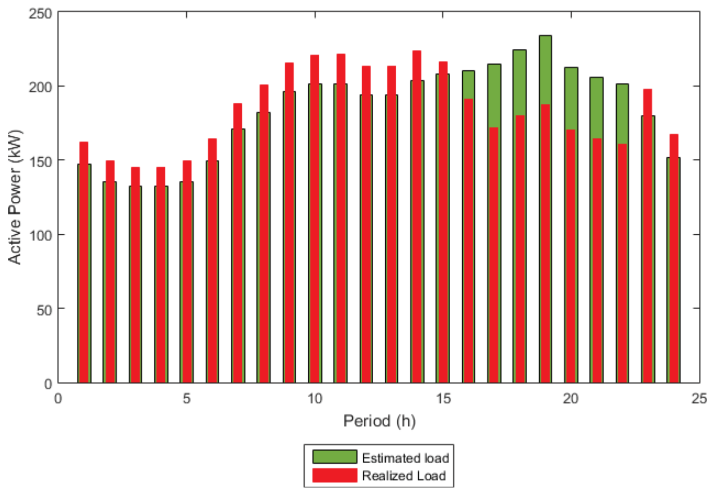

Source: The Author (2021).

With load shifting availability and reactive dispatch from BESS and PVs it is possible to reduce the amount of load that is shifted, as well as reduce power losses and operational costs (2.6% of cost reduction). Moreover, improvements in the voltage levels are obtained, with the minimum voltage happening at bus 86 with 0.94 pu, and for all other buses, the minimum voltage reached 0.95 pu.

4.3.7 Inserting Microgrids

Presuming the operation of microgrids in placement of flexible loads, as aforementioned in section 4.2, when the power grid presents only load and PV generation, it is possible to get the optimization convergence without changes in the proposed operation of the microgrids (FIGURE 37). For this scenario, the operational costs are reduced, since there is low load in the main grid, due to the disconnection of the MGs during part of the day, besides the provisioning of power from the MGs to the grid during the peak period.

FIGURE 37 - ESTIMATED AND REALIZED LOAD PROFILES FOR THE MICROGRID PLACED AT BUS 64.

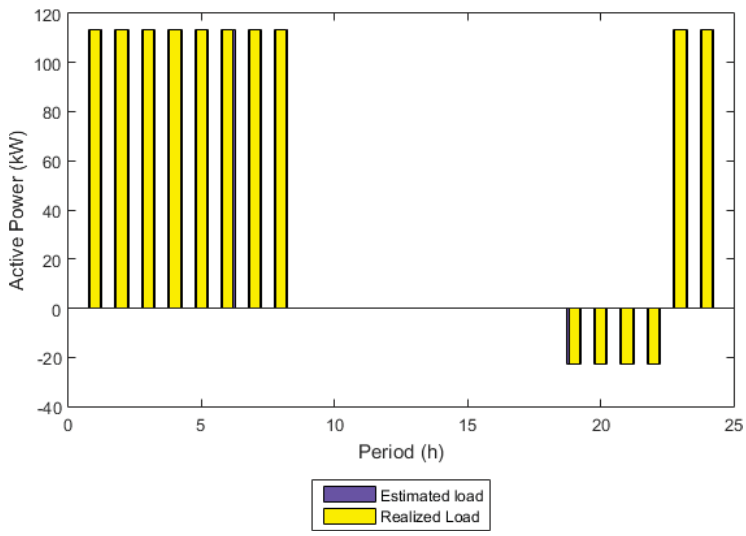

Source: The Author (2021).

Assuming the possibility of a load increase in the feeder or even in the microgrids, it could be necessary to propose a new behavior for the MGs to ensure a safe operation of the distribution grid. In this case, it is up to the DSO to inform the expected profile for the internal control of the MGs allowing the provisioning of a new operation plan to be run with the MPOPF, as shown in FIGURE 38.

FIGURE 38 - ESTIMATED AND REALIZED LOAD PROFILES FOR THE MICROGRID PLACED AT BUS 64 AFTER THE MPOPF LOAD SHEDDING, RESULTING IN A PROPOSITION OF A NEW MG PROFILE (YELLOW).

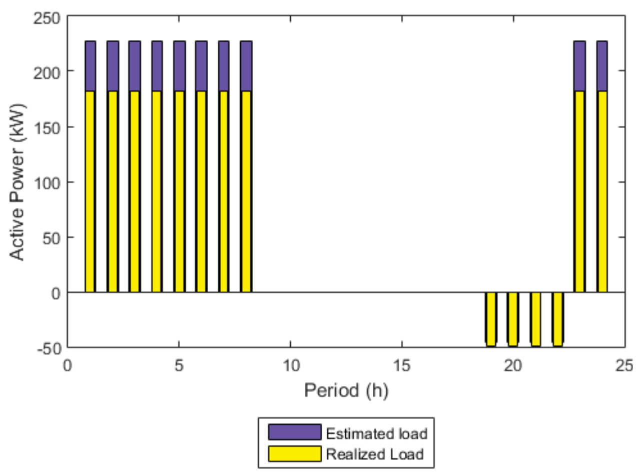

Source: The Author (2021).

The network behavior was evaluated with the insertion of multiple microgrids, and the previously tested equipment was gradually associated. The results regarding losses and costs are presented in TABLE 7. For scenarios 1 to 6, it was considered only the possibility of load shedding of the MGs by the DSM, resulting in a total demand of 84.74 MWh for scenarios 1,2 and 3, 87.74 MWh for scenarios 4 and 5, 85.85 MWh for scenario 6 and finally 86.42 MWh for scenario 7, which present load shifting realized from DSM of the MGs. This variation in daily demand values is a result of the proposed load shedding percentage for each of the scenarios. With the connection of D-SVC, it was possible to increase load supplying and still obtain the lowest percentage levels of circuit losses. With the entry of EVs, and therefore the increase in the unmanageable load, it was necessary to cut part of the microgrid load, resulting in lower demand throughout the day. In the last scenario, however, with the possibility of load shifting, it was possible to increase the demand supplied compared to scenario 6 since, instead of cutting the load of the MGs, it was proposed to shift them.

TABLE 7 - RESULTS FROM DIFFERENT SCENARIOS AFTER GRADUALLY EQUIPMENT CONNECTION.

Scenario		Power Losses (%)	Operational Costs (USD)	BESS Degradation Costs (USD)
1	MG + DSM + PV (pf = 1)	1,37	6,258.65	-
2	MG + DSM + PV (RD)	1,29	6,250.92	-
3	MG + DSM + PV (pf =1) + BESS (RD)	1,33	6,161.40	1,174.58
4	MG + DSM + PV (RD) + BESS (RD)	1,23	6,155.65	1,174.36
5	MG + DSM + PV(RD) + BESS (RD) + D-FACTS	1,22	6.155,54	1,174.36
6	MG + DSM + PV(RD) + BESS (RD) + D-FACTS + VEs	1,29	6,260.82	1,174.35
7	MG + DSM (load shifting) + PV(RD) + BESS (RD) + D-FACTS + VEs	2,00	6,310.32	1,172.90

* RD: Reactive Dispatch

Source: The Author (2021).

The most interesting results came from scenario 7, in which all equipment is considered connected to the grid simultaneously, requiring lots of decisions from the MPOPF. In this way, the following figures present some results from this scenario. FIGURE 39 and FIGURE 40 present the active and reactive power balances at the substation, respectively.

From FIGURE 40 it is visible the operation of D-SVC in addition to fixed capacitor banks since its behavior varies along the day, being detailed in FIGURE 41. With the possibility of reactive dispatch from many types of equipment, the substations started to absorb part of the reactive power through the system.

FIGURE 39 - ACTIVE POWER BALANCE AT THE SUBSTATION BUS FOR 90 BUSES TEST FEEDER AT SCENARIO 7.

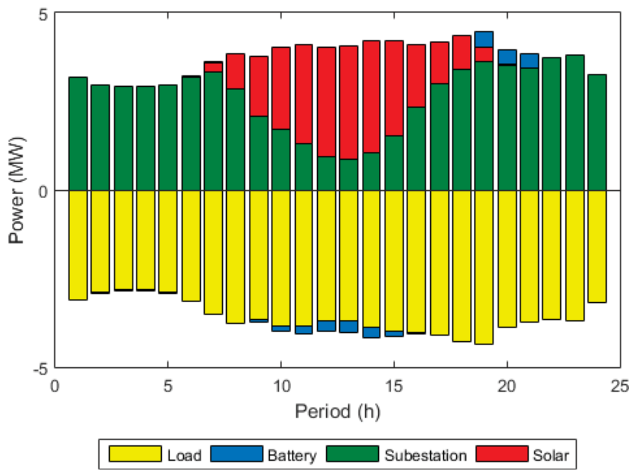

Source: The Author (2021).

FIGURE 40 - REACTIVE POWER BALANCE AT THE SUBSTATION BUS FOR 90 BUSES TEST FEEDER AT SCENARIO 7.

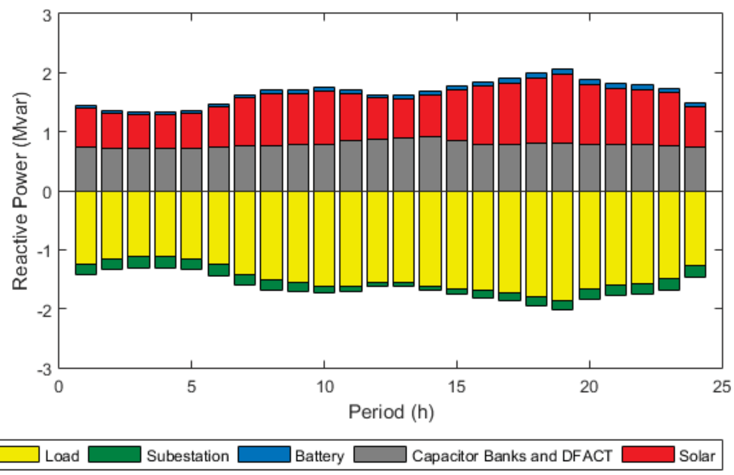

Source: The Author (2021).

FIGURE 41 - D-SVC BEHAVIOR AT SCENARIO 7.

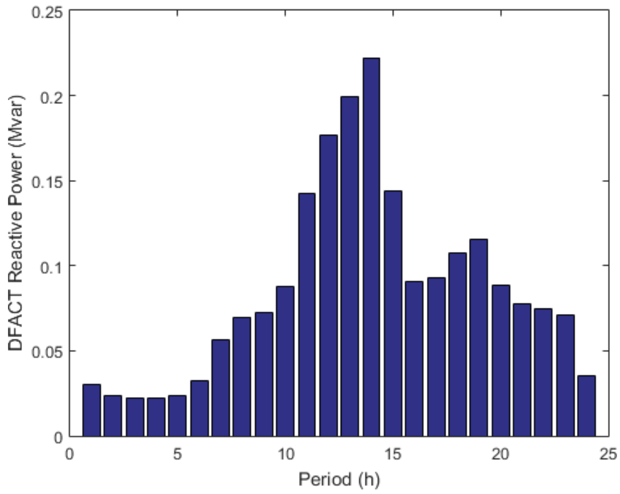

Source: The Author (2021).

With the implementation of the reactive control in different devices, the voltage levels increase significantly, in a way that all buses present values inside of the adequate range during all day, as seen in FIGURE 42.

FIGURE 42 - VOLTAGE BEHAVIOR FOR ALL 90 BUSES AT SCENARIO 7.

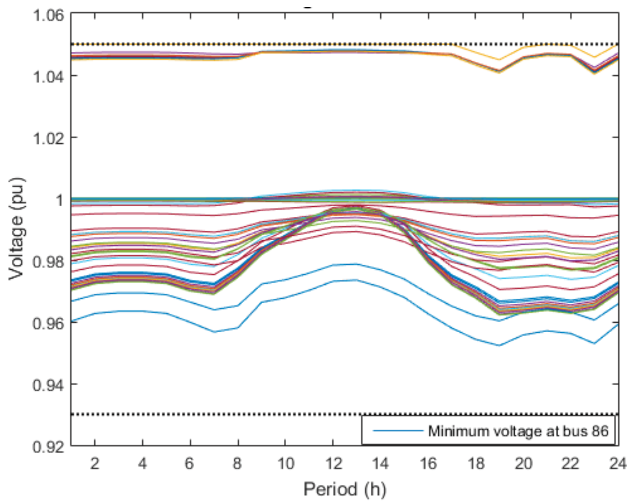

Source: The Author (2021).

Concerning the microgrid operation in scenario 7, just small changes were required by the DSO, being the biggest one at the MG located at bus 64, in which is proposed a load reduction at 7h and 22h, being this demand relocated during the period from 2-5h and at 8h, as shown at FIGURE 43.

FIGURE 43 - ESTIMATED AND REALIZED LOAD PROFILES FOR THE MICROGRID PLACED AT BUS 64 AT SCENARIO 7.

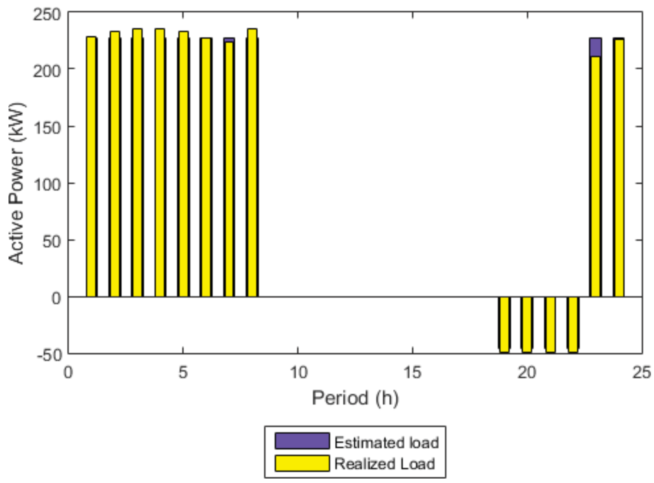

Source: The Author (2021).

Regarding the optimization convergence of the MPOPF for scenario 7, it happened in 29 iterations.

4.4 REAL DISTRIBUTION GRID APPLICATION

4.4.1 REAL DISTRIBUTION GRID DESCRIPTION

Another circuit was simulated with the MPOPF proposed, but now corresponding to a distribution system from Curitiba, Paraná, Brazil. According to the data provided by the COPEL power utility, this feeder presents 2,119.08 kW of installed power, of which 38% corresponds to low voltage consumers and 62% to medium voltage consumers and it has 359 buses and 358 lines. The drawing of the feeder is illustrated in FIGURE 44.

From FIGURE 44 legend ssdbt means low voltage lines; ssdmt are medium voltage lines, sub corresponds to the substation; ucbt is the low voltage consumers; ucmt are medium voltage consumers; unsemt are medium voltage switches, and untrd are distribution transformers that connect LV to MV (there are a total number of 64 in the circuit).

FIGURE 44 - REAL DISTRIBUTION FEEDER.

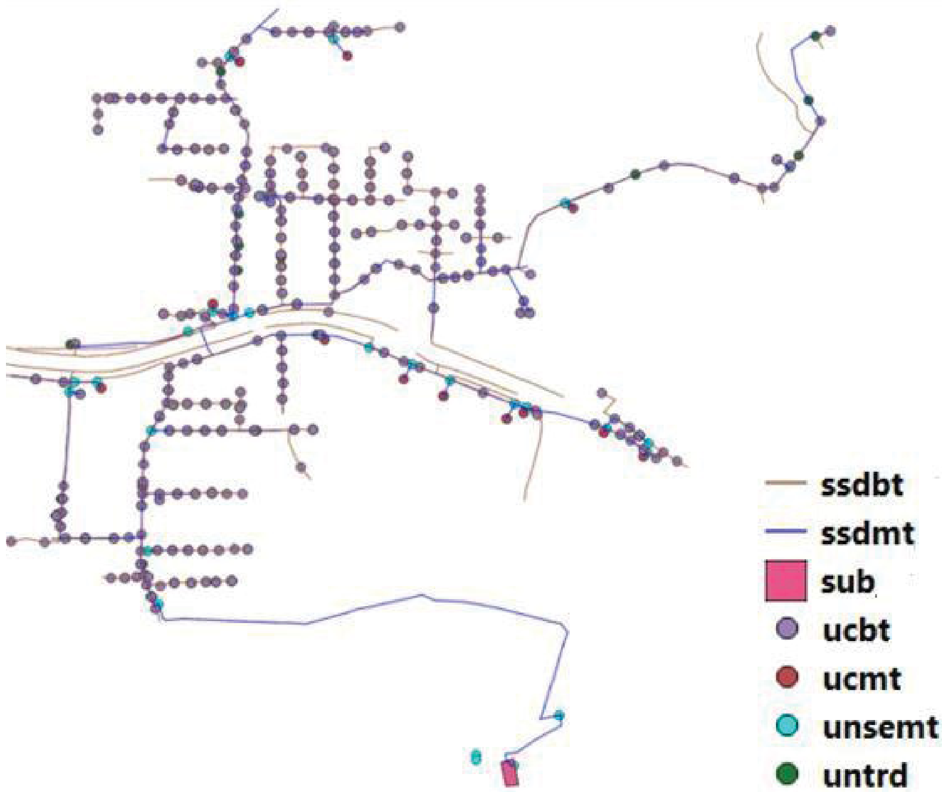

Source: The Author (2021).

For the load profile, real data information was used in the correspondent scenarios of summer and winter. Analyzing the load data of an entire month, the mean value and the standard deviation around the mean are represented in FIGURE 45 for summer and in FIGURE 46 for winter. Those profiles were normalized and applied for all load buses in the circuit.

FIGURE 45 - ACTIVE POWER PROFILE FOR REAL DISTRIBUTION FEEDER FOR SUMMER, BEING THE FILLED LINE THE MEAN AND THE DASHED LINE THE STANDARD DEVIATION AROUND THE MEAN.

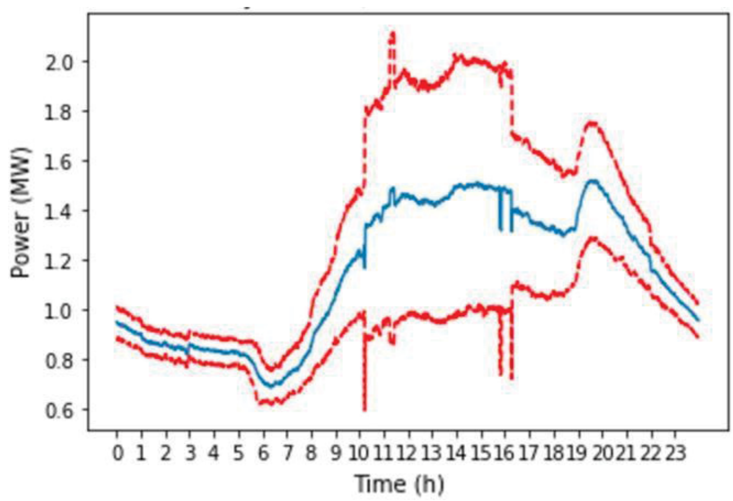

Source: The Author (2021).

FIGURE 46 - ACTIVE POWER PROFILE FOR REAL DISTRIBUTION FEEDER FOR WINTER, BEING THE FILLED LINE THE MEAN AND THE DASHED LINE THE STANDARD DEVIATION AROUND THE MEAN.

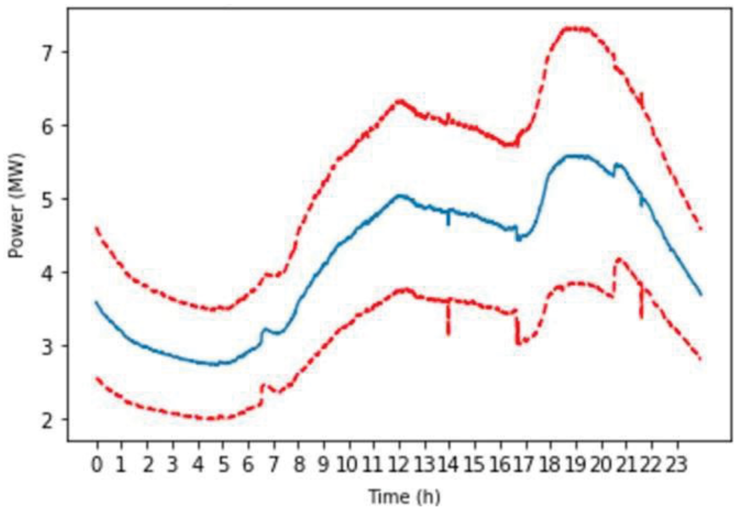

Source: The Author (2021).

Additionally, to the load profile analysis, the energy consumption values were also evaluated, allowing the definition of a load utilization factor in order that the total energy consumption of the simulated month presents the same value of the real measurements. For the summer months the energy consumption in the feeder is 27 MWh/day and for the winter it is 100 MWh/day.

Following Brazilian grid characteristics, circuit voltage levels are 220/127 V for LV and 13.8 kV for MV, and the frequency is 60 Hz.

Another important characteristic of the real distribution system is related to the voltage level at the substation bus. Following the technical norm NTC 905100 of Paraná State Power Utility - COPEL (COPEL, 2017) the substation voltage should change according to the demand level of the circuit, presenting the values defined in TABLE 8.

TABLE 8 - SUBSTATION VOLTAGE VALUES ACCORDING TO LOAD LEVELS

Load Stage	Minimum Voltage (pu)	Maximum Voltage (pu)	Period
Heavy	0.9927	1.00	18h00 – 22h00
Intermediate	0.9783	0.9927	08h00 – 17h00 23h00 – 00h00
Low	0.9565	0.9783	00h00 – 07h00

Source: COPEL (2017).

This feeder does not present any voltage regulator, capacitor bank, or D-FACTS allocated, not even DG or BESS.

In the context of the Research and Development (R&D) project PD-02866-0511/2019, a real microgrid was connected to this feeder, working as a pilot project connected to the distribution feeder. This microgrid is placed at Barigui Park, which is the largest public park in Curitiba City, and is composed of photovoltaic solar generation, battery energy storage, flexible loads, and a carport system.

To evaluate its integration with the real distribution feeder, the MPOPF methodology presented in this paper will be integrated in a hierarchical way of control, communicating with microgrid internal optimization control. It will be considered different operational schedules for MG, being evaluated in two different seasons: summer and winter, illustrated in FIGURE 47 and FIGURE 48, respectively.

FIGURE 47 - TYPICAL ACTIVE POWER SCHEDULE FOR THE MG IN SUMMER.

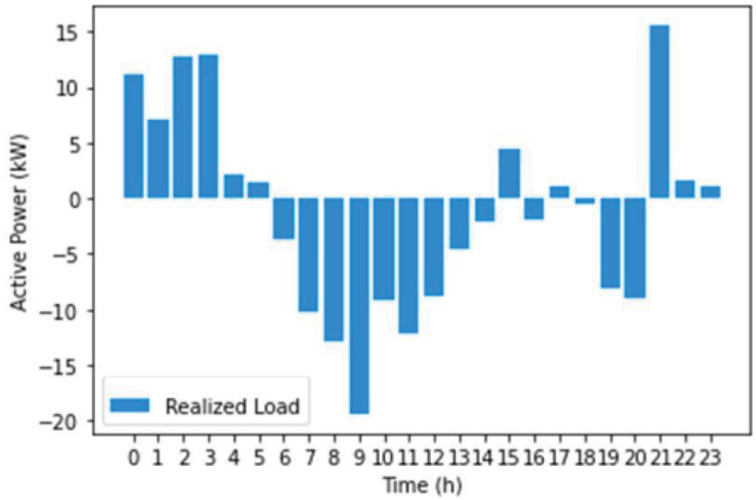

Source: The Author (2021).

In addition, for the present study, the distribution grid will be transformed into an ADN, with solar DG penetration and the placement of a BESS system. It is important to highlight that these elements aggregated on the grid for the study will be modeled in the same way that was previously done for the 90 buses test feeder.

FIGURE 48 - TYPICAL ACTIVE POWER SCHEDULE FOR THE MG IN WINTER.

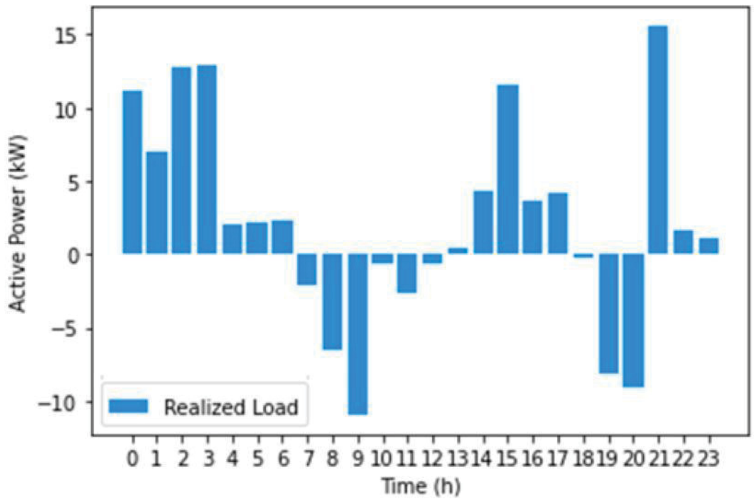

Source: The Author (2021).

Regarding the MPOPF execution, aiming to improve the computational time, especially for the real feeder, a new strategy was proposed, as illustrated in FIGURE 49 flowchart. As the real feeder has many buses (a total of 359 buses), and the incidence matrices are sized as (*nb.nper*), the computational time spent to build these matrices is high. Since some of the matrices building only depends on the graph characteristics of the circuit, a pre-processing was defined, resulting in the storage of the matrices. For the different scenarios, only the optimization process needs to be executed. So, getting access to the pre-defined matrices, the optimization can be processed much more quickly than when the matrices organization is considered inside of the entire process. The computational times to run these simulations will be presented later.

FIGURE 49 - FLOWCHART OF NEW STRATEGY OF MPOPF DIVIDED INTO PRE-PROCESSING AND OPTIMIZATION PROCESS.

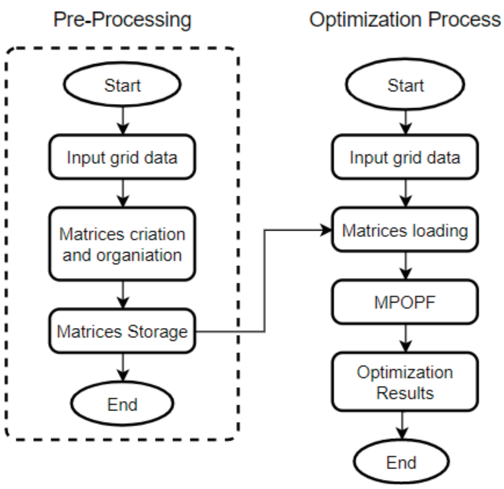

Source: The Author (2021).

4.4.2 REAL DISTRIBUTION GRID RESULTS

As presented at section 3.5 the objective function of the MPOPF has some weights defined to distribute the importance of the multiple goals that are being optimized.

Those values are defined by the execution of innumerous tests and combinations until the best simulation results is achieved. As aforementioned, the sum of all weights should be equal to one, so a normalization process can be performed to reach this condition.

For the real feeder simulations, the values of the weights for each simulation scenario are presented at TABLE 9.

TABLE 9 - NORMALIZED VALUES OF OBJECTIVE FUNCTION WEIGHTS

Weights	Base Case	RF*+MG	RF+MG+PV	RF+MG+PV+BESS
w_c	0.5	0.045	0.045	0.036
w_p	0.5	0.045	0.045	0.036

w_{bat}	-	-	-	0.163
w_{load}	-	-	-	0.036
w_{gd}	-	0.455	0.455	0.363
$w_{targetload}$	-	0.455	0.455	0.363

*RF: Real Feeder

Source: The Author (2021).

4.4.2.1 Real Feeder – Base Case

For the real feeder, the base case corresponds to the current grid configuration, that is, with the only load installed. The total daily energy consumption is 27 MWh for summer months and 100 MWh for winter. Considering these load demand and the load behavior for the two scenarios considered, this feeder presents total power losses of 0.35% (94 kWh) and a total operational cost of 2,687.48 USD for summer, and 1,26% (1.26 MWh) of losses and 9,987.78 USD of cost for winter load profiles.

The active power balance in this scenario is presented in FIGURE 50 (summer) and FIGURE 51 (winter), being all the power load supplies by substation power injection.

FIGURE 50 - ACTIVE POWER BALANCE FOR REAL DISTRIBUTION FEEDER ON BASE CASE SCENARIO FOR SUMMER (SE IS THE SUBSTATION BUS).

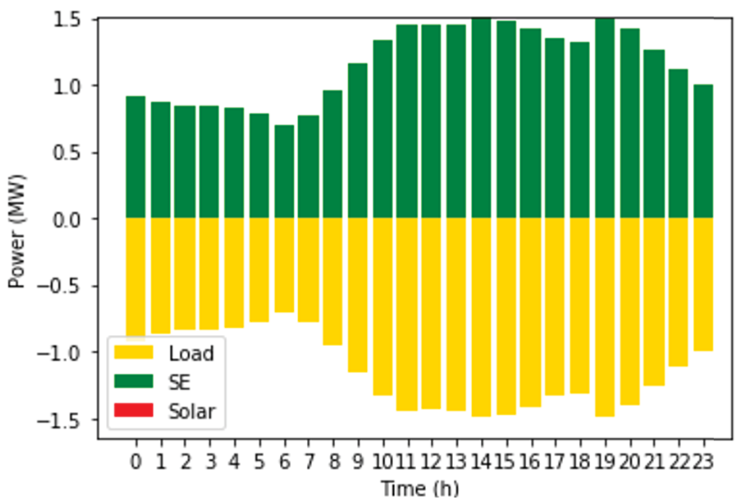

Source: The Author (2021).

FIGURE 51 - ACTIVE POWER BALANCE FOR REAL DISTRIBUTION FEEDER ON BASE CASE SCENARIO FOR WINTER.

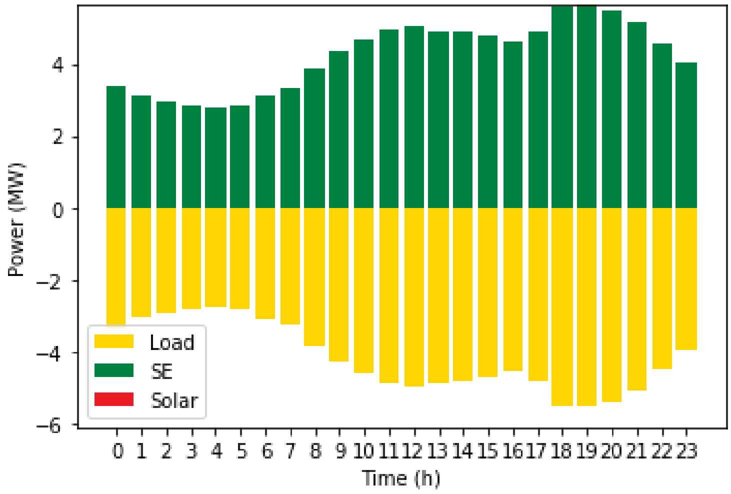

Source: The Author (2021).

Voltage behavior for all buses is presented in FIGURE 52 and FIGURE 53, in which is seen the voltage levels at the substation bus as previously defined in TABLE 8. For all other circuit buses, there are no voltage violations, and the behavior changes following the corresponding load variation.

FIGURE 52 - VOLTAGE BEHAVIOR FOR ALL BUSES IN REAL FEEDER BASE CASE FOR SUMMER LOAD PROFILE.

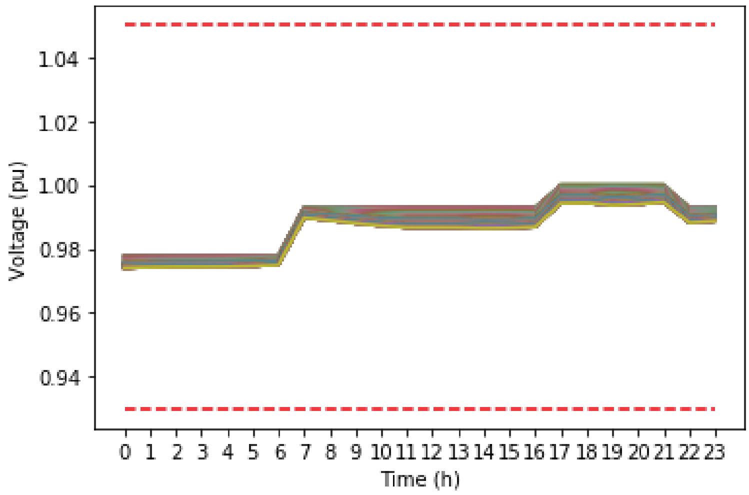

Source: The Author (2021).

FIGURE 53 - VOLTAGE BEHAVIOR FOR ALL BUSES IN REAL FEEDER BASE CASE FOR WINTER LOAD PROFILE.

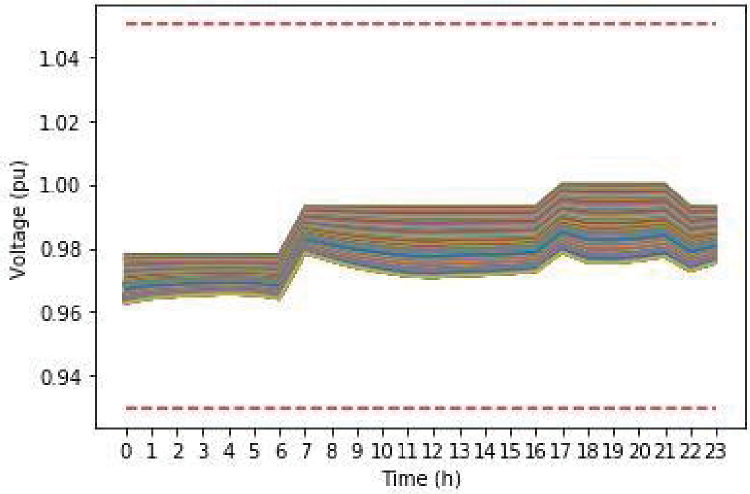

Source: The Author (2021).

4.4.2.2 Real Feeder with the Connection of the Pilot Microgrid

For the operation of the pilot microgrid, an internal optimization was developed and result in the load profiles shown in FIGURE 47 and FIGURE 48. This load profile was applied at the bus where the microgrid is connected.

From the results, the operational costs were lower than in the base case scenario. This happens since there is power injection from the microgrid during some periods and the power demand in this point of the circuit is also lower in comparison to the case when it was just a load. The values obtained with the MG operation are presented in TABLE 10.

Concerning the voltage behavior, it was similar to the one seen for the base case scenario (FIGURE 52 and FIGURE 53) since the levels of power injected and consumed by the microgrid are small compared to the feeder demand.

TABLE 10 - RESULTS FROM THE REAL FEEDER WITH MICROGRID CONNECTION FOR DIFFERENT LOAD AND MICROGRID PROFILES.

Real Feeder with MG	Power Losses	Operational Costs
Summer Profiles	0,33%	2,630.44 USD
Winter Profiles	1.27%	10,103.89 USD

Source: The Author (2021).

Regarding the behavior of the microgrid, there was no need to propose another operation point for it since the result of its internal planning allowed an operation point that that does not violate any operation condition of the power grid.

FIGURE 54 presented the active power balance with the small power injection from the microgrid (black).

FIGURE 54 - ACTIVE POWER BALANCE FOR REAL DISTRIBUTION FEEDER WITH THE CONNECTION OF THE MICROGRID FOR WINTER.

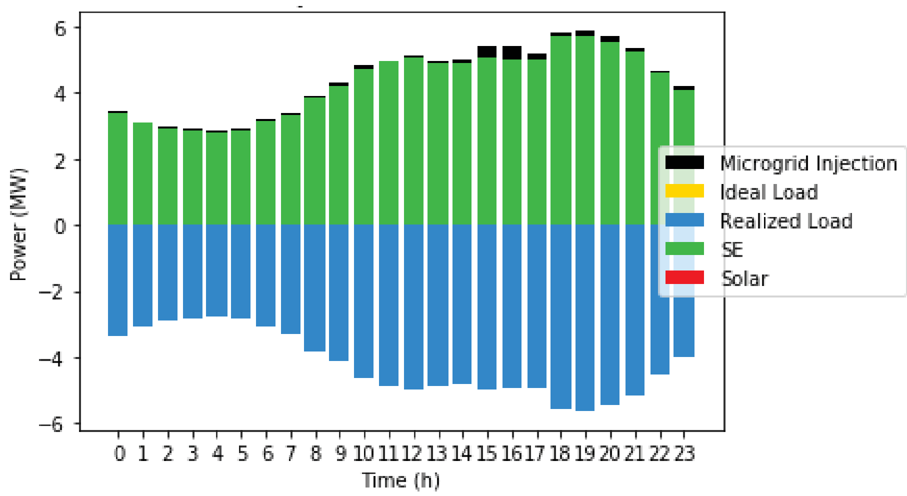

Source: The Author (2021).

4.4.2.3 Real Feeder as Active Distribution Network

Considering a future scenario in which the feeder starts to present the connection of more distributed energy resources in addition to the microgrid, the analysis was performed assuming a 30% penetration of distributed generation in this feeder. The allocation of this penetration was done proportionally in the load buses, considering that part of the equivalent loads modeled in each bus may present PV systems.

TABLE 11 shows the results when it was simulated the 30% of PV penetration during summer and winter scenarios of load and MG.

TABLE 11 - RESULTS FROM REAL FEEDER WITH MICROGRID CONNECTION FOR 30% OF PV PENETRATION AT SUMMER AND WINTER SCENARIOS.

30% PV penetration scenarios	Power Losses	Operational Costs
Summer	0,26%	2,327.06 USD
Winter	1,02%	8,969.46 USD

Source: The Author (2021).

With the introduction of solar photovoltaic generation, the power losses decrease, since part of the load is supplied by the existing generation nearby, reducing the amount of energy that needs to be delivered by the substation. In terms of voltage behavior, there is an increase in voltage values during the solar generation period for almost all buses, as seen in FIGURE 55 in comparison with FIGURE 52.

At least, a BESS was connected in a point of the where 80% of the load is located downstream. For this analysis 30% of PV penetration was considered and the scenarios of summer and winter were evaluated.

FIGURE 55 - VOLTAGE BEHAVIOR FOR ALL BUSES IN REAL FEEDER FOR WINTER LOAD PROFILE WITH MICROGRID AND 30% OF PV PENETRATION. HIGHLIGHT FOR THE PERIOD WITH VOLTAGE INCREASE.

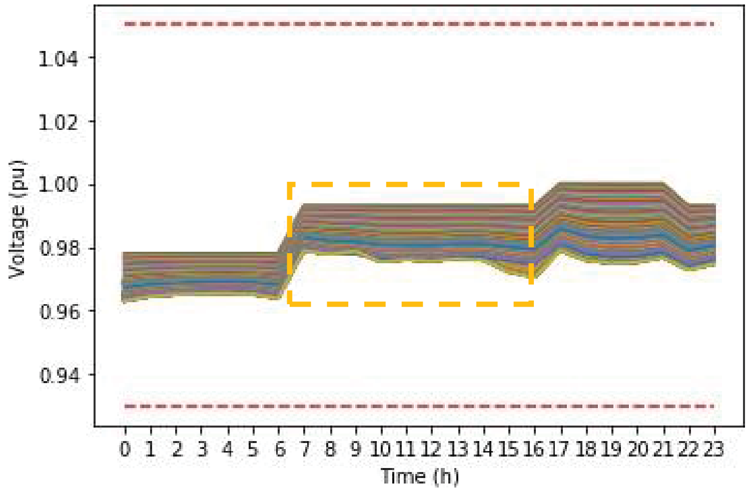

Source: The Author (2021).

From the results presented at TABLE 12, it is verified that power losses get reduced when compared to the scenario with only loads, since BESS can contribute to provide power closer to loads. In terms of operational costs, they are also lower than in previous scenarios due to the operation of BESS, that realizes the discharge during most costly period (regarding that white tariff is being considered), as show at FIGURE 56.

Battery operational behavior both for summer and winter are similar, presenting the behavior illustrated at FIGURE 56, in which the charging process occurs during the day (lower tariff and PV generation) and the discharge happens during the high tariff cost period.

TABLE 12 - RESULTS FROM THE REAL FEEDER WITH MICROGRID CONNECTION, 30% OF PV PENETRATION, AND BESS

Real Feeder + MG + 30% PV + BESS	Power Losses	Operational Costs	BESS Degradation Costs
Summer	1.01%	2,293.94 USD	445.25 USD
Winter	1.58%	8,886.76 USD	1,105.31 USD

FIGURE 56 - BESS POWER AND ENERGY BEHAVIOR WHEN CONNECTED TO THE REAL FEEDER WITH WINTER LOAD PROFILE AND 30% OF PV PENETRATION.

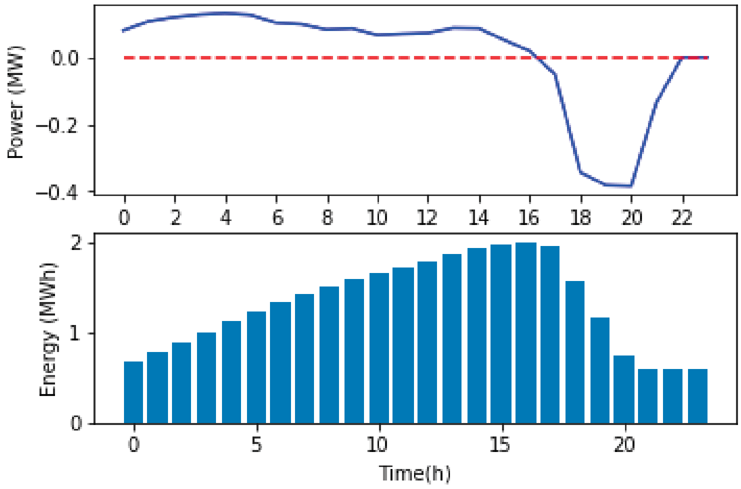

Source: The Author (2021).

Regarding voltage behavior, when BESS discharge happened, the voltage profile increased along all buses (FIGURE 57) due to the injection of active and reactive power (BESS is operating with pf=0,92). Active power injection close to the load center and during the peak demand contribute to supply the load, with lower losses, contributing to increase voltage levels.

This is a robust distribution feeder, since it does not present any power quality problem, even with the connection of active elements such as microgrid, distributed generation and BESS. This is an example of a distribution feeder that is currently ready for future grid transformations.

FIGURE 57 - VOLTAGE BEHAVIOR FOR ALL BUSES IN REAL FEEDER FOR WINTER LOAD PROFILE WITH MICROGRID, 30% OF PV PENETRATION AND BESS.

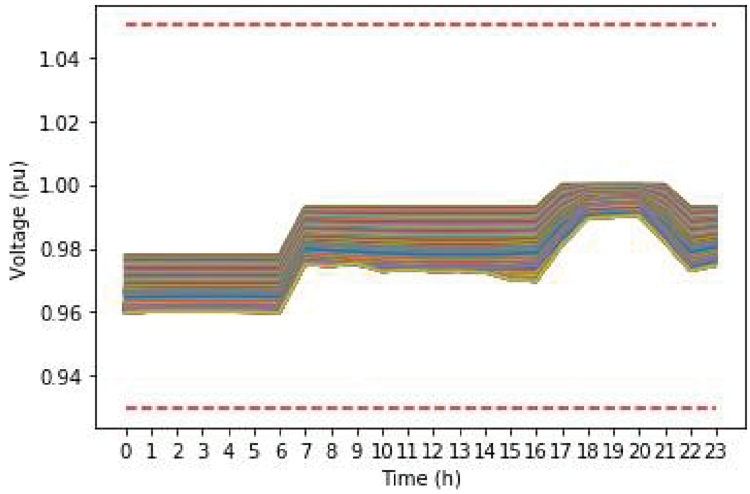

Source: The Author (2021).

4.4.2.4 Computational Performance

The computational performance of the simulations with the real distribution feeder was also evaluated. It is important to highlight that all the problem formulation was implemented in Python language, not been used any solver or even toolbox.

Using the pre-processing step to organize the matrices (FIGURE 49), the times of the optimization process for the different scenarios simulated are presented at TABLE 13. These time values were obtained in a computer with 16 GB of RAM memory and Spyder IDE was used to run the Python script.

Initially the simulation is performed with a typical variables initialization, resulting in a higher number of interactions and best performance time. Once the scenario has already been simulated, for the next time it uses the solution of the previous one to variables initialization, allowing to improve the optimization performance, since it starts close to the optimum point.

TABLE 13 - OPTIMIZATION TIMES FOR DIFFERENT SIMULATION SCENARIOS WITH REAL DISTRIBUTION FEEDER WITH INITIALIZATION BASED ON PREVIOUS SIMULATIONS

SCENARIO	SUMMER		WINTER	
	TIME (SECONDS)	NI**	TIME (SECONDS)	NI
BASE CASE	95.7	3	96.5	2
RF* + MG	143.4	5	147.5	5
RF+MG+PV	117.9	4	166.9	5
RF+MG+PV+BESS	312.8	12	307.1	12

*RF: Real Feeder; ** NI: number of interactions

Source: The Author (2021).

4.5 FINAL CONSIDERATIONS ABOUT SIMULATION RESULTS

Distribution grids are facing the biggest changes in their operation, mainly due to the insertion of new elements as distributed energy resources. In this way, it is necessary to model these new elements allowing the distribution system operator to plan the power grid operation inside of power quality levels.

The multiperiod optimum power flow proposed in the current work consists of a tool to optimize the entire grid operation, with the insertion of DERs considering different scenarios of its operation.

Additionally, the insertion of DERs and its active power provisioning through the main grid, the ancillary service of reactive power control was also considered in the MPOPF. In this way, a reactive dispatch from equipment that present inverters were done by the optimization methodology, resulting in improvements of voltage levels.

With the idea of an ADN scenario in mind, new equipment as D-FACTS were also considered connected to the main distribution grid. For this work, a D-SVC was placed in a branch with voltage problems, and its operation was also optimized, allowing to improve voltage levels, power losses, and the hosting capacity of DG into the distribution grid.

First, the 90 buses test feeder was evaluated in a different scenario, from a base case only with load, voltage regulator, and fixed capacitor banks to a scenario with PV, BESS, DSM, MGs, D-SVC, and VEs all connected simultaneously to the main grid.

At least a real distribution feeder, that currently presents only loads, was evaluated with the insertion of distributed generation and a BESS, allowing the analysis of how this equipment can impact real distribution system operation. In this case, the proposed MPOPF also proved to be a robust simulation tool for real systems, even when the circuit grows in complexity.

5 HIERARCHICAL MODEL

5.1 HIERARCHICAL MODEL BASIC CONCEPTS

Considering the integration of microgrids on the distribution grid, the main grid optimization can be done considering the microgrid dispatch, interacting with it in a hierarchical structure, where the master will be the power utility and the slave will be the microgrid optimization.

Some works are already found on the literature proposing different hierarchical approaches.

Addressing the bias of hierarchical control by the distribution network, considering the insertion of the microgrid, the work developed by Palizban, Kauhaniemi and Guerrero (2014) considers the integration of microgrids with the distribution network using hierarchical control with five levels, where the first three refer to controls of the grid in conjunction with the storage system allocated to the distribution grid, the fourth level refers to the integration with the microgrid and, finally, the fifth level consists of internal control of the microgrid. In the model proposed by the authors, the grid is represented by a model with the connection of the active elements being a storage system storage system and the microgrid, being the whole modeled in virtual power plants.

The work of Sanseverino et al (2015) and Agundis-Tinajero et al (2018) propose the use of the three-phase optimal power flow for an isolated system with multiple microgrids. In these papers, the FPO is used with the intention of minimizing losses from the definition of the optimal dispatch of the generation systems belonging to the set of microgrids, in addition to considering the set of constraints linked mainly to voltage limits. The approach of both works is very similar, highlighting that the second one presents the modeling test in Labview. Both works show that the FPO is appropriate for calculating the optimal operation points of the generators that compose the specific microgrids, respecting the operational restrictions, as well as reducing losses.

Moreover, the work of Chang, Martínez, and Cortes (2017) considers the existence of microgrids connected to the grid in a way that they can contribute with the frequency regulation market through the management of the resources available. In the approach proposed by the authors, the hierarchical control is done with the distributed FPO applied to microgrids connected to the power grid to improve the frequency regulation of the grid. The authors consider microgrids composed of distributed generation systems and the control performed by the FPO comprises the optimization of frequency regulation and minimizing costs, with microgrids being the only manageable energy resources available.

The integration of microgrid control and the power system management is very important, since it allows the optimum coordinated operation. In this context, is proposed a hierarchical model that will integrate on the MPOPF the results provided by the microgrid optimization itself, corresponding to a tertiary control level which provided setpoints for a day ahead considering the status of the microgrid and its connection in the distribution grid (YAZDANIAN, MEHRIZI-SANI, 2014; GUERRERO et al., 2013).

The work proposed by Che et.al. (2015) presents the application of a hierarchical control of multiple AC and DC microgrids in a community microgrid, focusing on the economic dispatch of the microgrid group, the possibility of islanded operation of the community microgrid, as well as the grid-connected operation. For the primary and secondary control, the authors implemented the droop control, while the tertiary control corresponds to the economic and optimum operation of the MGs as a group. From the results, the hierarchical control implemented presents the optimum economic dispatch from all the three microgrids to the power grid, as well as the best operation in the islanded mode, improving the voltage and frequency levels.

It is important to highlight that the large number of papers founded on the literature proposes a hierarchical model inside of the microgrid, with primary, secondary and tertiary controls, as did by Che et al (2015), or proposes a hierarchical control for a group of MGs.

The work proposed by Zhao et al. (2018) considers the integration of microgrids into a hierarchical model with the main grid, considering the system-of-systems methodology. In this case the authors perform an optimization of the energy management at the level of individual MGs using a multiple-stage robust optimization, and for the multi-microgrids level it focused on the power transactions between microgrids, being this process based on a decomposition problem. This process is repeated until a convergence point is reached.

Different hierarchical control approaches can be found for microgrid integration into the distribution grid. Che et al. (2015) proposes an enhanced microgrid power flow considering a Newton approach to power-sharing and voltage regulation and a modified Jacobian matrix for secondary control, implementing a droop control. The work of Feng and Zhang (2020) proposes a multiple ac and dc community microgrid integration considering an economic dispatch that allows the energy flow between microgrids and from microgrids to the main grid, considering the voltage and frequency constraints. This approach is like the one proposed in the present work, which considers the internal microgrid optimization, as well as the integration with the main grid, considering technical and economic aspects.

The hierarchical structure proposed in this thesis consists in a master-slave structure, where the slave level acts as a tertiary control level to provide the dispatch for a day ahead, using a centralized structure, and the master corresponds to the power utility which receives all the information from the microgrids and interfere in the operation proposed, to ensure power quality and reliability of the entire grid operation (BLASI et al., 2022).

The microgrid realizes its own optimization using a Multiperiod Optimum Power Flow solved using a mixed-integer linear model based on the modeling proposed by Lara Filho et al. (2021), considering the available resources and power demand, reaching out an optimum dispatch.

This dispatch from each microgrid will be provided for the power utility optimization (master level), which will execute the non-linear Multiperiod Optimum Power Flow, based on the same methodology proposed on the previous chapters of this work. If the power grid dispatch could not be performed with the proposed dispatch from the MGs, i.e. reaching any constraint, a new dispatch for the MG is proposed by the power utility optimization, as a master level. In this way, the MG optimization receives the proposed dispatch from the DSO and tries to fit to it, proposing a new MG dispatch. This process is repeated until reaches the convergence point without reaching out any constraint.

5.2 MODELING

The main goal of the hierarchical model proposed to define the optimum operation of the power grid and the microgrid, where operational and cost constraints are considered simultaneously in a solution considering an acceptable tolerance. To reach this objective, some criteria need to be defined:

- The main grid primary voltage profile should be maintained within a safety range;
- The operating cost of the main grid and from the microgrid will be minimized;
- Control the active and reactive power flow between the microgrid and the main grid to ensure the energy balance;
- Manage the power injections of the MGs to ensure the power grid quality levels and reliability;
- Realize a tertiary control from hourly forecasts of power dispatch suggesting actions for the microgrids;
- Decomposition of the problem into a master-slave optimization, where the master part optimizes the main grid, including the voltage adjustment, flexible loads management, energy storage operation, and active and reactive power management; and the slave part which optimizes the microgrid, including the flexible loads management, energy storage operation, controllable loads dispatch and active power balance.
- Feedback the results of the slave problem to the master until a convergence point is reached that reconciles the objectives of each problem, which are coordinated through a centralizing unit;
- In the master model, the microgrid is represented as a single bus equivalent that injects or absorbs power, while in the slave problem the modeling of the microgrid is performed in detail, considering the internal network of each microgrid;
- Use a planning horizon of one day ahead (24 h), and each period contemplates an interval of Δt equal to 1 h.

5.2.1 Modeling the Master Problem

For the power grid optimization, it is used the MPOPF model presented in chapter 3. The main grid model follows exactly the same process and presents the same elements, as distributed generation, voltage regulators, battery energy storage system, as well as the microgrids.

The multiple microgrids are considered as flexible loads that present a load behavior with positive (load behavior) and negative (generation behavior) values. The same constraints as well as the multiple objectives of the optimization are kept according to the equipment considered on the grid.

The same ***gamma*** variable, defined on equation 18, was used to avoid the deviation of the microgrid behavior proposed by the microgrid optimization.

5.2.2 Modeling the Slave Problem

For this case the slave problem corresponds to the day-ahead optimum operational planning for the microgrids, providing the optimum behavior of its elements. This model is presented as part of Blasi et al. (2022), being developed and completely described by Lara Filho (2021). This process will be called Microgrid Optimization Model (MGOM). This methodology will be briefly described in this section, since it was not developed by this author, but more information can be found in the references.

As the microgrids have similar equipment as the main grid, it can be modeled in the same way, but considering small portions as well as the possibility to operate islanded from the main grid.

The internal grid of a microgrid, in low or medium voltage can be mathematically modeled by non-linear equations. However, to improve the calculation performance, most part of the formulation allows a problem linearization. One of the simplifications that can be done in this way is to consider a single-bus model for the microgrid, which is fine to be used for small low voltage microgrids, being this approach used for this proposed model. The microgrid internal optimization model was implemented on the Gurobi optimizer integrated with Python 3.8 language.

Microgrids considered present energy resources, such as distributed generation, energy storage systems and flexible loads. The islanded operation of the microgrid is also considered, happening in this case for scheduled events.

The microgrid optimization objective function is also the cost minimization, being in this case the cost composed by the battery degradation cost, the load shedding cost, and an energy cost, as presented on equation (47).

$$\min \sum_{t=1}^{N} Cb_t + LS_t . Tls_t + \eta \tag{47}$$

where:

Cb_t: cost of battery degradation in the period t;

LS_t: load shedding in the period t;

Tls_t: load shedding cost in the period t;

t: period that is being evaluated;

N: total number of periods calculated, being in this case 24, since is considered the dispatch of a day-ahead;

η: auxiliary variable that represents the energy cost, and can be defined by (48):

$$\eta = \sum_{t=1}^{N} Grid_t . T_t + (|Pd_{ideal,t} - Pd_{realized,t}|). T_{pen} \quad (48)$$

where:

$Grid_t$: power consumption (positive values) or injection (negative values) of the microgrid into the power grid in the period t ;

T_t: energy price at the period t;

$Pd_{ideal,t}$: ideal active power flow between the MG and the distribution grid in the period t;

$Pd_{realized,t}$: realized active power flow between the MG and the distribution grid in the period t;

T_{pen}: penalty pricing for the difference between the ideal and the realized power flow between the MG and the main power grid.

The ideal power transaction for the period t is calculated using the ***gamma*** variable, defined on equation 18, which comes from the master problem (MPOPF), and the realized power flow from the previous interaction, for the same period.

$$Pd^{i}_{ideal,t} = Pd^{i-1}_{realized,t} . gamma^{i}_{t} \quad (49)$$

where:

i: iteration from the hierarchical process.

For the microgrid operation and dispatch was considered the same approach presented at Blasi et al. (2022) and Lara Filho (2021), being summarized in the sequence.

For the battery inside of the microgrid, its power flow behavior needs to be modeled considering that is not possible to directly inject power into the grid, and its power should be firstly provided to the microgrid itself. In this way, the following formulation is used:

$$Grid_t = Er1_t + Er2_t \tag{50}$$
$$Er1_t = L_t^{NP} + L_t^{CP} - G_{pv} + A_t^c - LS1_t \tag{51}$$
$$Er2_t = L_t^P + L_t^{CONT} - A_t^d - LS2_t \tag{52}$$

where:

$Er1_t$: energy balance that cannot be supplied by the microgrid battery in a period t;

$Er2_t$: energy balance that can be supplied by the microgrid battery in a period t;

L_t^{NP}: non-controllable critical load in a period t;

L_t^P: non-controllable priority load in a period t;

L_t^{CP}: load from the carport system from the microgrid in a period t;

L_t^{CONT}: controllable load of the microgrid in a period t;

G_{pv}: generation from the microgrid photovoltaic system in a period t;

A_t^c: amount of energy stored (charged) in the microgrid battery in a period t;

A_t^d: amount of energy discharged from the microgrid battery in a period t;

$LS1_t$: load shedding without microgrid batteries in a period t, being limited by $0 \leq LS1_t \leq L_t^{NP}$;

$LS2_t$: load shedding with microgrid batteries in a period t, being limited by $0 \leq LS2_t \leq L_t^P$.

5.2.3 Modeling the Hierarchical Problem

The proposed process to interconnect the information between the active primary distribution network (obtained by the MPOPF Model) and the microgrids (obtained by the MGOM Model) is described in the following algorithm and summarized in the flowchart presented at FIGURE 58, being described in details in the sequence.

FIGURE 58 - HIERARCHICAL MASTER-SLAVE MODELING PROPOSED WITH POWER GRID AND MICROGRID OPTIMIZATION.

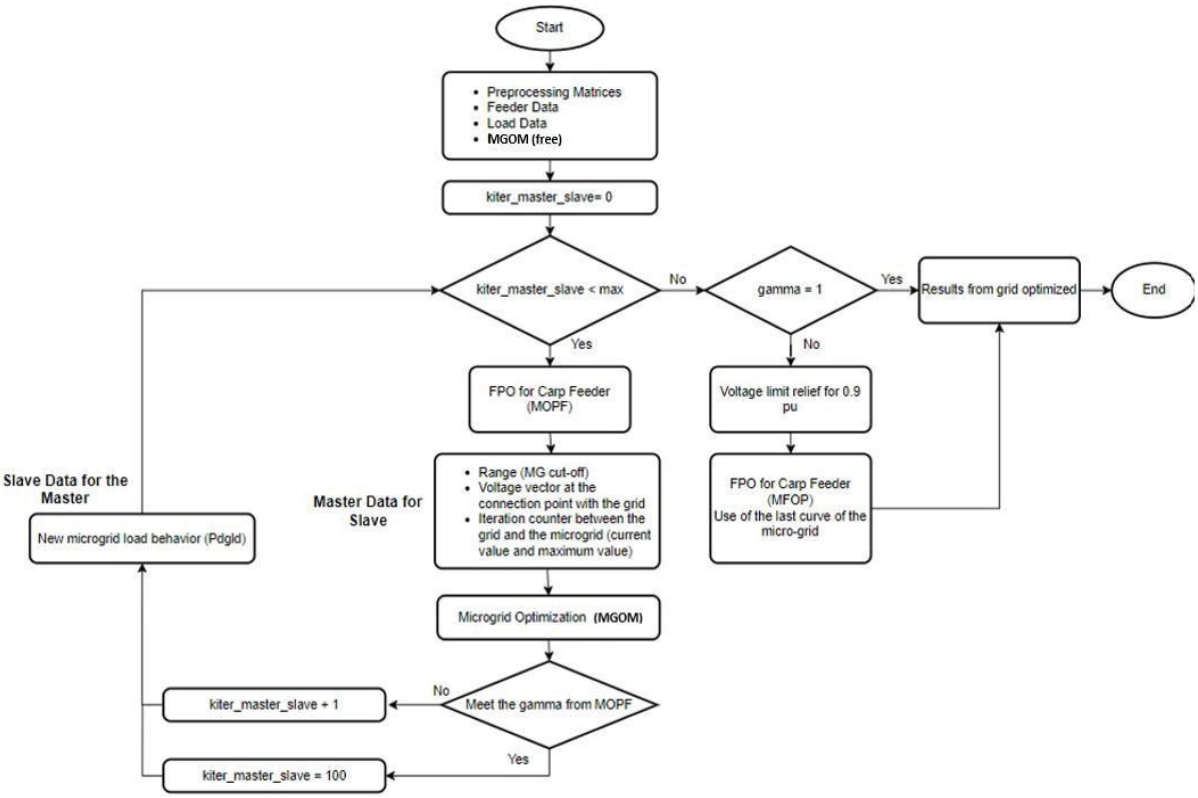

Source: The Author (2022).

The flowchart can be detailed from the proposed algorithm by the following set of steps:

Step 1: Declare input parameters.

Step 2: Make $kiter_{masterslave}$ = 0.

Step 3: Run first simulation of MGOM, which provides optimal power injection value by the microgrid view, namely as FPd_{MGOM} .

Step 4: Initialize the variables, load the ones already calculated in pre-simulation and run MPOPF to obtain FPd_{MFOP}, which is the optimal power injection value to be performed by the microgrid, but prioritizing the feeder. If there is a convergence of the MPOPF, go to **Step 5**, otherwise go to **Step 9**.

Step 5: If $kiter_{masterslave}$ is greater than the maximum number of resupply (kmax) go to **Step 8**. If there is dispatch deviation of FPd_{MFOP} from FPd_{MGOM}, go to **Step 6**. Otherwise, make $kiter_{masterslave}$ = 100 and go to **Step 9**.

Step 6: Run MGOM and recalculate new FPd_{MGOM}. If the new value of FPd_{MGOM} satisfies the value of FPd_{MFOP} (calculated in **Step 5**), go to **Step 9**. Otherwise, make $kiter_{masterslave}$ = $kiter_{masterslave}$ + 1.

Step 7: Perform MPOPF optimization process and obtain new of FPd_{MFOP} and go to **Step 5**.

Step 8: If microgrid injection cannot be adjusted after *kmax* iterations, simulate MPOPF with minimum voltage reduced to 0.9 pu and using last load value set by MGOM (FPd_{MGOM}).

Step 9: END

If after *kmax* iterations between Step 2 to 5, no load shedding of the microgrid is achieved, there will be two options: the mandatory easing of power injection proposed by MPOPF is recommended, as it trumps feeder operational safety, or the MPOPF is executed with relaxation of the minimum voltage levels (Step 9) to meet the power injection proposed by MGOM.

5.3 HIERARCHICAL MODEL SIMULATION

5.3.1 Scenarios definition for the Hierarchical Model Simulations

For the hierarchical model simulation, it was used the real distribution grid modeled, presented on Chapter 4.4 of the current work. However, the microgrid model has changed. On section 4.5.2, the microgrid corresponds only to a node of the grid that can provide or absorb power. At this point, the microgrid dispatch is being modeled and optimized, and its behavior will change according to the interactions with the main grid, as described on Chapter 5.2.

From the MFOP point of view, the MG was modeled as an equivalent bus of the system. However, as in this case the MG optimization is being realized by the MGOM, it is important to model and present the Barigui MG structure, as represented at FIGURE 59.

It is possible to see that the battery system (SAE) of the microgrid can be connected/disconnected from the main power grid, as well as can be directly connected to the microgrid loads. The solar photovoltaic generation system, as well as the carport, cannot operate islanded from the main grid, and are not switchable as the batteries and the loads.

FIGURE 59 – BARIGUI MICROGRID SCHEMATIC DIAGRAM.

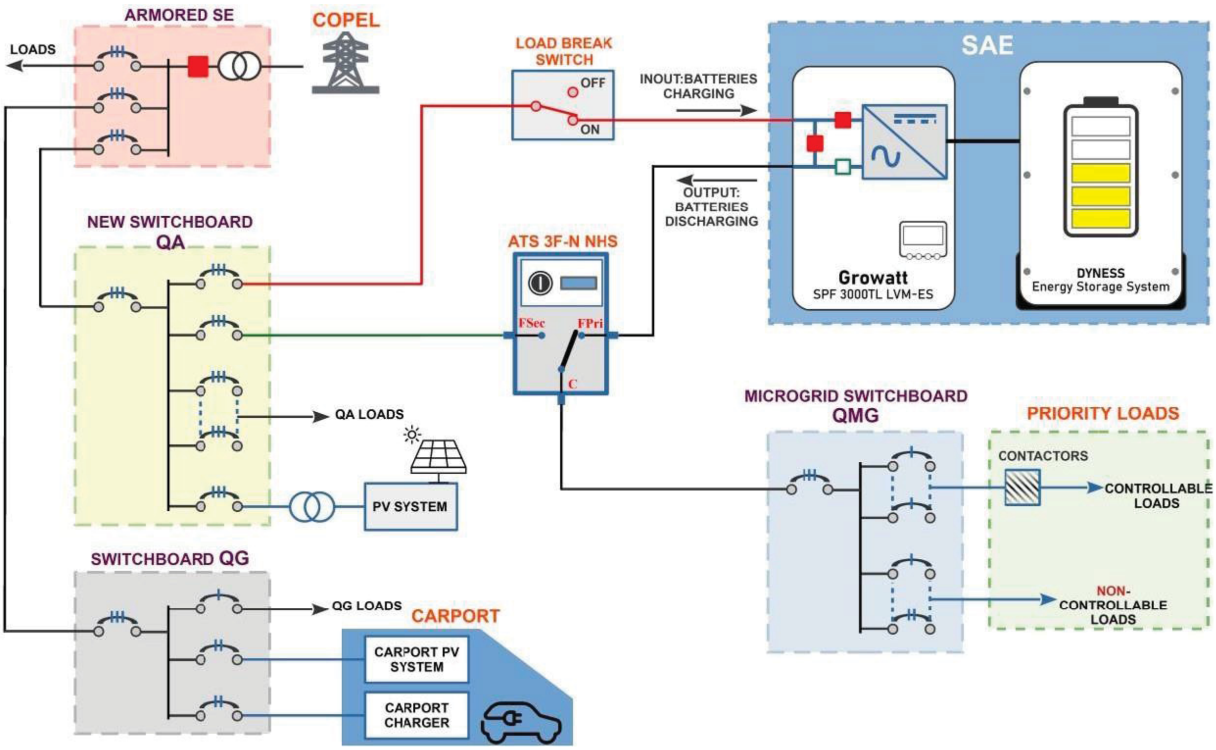

Source: The Author (2022).

For the hierarchical model simulation, the following simulation scenarios were defined:

- **Scenario 1**: original load for the feeder and the Barigui microgrid;
- **Scenario 2:** condition of programmed microgrid isolation (schedule islanding);
- **Scenario 3:** feeder and microgrid with increased load;
- **Scenario 4:** consideration of the most complex grid scenario, with the presence of distributed generation and batteries, as well as the microgrid, with load increased.

5.3.2 Hierarchical Model Simulations Results

5.3.2.1 Scenario 1: original load for the feeder and the Barigui microgrid

The initial dispatch proposed by the MGOM model is presented in FIGURE 60. For this dispatch, it is possible to observe that the charging of electric vehicles (in pink) is performed during the period from 11:00 a.m. to 4:00 p.m., minimizing the operating cost of the microgrid. The controllable loads are allocated from 9:00 a.m. to 12:00 p.m. and 3:00 p.m, and the battery discharge (in red) are happening in the periods of 6:00 p.m. and 7:00 p.m. since in this period the photovoltaic generation is ending, and the energy price is higher. The battery charge happens at hour 23 (green color), since this presents a lower price and load for the system. Additionally, no load shedding (gray color) is observed in this scenario.

FIGURE 60 - PROPOSED DISPATCH BY THE MGOM FOR THE PILOT MICROGRID, FOR SCENARIO 1 OF THE HIERARCHICAL MODEL ANALYSIS.

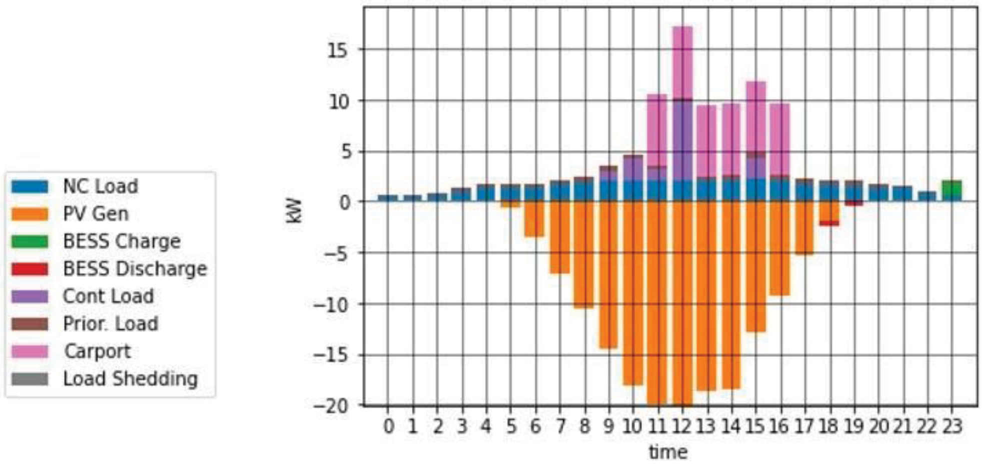

Source: The Author (2022).

From the hierarchical process point of view, at this moment there was no feedback from the main grid yet. This first run ($kiter_{masterslave}$ = 0) provides the optimal power injection value from the microgrid point of view. In this case, the total cost of dispatching the microgrid is -26.27 BRL, which means that at the end of the day, there is more power injection into the network than consumption from the MG.

There is no need for the feedback process (so, make $kiter_{masterslave}$ = 100), because no restrictions were violated, and the main grid operation took place within the operational limits. In this case, both grid and migrogrid dispatches were already optimized in the first steps of the process.

Thus, the microgrid behavior does not need to be changed, and the operation proposed by the MGOM is accepted by the MPOPF calculation. In this case, the hierarchical feedback does not need to be performed. FIGURE 61 shows the dispatch of the microgrid from the point of view of the main grid, which shows that the load/injection performed, and the load/injection desired by the microgrid is the same, without the need for changes.

FIGURE 61 – MICROGRID DISPATCH FROM THE MAIN GRID POINT OF VIEW, FOR SCENARIO 1 OF THE HIERARCHICAL MODEL ANALYSIS.

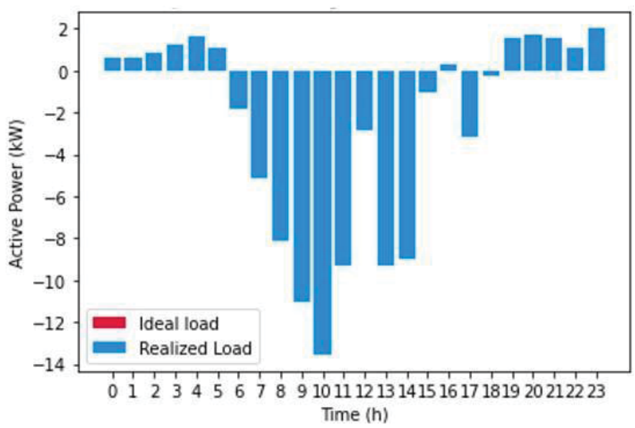

Source: The Author (2022).

Regarding the voltage levels, are verified that all buses are operating inside of the voltage limits (from 0.93 to 1.05 pu), as presented on FIGURE 62. In addition, the voltage levels follow what is specified according to the load behavior (light, medium, and heavy), showing a small variation between feeder buses in relation to the specified voltage at the substation.

FIGURE 62 – VOLTAGE BEHAVIOR FOR ALL BUSES OF THE FEEDER, FOR SCENARIO 1 OF THE HIERARCHICAL MODEL ANALYSIS.

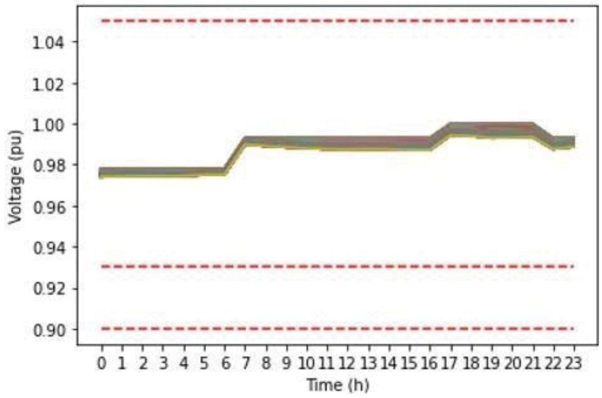

Source: The Author (2022).

5.3.2.2 Scenario 2: condition of programmed microgrid isolation (schedule islanding)

In this case, it is considered a planned island operation of the microgrid during the periods from 1:00 p.m. to 3:00 p.m. In this case, the MG battery can only supply the critical loads on the MG. For this scenario, the microgrid dispatch proposed by the MGOM is presented on FIGURE 63. During the islanded period there is no charging of EVs and, there are no allocation of controllable loads, and the non-critical loads are cut off, being only the critical loads supplied by the discharge of the battery system. Once the islanding operation ends, the battery is charged again in the next period.

FIGURE 63 - PROPOSED DISPATCH BY THE MGOM FOR THE PILOT MICROGRID, FOR SCENARIO 1 OF THE HIERARCHICAL MODEL ANALYSIS.

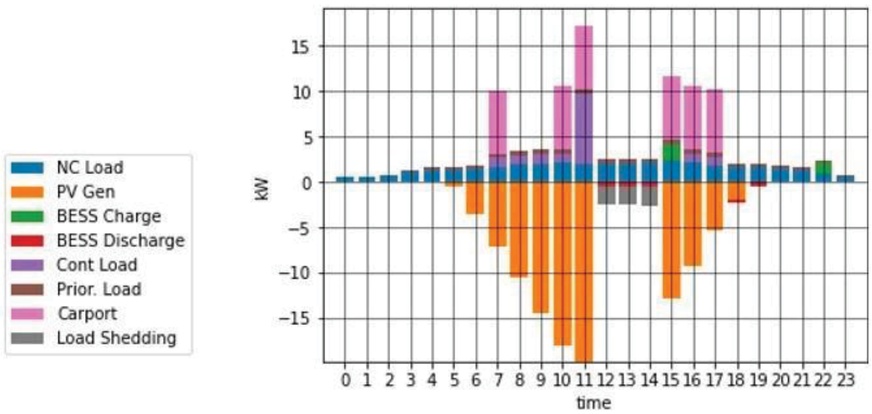

Source: The Author (2022).

Reminding the Barigui MG structure (FIGURE 59), when the MG is islanded, the solar generation is not kept with the MG structure, being both generation systems (PV and carport) still connected with the main grid. By not using photovoltaic generation, as it is not connected in the same frame as the priority loads, the costs of the microgrid increase to 32.59 BRL.

The behavior of the power injection of the microgrid to the main grid is shown at FIGURE 64 in which during the programmed islanding period, there is no energy transition with the main grid. Therefore, in other planning periods there was no necessity of change the behavior proposed by the MGOM.

FIGURE 64 - MICROGRID DISPATCH FROM THE MAIN GRID POINT OF VIEW, FOR SCENARIO 2 OF THE HIERARCHICAL MODEL ANALYSIS.

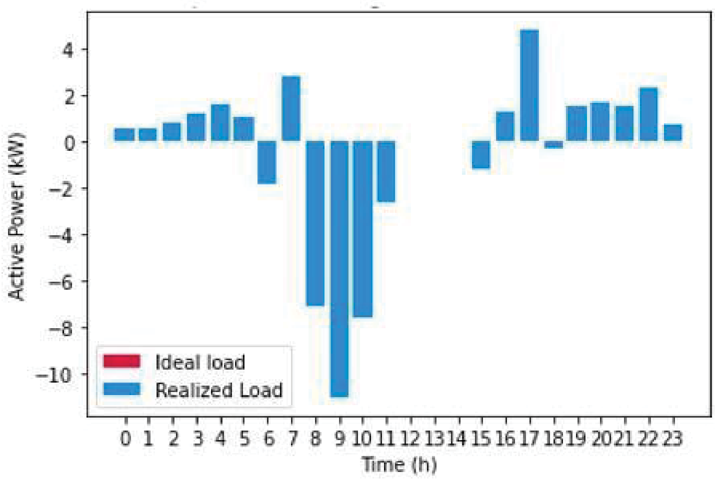

Source: The Author (2022).

5.3.2.3 Scenario 3: feeder and microgrid with increased load

Since the feeder load and the Barigui microgrid load present low values, there are no problems with the voltage values, and no operational and violated constraints. In this way, no iterative process occurs within the hierarchical model, as presented in the previous scenarios.

To force the feedback actuation and, therefore, verify the hierarchical model, the load values of the active network feeder were increased 9 times and the load values of the microgrid were increased 20 times. These values were defined after exhaustive tests with several other lower values, which did not cause problems for the operation of the network.

Below is the sequence of steps performed for this case:

- Initialization of the counter for the iteration between the methodologies, $kiter_{masterslave} = 0$; FPd_{MGOM}
- Run the first simulation of the MGOM model. This step provides the optimal power injection value through the microgrid point of view (FIGURE 65). In this case, the dispatch corresponds to the behavior of load and generation in the summer, increased by 20 times;
- Run the MPOPF model. In this step, all the constraints are checked and a new microgrid operation is proposed by the MPOPF as shown in FIGURE 66. The proposed load shedding considers the voltage violation that happens especially between 7 p.m. and 8 p.m. In this way, the proposed operation considers a reduction in the microgrid's load, which tends to improve the voltage magnitude profile, thus avoiding undervoltage.

FIGURE 65 - PROPOSED DISPATCH FROM THE MGOM FOR THE MICROGRID BEFORE THE FEEDBACK PROCESS

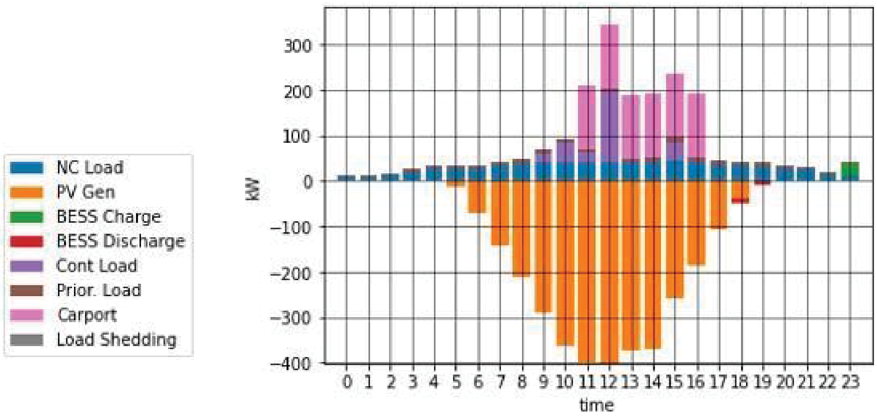

Source: The Author (2022).

FIGURE 66 - PROPOSED DISPATCH FROM THE MPOPF FOR THE MICROGRID BEFORE THE FEEDBACK PROCESS.

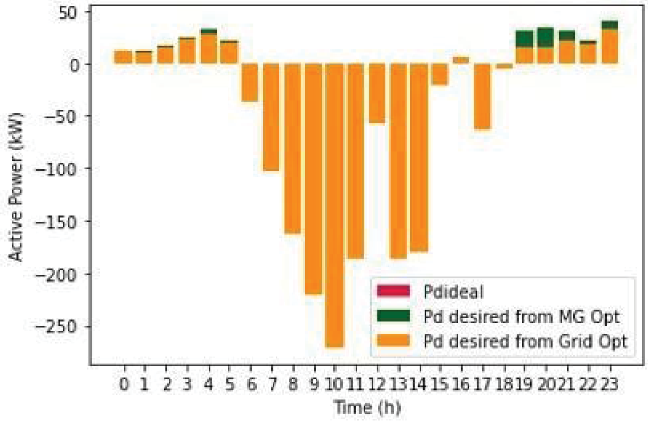

Source: The Author (2022).

A new microgrid dispatch (MGOM) is run using the proposed dispatch of MPOPF (FIGURE 67). There is a load reduction at periods suggested by the main grid, but not enough as suggested by the main grid optimization. In this case the load shedding occurs from 7 p.m. to 8 p.m. Furthermore, to better adapt to the suggestion of the MPOPF, the MGOM also reduces part of the battery charge and discharge.

From the point of view of the main grid, it would be necessary to further reduce the load during the 7 p.m., 8 p.m., and 11 p.m. periods (FIGURE 68). Therefore, there is a new feedback process, thus sending a new range, allowing the microgrid to make the adjustments on its energy resources to the requests made by the main grid.

FIGURE 67 - PROPOSED DISPATCH FROM THE MGOM FOR THE MICROGRID AFTER THE FIRST INTERACTION ON THE FEEDBACK PROCESS.

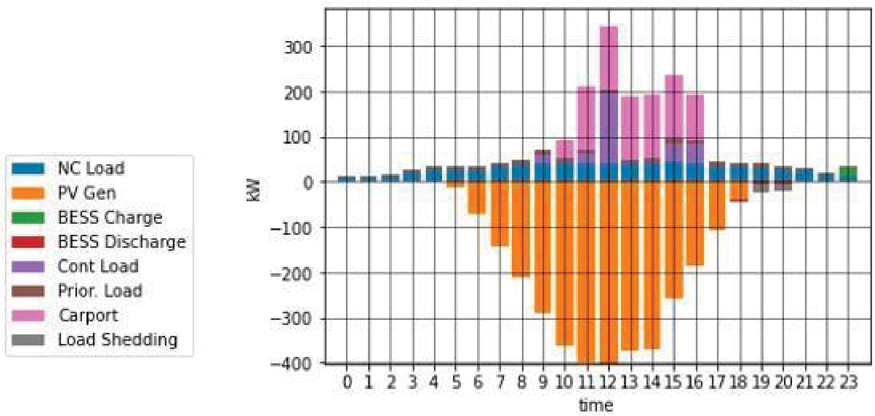

Source: The Author (2022).

FIGURE 68 - PROPOSED DISPATCH FROM THE MPOPF FOR THE MICROGRID AFTER THE FIRST INTERACTION ON THE FEEDBACK PROCESS.

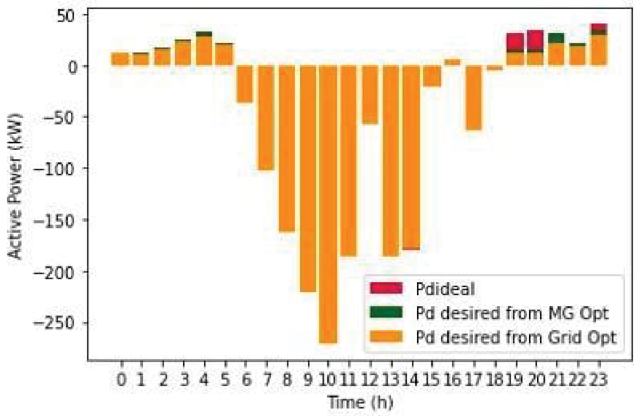

Source: The Author (2022).

After the increase in load shedding and reduction in the use of batteries, a new dispatch is proposed. However, even with the adjustments, the load shedding is very costly for the microgrid during peak hours, which is exactly when the MPOPF requests the reduction in load. Therefore, even after three feedback from the hierarchical process, the microgrid cannot adapt to the power requested by the MFOP, as shown in FIGURE 69 and FIGURE 70.

FIGURE 69 - PROPOSED DISPATCH FROM THE MGOM FOR THE MICROGRID AFTER THE THIRD INTERACTION ON THE FEEDBACK PROCESS.

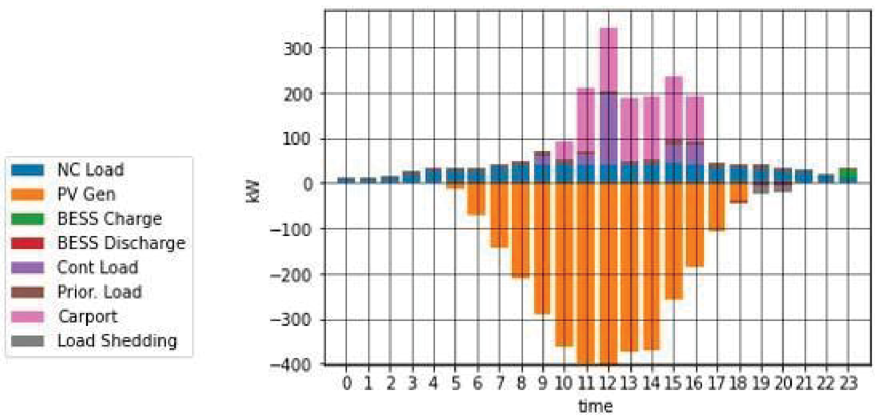

Source: The Author (2022).

FIGURE 70 - PROPOSED DISPATCH FROM THE MPOPF FOR THE MICROGRID AFTER THE THIRD INTERACTION ON THE FEEDBACK PROCESS.

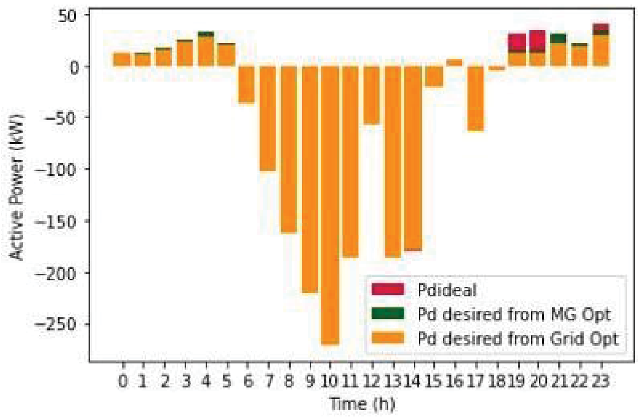

Source: The Author (2022).

As it was not possible to solve the constraint violation by the redispatch of the MG, the main grid reduces the minimum voltage constraint to 0.9, and the dispatch from the microgrid is accepted by the main grid under these conditions. The behavior of the load at the end of the hierarchical process is presented at FIGURE 71 in which the difference between the dispatch initially proposed by the microgrid (ideal load) and the dispatch carried out (realized load) is shown, both from the point of view of the main grid.

FIGURE 71 - PROPOSED DISPATCH FOR THE MICROGRID AT THE END OF THE HIERARCHICAL PROCESS.

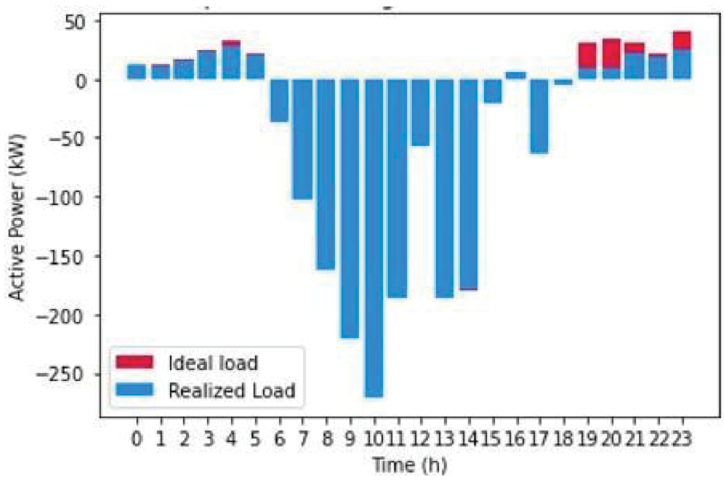

Source: The Author (2022).

Regarding the voltage behavior, FIGURE 72 shows the voltage profile of all buses at the end of the hierarchical model iterations. With the new microgrid dispatch it was yet possible to guarantee the voltage of all buses within the operational limits.

FIGURE 72 - VOLTAGE PROFILE OF ALL BUSES OF THE FEEDER AFTER THE HIERARCHICAL PROCESS FOR THE MG DISPATCH.

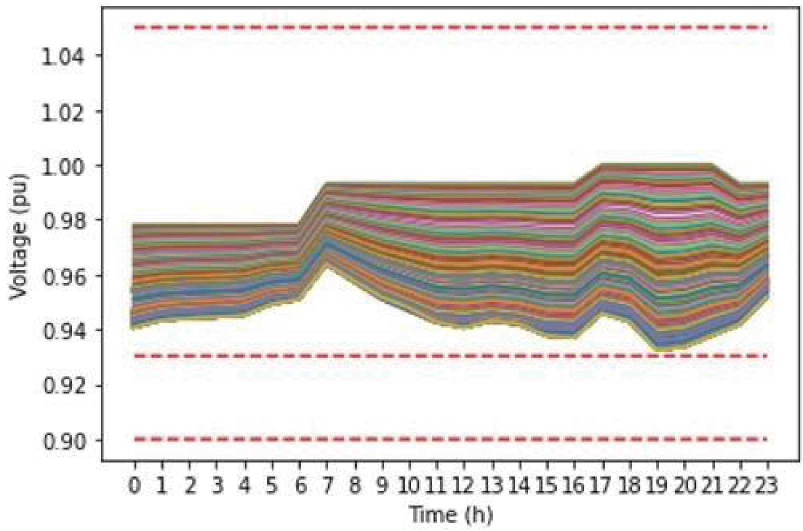

Source: The Author (2022).

Regarding the costs, in the first iteration, the total costs of the microgrid were -525.40 BRL, in which the controllable loads are allocated within the commercial period and the battery is discharged at 6 p.m. and 7 p.m. and charged at 11 p.m.

In the second iteration, when there was the feedback of the MFOP and the definition of a new range for readjustment in the microgrid dispatch, the total cost was -380.41 BRL, since there was a need to reduce the load between the periods 6 p.m. to 8 p.m., decreasing the financial benefit. For this scenario, after the iteration of the hierarchical process, the microgrid carried out a 6.93% reduction in its load compared to the initial proposition.

The final behavior of the network presents a total power loss of 3.2% (8.088 MWh) and operating costs of 141,319.57 BRL. It should be noted that in this scenario the costs are higher since the demand supplied by the feeder is 9 times higher than the load in the original scenario, which represents a total of 252 MWh throughout the day.

5.3.2.4 Scenario 4: consideration of the most complex grid scenario, with the presence of distributed generation and batteries, as well as the microgrid, with load increased

In this scenario, the operation of the network was considered with the allocation of distributed PV systems and batteries operating simultaneously along the feeder, as an active distribution network. In other words, this scenario looks at future cases in which the feeder also has distributed energy resources (similarly to the considerations done on the MPOPF analysis on chapter 4.5.3).

The analysis was carried out considering the penetration of 30% of distributed PV generation in this feeder and the connection of a BESS (1MW/2MWh) in a point with 80% of the load located downstream.

For this scenario, the loads of the main grid and of the microgrid were increased to evaluate the behavior of the hierarchical model under conditions of stress for the system, getting the same values as presented on scenario 3. However, for this case, there is a slack due to the insertion of BESS and GD; thus, the MPOPF does not require readjustment, providing a cost in the microgrid of -525.37 BRL.

FIGURE 73 shows the microgrid dispatches, which is similar and proportional to the microgrid dispatch without increased load. Similarly, FIGURE 74 also shows the MG behavior from the point of view of the main grid.

FIGURE 73 - MICROGRID'S DISPATCH FROM MGOM IN THE SCENARIO OF AN ACTIVE NETWORK WITH INCREASE LOAD.

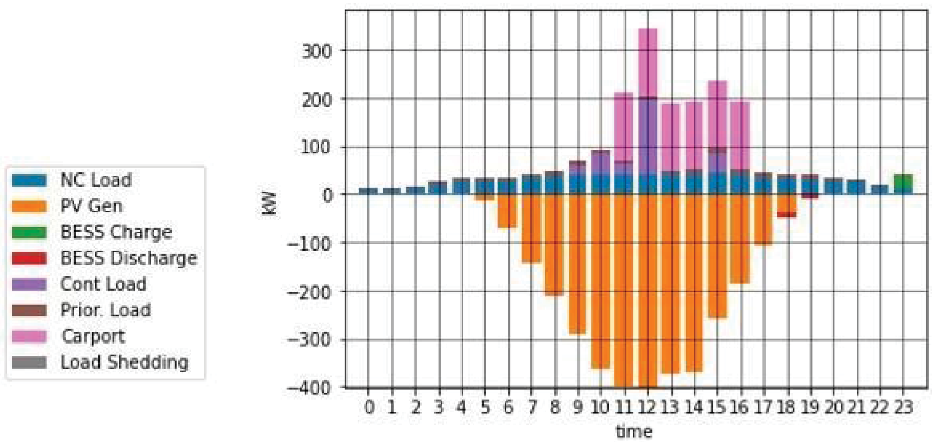

Source: The Author (2022).

FIGURE 74 - MICROGRID'S DISPATCH FROM MFOP POINT OF VIEW IN THE SCENARIO OF AN ACTIVE NETWORK WITH INCREASE LOAD.

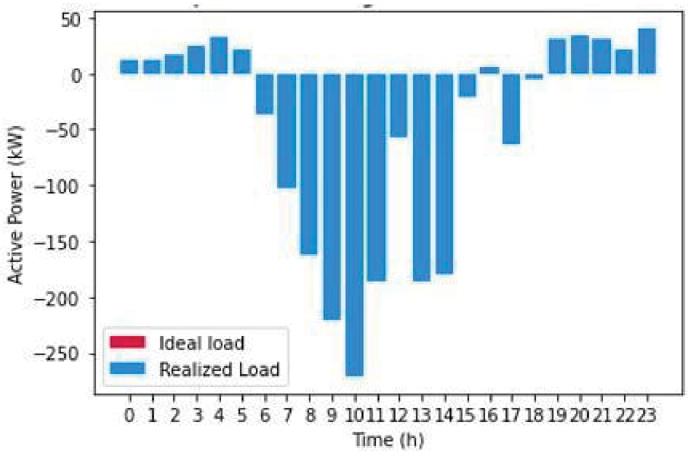

Source: The Author (2022).

Regarding other characteristics of the network operation for this scenario with a larger number of elements, it appears that the losses are 3.31% (8.35 MWh), remaining the levels obtained in the previous simulations. Concerning the costs of operation of the network, these are 134,761.88 BRL including the cost of battery depreciation of 6089.52 BRL.

The battery operation stores 1.537 MWh throughout the day and provides 1.309 MWh of energy. At FIGURE 75, the behaviors of power (upper part of the figure) and energy (lower part) are presented. It can be observed that the charge occurs in the first hours of the day, which corresponds to the low load period of the feeder, thus presenting lower impact on feeder operation. The discharging, on the other hand, happens at the peak load time of the feeder, contributing to the fulfilment of the load.

Finally, regarding the voltage behavior, since this scenario has increased load, there is a tendency for voltage violation. However, with the battery dispatch, it is possible to perform the network operation in a satisfactory manner, without under or over voltage in any of the feeder buses, as presented in FIGURE 76.

FIGURE 75 - BEHAVIOR OF THE BATTERY FOR THE ACTIVE DISTRIBUTION NETWORK SCENARIO WITH INCREASE CHARGE

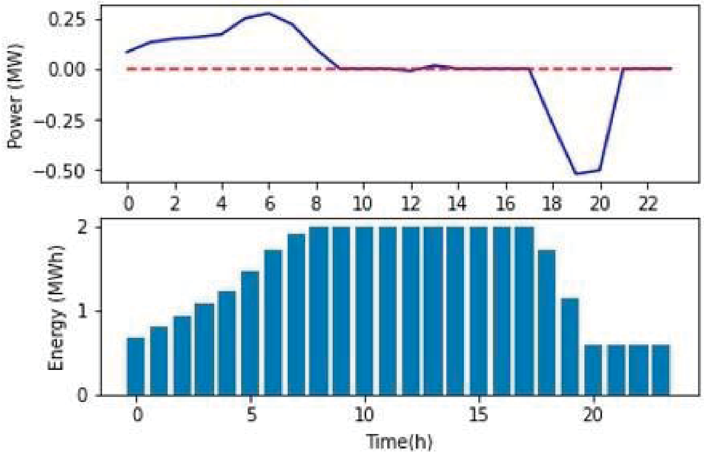

Source: The Author (2022).

FIGURE 76 - BEHAVIOR OF VOLTAGE AT ALL BUSES FOR THE SCENARIO OF ACTIVE DISTRIBUTION AND LOAD INCREASE~NETWORK

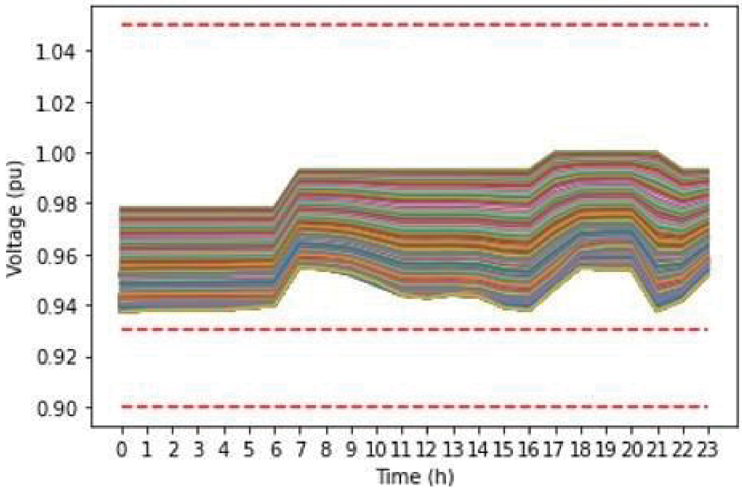

Source: The Author (2022).

5.4 FINAL CONSIDERATIONS ABOUT THE HIERARCHICAL MODEL

The hierarchical model corresponds to the integration of two distinct methodologies: an internal optimization of the dispatch of microgrids, and the optimization of the distribution network operation.

From this model, it was possible to test different scenarios considering the application of a real distribution grid and a pilot microgrid implemented in the city of Curitiba/Brazil. Different feeder load levels, and microgrid operations were evaluated as well as a future scenario of the grid as an active distribution network.

Since the simulated feeder is robust and present a low load demand, the microgrid connection, and the operation of the distribution network itself does not require the feedback process in the hierarchical model, i.e., the network is able to organize itself to guarantee operation within the operational limits.

Therefore, aiming to test the operation of the hierarchical model it was necessary to increase the load, allowing the connection between the methodologies, testing the feedback process, and allowing the joined optimization of the grid and microgrid optimization. The points evaluated are the grid losses along a day, the microgrid operation cost for the proposed and realized dispatch, the difference between the microgrid dispatches, grid operation costs, and the voltage profile of all buses in the feeder.

For the scenarios with the entry of the pilot microgrid in the feeder, the operating costs decrease in relation to the scenario without the microgrid. This happens since the microgrid contributes to the injection of power into the grid, as well as reducing the load, since part of it is supplied by the microgrid's own resources. When considering the operation of an active grid, the injection of distributed generation, as well as the battery operation contribute to meeting the feeder demand and consequently reduce the operation costs. Although, in scenarios of increased load, it is necessary to perform the joint operation of the grid with the microgrid to ensure operation within operational limits, especially aiming to respect the voltage constraints. Even so, due to the operation of the hierarchical model it is possible to communicate the optimal dispatch from the grid's point of view to the microgrid, allowing it to propose a redispatch and, therefore, a new grid optimization.

Additionally, for the scenarios with load elevation on the feeder, more expressive losses occur, being proportional to the increase of power flowing through the feeder, but the obtained values do not correspond to operational problems, since they do not exceed 5% of the feeder's daily demand. Furthermore, in relation to the voltage profile behavior, for the light load scenarios, there is little voltage variation on the feeder's buses in relation to the magnitude of the substation's output voltage. Nevertheless, in scenarios with higher loads, the impact on voltage behavior is verified in a manner that the voltage decreases with greater intensity along with the buses farther from the substation or that presents a higher load.

In general, microgrids and other distributed resources that can be incorporated into the distribution grid, if their operation and the DERs were appropriately optimized/allocated, contributing to decrease power losses and operation costs of active grids.

Furthermore, with more complex compositions of the distribution grid, it can be observed greater computational requirement to the model achieves the convergence, demanding more computational time, and a greater number of iterations for each optimization process.

6 REAL-TIME SIMULATION AND DIGITAL-TWIN

6.1 REAL-TIME SIMULATION CONCEPTS

Starting with the concepts of real-time simulation, this corresponds to a type of simulation used for electromagnetic transient analysis; power systems modeling and simulation; and control prototyping techniques.

What differentiates a real-time simulation from other types of simulation is the time response. In this case the time response must be coherent with the time response of the studied phenomena. To be able to respond in this time frame, the real-time simulation uses some specific approaches, like the discrete-time and constant time-step.

In a real-time simulation, a fixed time-step is defined, since to solve mathematical functions and equations at a given time-step, each variable or system state is solved successively as a function of variables and states at the end of the proceeding time-step.

During a discrete-time simulation, the time-step size should be longer enough to be able to compute all equations and functions representing a system during a given time-step. For each time-step, the real-time simulator, responsible by execute the simulation on a proper time, will execute some tasks (as illustrated at FIGURE 77): 1) reading inputs and data from the model, and also generating outputs; 2) solve model equations; 3) exchange results with other simulation nodes; 4) wait for the start of the next time-step.

If the fixed time-step is not respected because the tasks take more time to be done, the simulation will present instability since some time-steps will be skipped by the process that will be trying to resynchronize with the clock and thus, wrong results will be presented. This effect is commonly known as overrun.

The first challenge of a real-time simulation is to select the proper time-step for the model. It is also necessary to think about the computing power required based on the complexity of the simulated system, since this will directly affect the performance of the simulation in time.

FIGURE 77 - ILUSTRATION OF FIXED TIME STEP USAGE ON A REAL-TIME SIMULATION

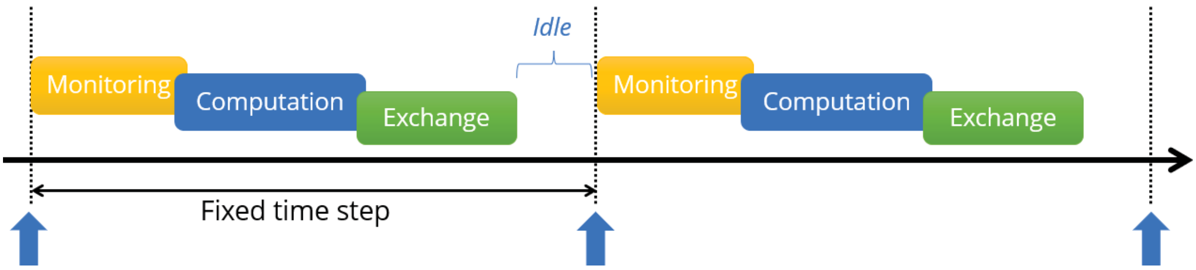

SOURCE: The Author (2023).

FIGURE 78 outlines typical time-step and computing power requirements for a variety of applications. The left side of the chart illustrates mechanical systems with slow dynamics that generally require larger time-steps, meanwhile on the right side are presented applications that requires very small time-steps, usually related to power electronics applications.

FIGURE 78 – TYPICAL SIMULATION TIME-STEP BY APPLICATION

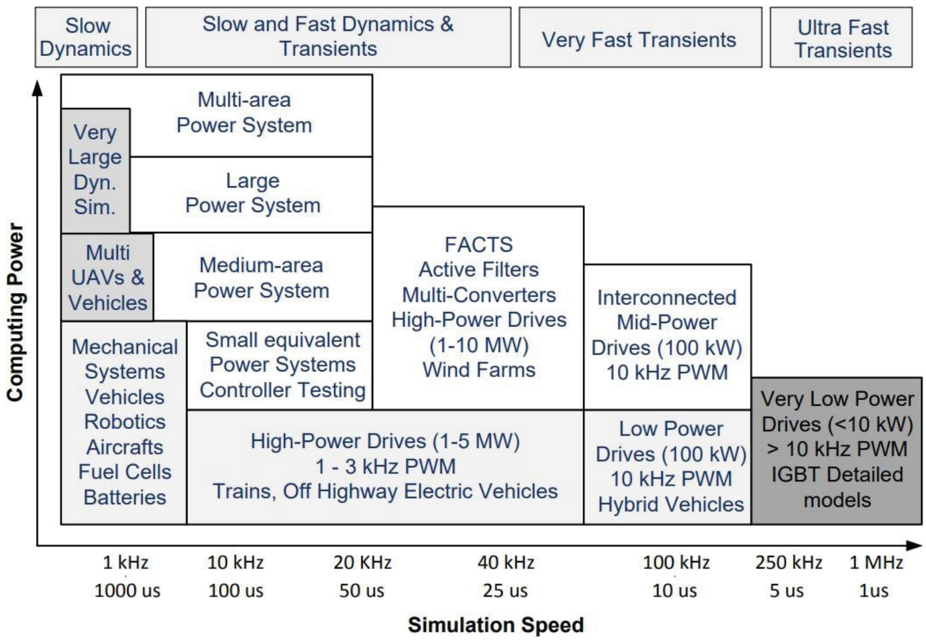

SOURCE: Belanger, J; Venne, P. Paquin, J-N. (2010).

Time-steps up to tens of milliseconds could be processed on the CPU core of the simulators, considering the clock of the motherboard. For applications that require lower time-steps, like hundreds or tens of nanoseconds, the Field-Programmable Gate Array (FPGA) boards usage is required, due to its capability of reprogramming to optimize their usage for calculations.

Regarding the system complexity, as the more complex is the system, the more difficult to make its calculation time fit inside of the desired time-step. In this way a parallelization approach is used, where the model can be divided to run simultaneously at multiple CPU cores, being synchronized at the end of the time-step. There are multiple techniques used for this approach that will not be detailed in this document, since it is not the focus of this research.

The real-time simulation can be used for different approaches, which can be basically divided into four categories (FIGURE 79): model-in-the-loop (MIL); rapid-control-prototyping (RCP); hardware-in-the-loop (HIL); and power-hardware-in-the-loop (PHIL) (Belanger, J; Venne, P. Paquin, J-N., 2010).

The model-in-the-loop or software-in-the-loop (SIL) consists of a plant and controller being simulated at the software, where no external device is connected to the real-time simulator. It can be used as a first step in the development of a simulation since it can run faster or slower than real-time.

In RCP the plant controller is implemented on a real-time simulator, and it is connected to a real physical plant (or device), allowing to test the algorithms and parameters of the prototyped control.

For HIL applications, a physical controller is connected to the real-time simulator, where a virtual plant is being simulated. This simulation can, for example, use the controller previously defined via RCP that now is implemented on a physical hardware and will be connected to the simulation to test its behavior under different plant conditions.

The difference between HIL and PHIL consists of that on HIL only control signals are exchanged from the simulation to the external device, meanwhile in PHIL, power signals can be represented to interact with the device under test. To be able to do it, a power amplifier is required, converting low value signals from the simulator inputs and outputs, on voltages and current magnitudes that emulates power devices environments.

FIGURE 79 - REAL-TIME APPLICATIONS

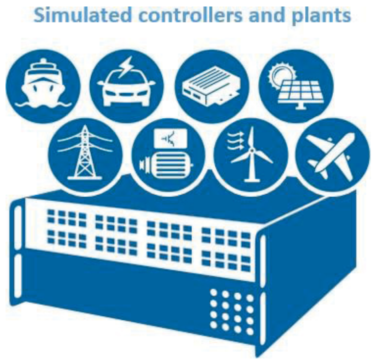

a) MIL/SIL

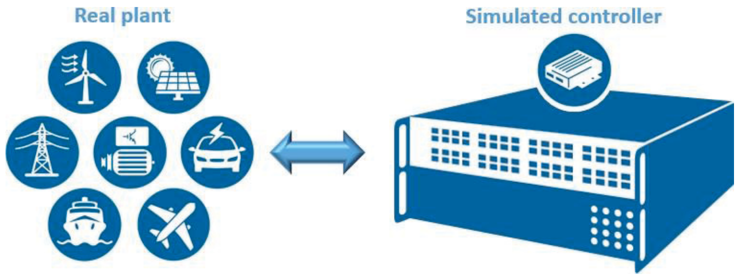

b) RCP

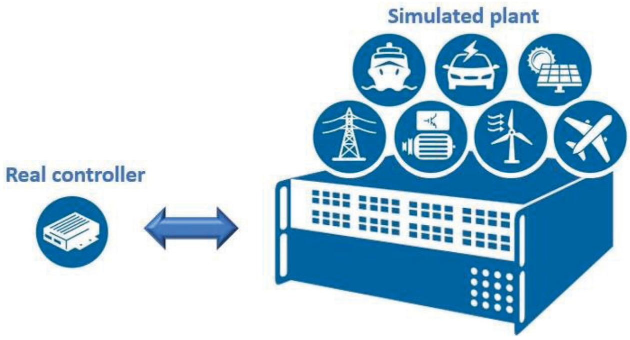

c) HIL

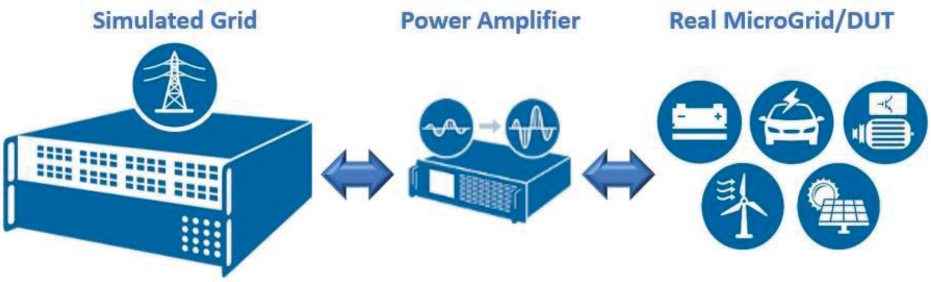

d) PHIL

SOURCE: OPAL-RT RT-LAB Training Material (2023).

6.2 DIGITAL-TWIN BASIC CONCEPTS

According to IBM, a digital twin can be defined as a virtual model that reflects the real physical object of study with great reliability. This object will be equipped with several sensors, to produce data that allows refining and validating the model.

Furthermore, the generated model can receive real data during the simulation, allowing the study performance problems and generate possible improvements. All of it with the aim of generating valuable insights that can be applied again to the original physical object (IBM, 2022).

Looking for the differences between a simulation and a digital twin approach, the following points can be highlighted:

- Both correspond to modeling with the objective of replicating systems and processes; however, the digital twin goes further and can be considered a virtual environment, with a higher level of detail;
- Simulations generally do not consider the response in real-time, taking more time to execute a time window, while the digital twin considers the execution in real-time, presenting results in the same time order of the dynamics of the phenomena studied, corresponding to the response time of the real system under analysis.

The first applications of digital twins were carried out by NASA in the 1960s for the Apollo program. However, it is possible to apply the concept of digital twins to different areas, among them, power systems, including focused on applications with microgrids.

The work proposed by Hong and Apolinario (2022) considers the modeling and integration of MGs in a distribution network, as well as the provision of ancillary services for the network based on available energy resources. In this case, the digital twin communicates with a neural network that brings uncertainty to the network elements and allows the study of different scenarios.

Bazmohammadi et al. (2021) presents a review of concepts and applications for microgrid digital twins. In terms of concepts, the citation made to Brosinsky, Song and Westermann (2019) stands out, which defines a digital twin as: “the virtual image of the physical object in the electric power system, which makes the data provided usable for various purposes in the center of control”. This concept corresponds to the approach present in the current work, where the emulation of communication with the supervisory system of the control center for sending and receiving data from the developed model, via communication protocol, will be considered.

One of the main challenges when working with digital twins is to keep the model updated, following the modifications on the real system. Additionally, the communication, receiving measurements from the real system should be defined in a reliable way, to ensure that the digital twin will be up to date to represent the real system behavior.

Considering the goal of this work to present different approaches for the microgrid integration on the main grid, the digital twin presents a different point of view in comparison with the optimum power flow, however it can complement the DSO studies when considering the MG integration. In the digital twin, the MG operation dynamics is considered during its operation, as well as the communication with the DSO SCADA system, allowing the monitoring and the DSO interview on MG operation.

6.3 DIGITAL-TWIN OF A REAL MICROGRID MODELING

The microgrid used for the elaboration of the digital twin corresponds to the pilot microgrid installed in Barigui Park, in Curitiba/Paraná, being the same one used for the previous studies presented on this work.

As at this point the microgrid topology will be detailed modeled, the description of the microgrid components is presents below:

- a 39 kW photovoltaic (PV) system;
- a carport with 3 kW of photovoltaic solar generation and a 7 kW electric vehicle (EV) charger;
- a 28 kWh battery energy storage system (BESS) with lithium ions
- controllable and non-controllable loads.

The microgrid model was developed up to the point of connection to the grid (Point of Common Coupling - PCC), detailing the energy resources, as well as the existing loads and connections.

The modeling was developed in OPAL-RT's HYPERSIM tool, which is focused on modeling electrical power systems. HYPERSIM was developed by OPAL-RT and IREQ institute from Hydro Quebec, being nowadays maintained by consortium composed by both companies and CEPRI (China) and RTE (France). The main goal is to have a tool focused on industry applications, with models tested and validated with real data.

As it is a real-time approach, it is necessary to define the time step of the simulation, that mean, what is the time interval in which the simulation will receive the data, carry out the calculation process, and send the corresponding outputs, either for the meters or for the communication protocol used. In this case, considering the dynamics of transients in the network, caused by input/connection and output/disconnection of loads and/or generation, as well as switching, it was possible to define the time step of 50 microseconds, which is also a typical time-step value used for power systems real-time simulations.

FIGURE 80 shows the modeling carried out, highlighting each of the structures modeled. In addition to modeling the existing energy resources, in this case solar generation and storage system (Battery Energy Storage System – BESS), the loads corresponding to the electric vehicle (EV) charging station, and the controllable and non-controllable loads are also modeled. The handling switches were also included in the modeling, which allow the entry and exit of loads as well as the DER systems. Furthermore, the resistance of the cables up to the point of connection to the main network was also considered.

For the generation and storage systems, some control flags for input data in the models were defined. The behavior of the model was validated with different measurements carried out in the field, allowing to obtain, through simulation, the same results of the real microgrid.

Different operating scenarios were considered in the simulations, such as: connection of a vehicle to a load in the carport system, considering periods with and without solar generation; microgrid islanding and operation under a fault condition.

FIGURE 80 - MICROGRID MODEL IMPLEMENTED IN THE HYPERSIM TOOL, HIGHLIGHTING EACH OF THE MODELED PLOTS

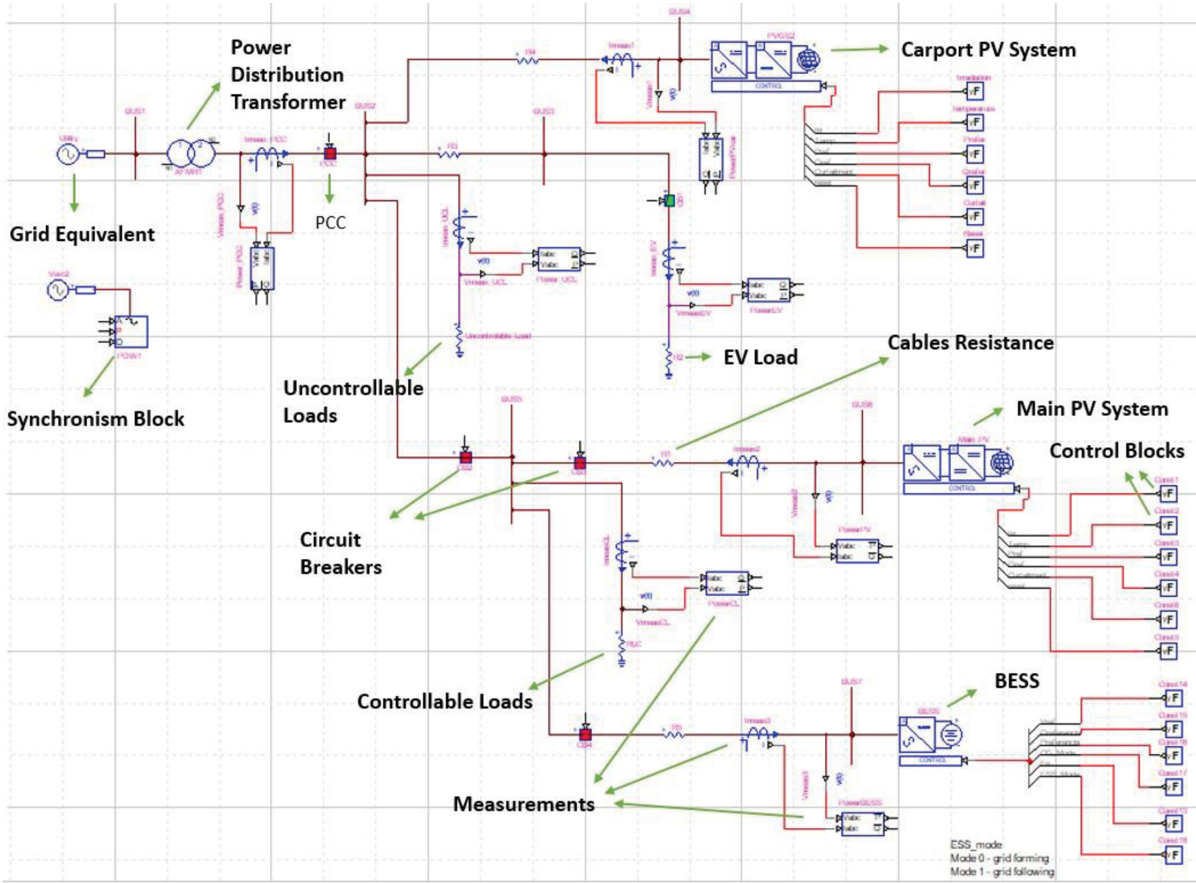

SOURCE: The Author (2023).

The simulation was performed using the OPAL-RT real-time simulator OP4610XG, using only one core for processing and the HYPERSIM 2023.1 version. In addition, it was possible to emulate the sending of data from the microgrid to the supervisory system of the distributor (SCADA) through the IEC 60870-5-104 communication protocol. This protocol was chosen since multiple DSOs are using it worldwide to communicate IEDs (Intelligent Electronic Devices) with their SCADA system. According to the IEC standard, the IEC 60870-5-104 protocol “provides a communication profile for sending basic telecontrol messages between a central telecontrol station and telecontrol outstations, which uses permanent directly connected data circuits between the central station and individual outstations” (IEC, 2006).

The IEC 60870-5-104 Slave was configured on HYPERSIM driver, and a TCP communication loopback will be done to the IEC 60870-5-104 Master communication system, which will emulate to the SCADA, being in this case emulated in the

FreyrSCADA IEC 60870-5-104 Client/Master Simulator application, installed on the windows PC. FIGURE 81 illustrates the simulation setup, where the power system simulation will be running on the real-time simulator and the communication link will be done through TCP/IP with the host PC, which will run the Hypersim console and the SCADA emulation.

FIGURE 81 - SIMULATION SETUP

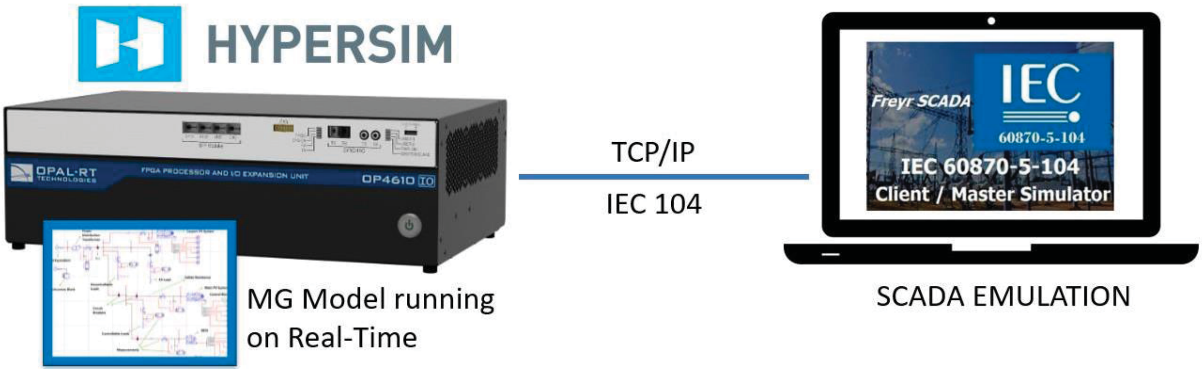

SOURCE: The Author (2023).

The power data of the microgrid elements is sent as a floating point, due to the data format being send to SCADA with the precision of three decimal places. The status of the PCC switch with the network is sent as a double point, since it varies from 0 to 7 according to the number and combination of phases that will be operated (OPAL-RT, 2023). In this case, the switch status will not just be a SCADA read-only variable, but a variable that can be operated, allowing the connection and disconnection of the MG being operated by the DSO.

6.4 MICROGRID DIGITAL-TWIN REAL-TIME SIMULATION

For the microgrid digital-twin simulation, three different scenarios were considered:

- EV connection for loading at the carport;
- MG islanding under a contingency;
- Fault inside of the MG.

The results for each scenario will be presented in the following sections.

6.4.1 EV connection for loading at the carport

The impact of connecting an electric vehicle for charging in the carport system was evaluated. In this case, two different situations were considered: first, during the day, where there is photovoltaic solar generation in both systems; and, at night, when there is no generation in the MG.

FIGURE 82 and FIGURE 83 presents the results of the average power at different points of the MG in the scenario where there is PV generation, and the EV starts to load.

FIGURE 82 - RESULTS FROM THE EV CONNECTION TO CHARGE AT THE CARPORT DURING THE DAY – PART 1

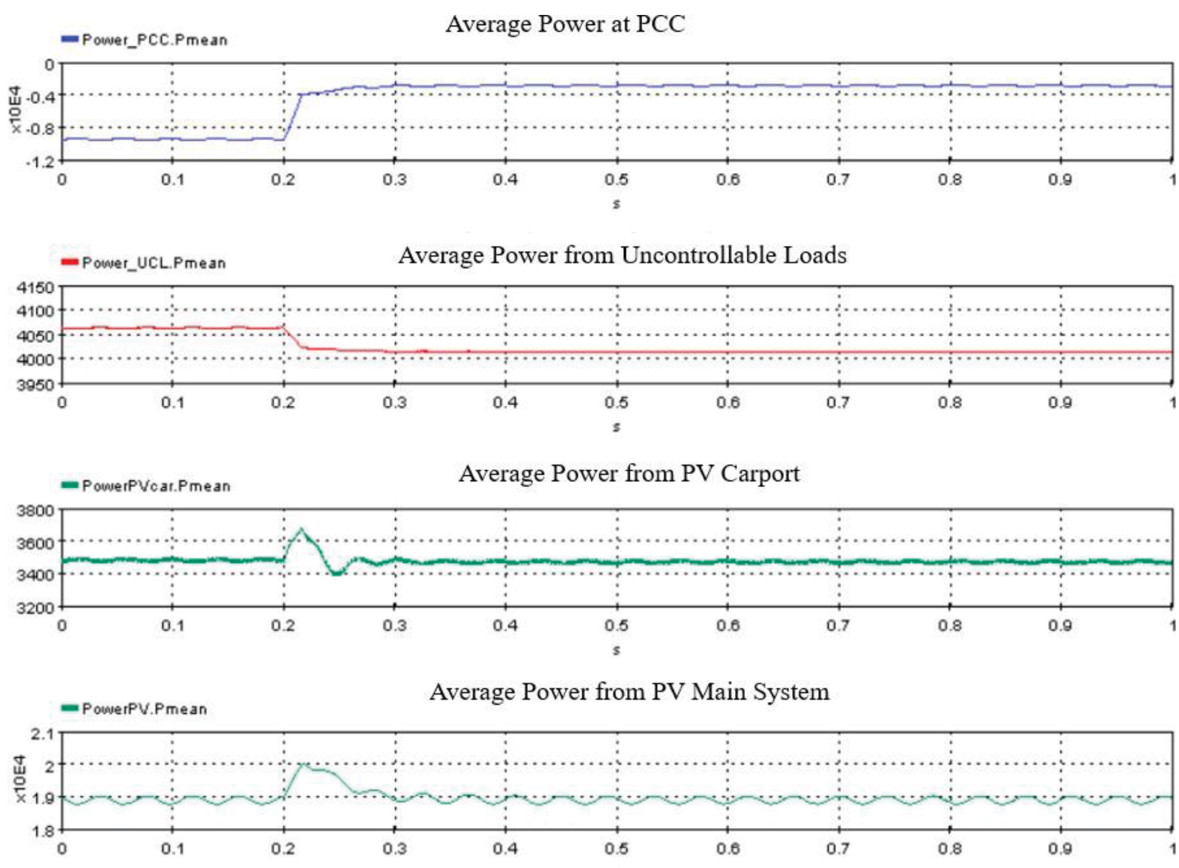

SOURCE: The Author (2023).

FIGURE 83 - RESULTS FROM THE EV CONNECTION TO CHARGE AT THE CARPORT DURING THE DAY – PART 2.

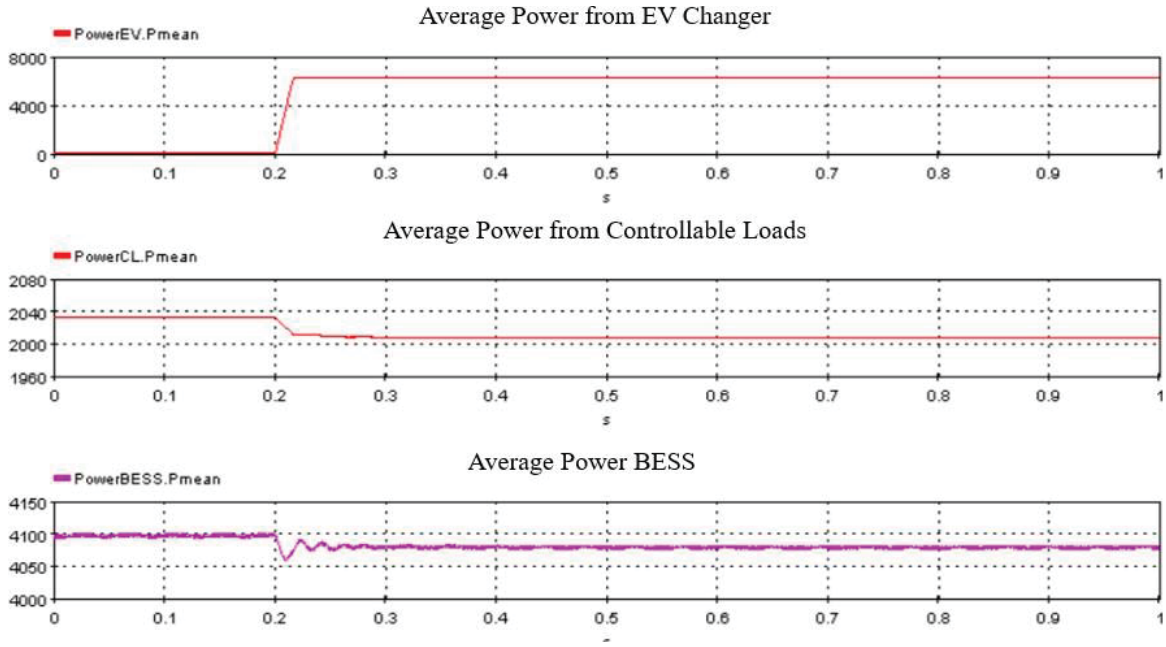

SOURCE: The Author (2023).

In terms of power in the PCC, it is verified that there is an export of 9.2 kW, but as soon as the EV starts the loading process, the MG starts to export only 2.2 kW, since 7 kW are consumed by the EV charger.

With the increase in the MG load, there is a variation of 1.075% in the controllable and non-controllable loads, which is caused by the reduction of losses in the microgrid cables, since the EV charger circuit starts to drain power, changing the behavior of the power flow in the MG.

Evaluating the scenario at night, without solar generation, the main difference in the behavior of the network with the EV load is related to the power flow in the PCC, as illustrated in FIGURE 84. Whereas in the scenario with solar generation the MG exports energy to the grid, without solar generation the MG consumes 10.9 kW, and with the entrance of the EV it starts to consume 17.2 kW.

FIGURE 84 – BEHAVIOR OF THE AVERAGE POWER AT THE PCC AND THE EV ENTRY POINT WHEN THERE IS NO SOLAR GENERATION – NIGHT.

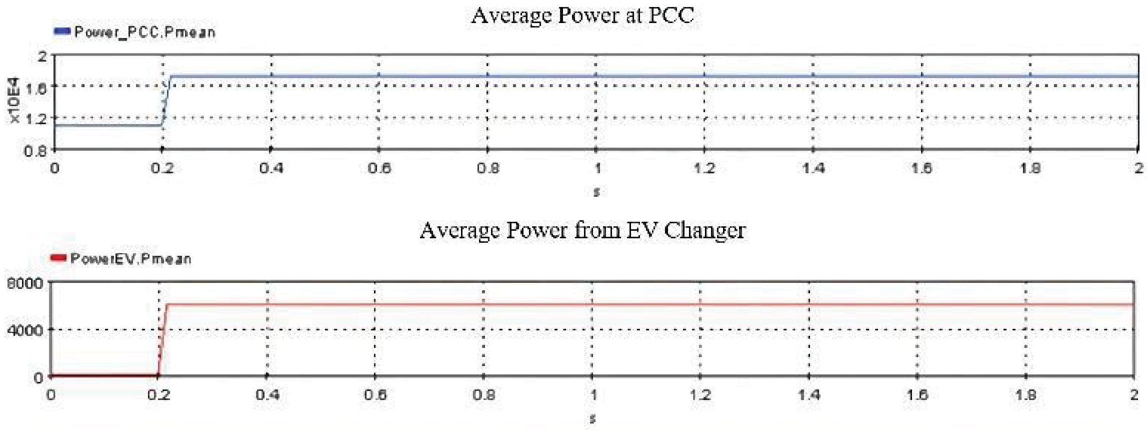

SOURCE: The Author (2023).

At FIGURE 85 it is illustrated the communication with the SCADA emulation at FreyrSCADA, where the active power at the PV carport and the PV main system values are send, as well as the status of the PCC switch. This emulates the DSO point of view from the MG operation.

FIGURE 85 - IEC 104 COMMUNICATION PROTOCOL IN HYPERSIM AND COMMUNICATION WITH FREYRSCADA IEC 60870-5-104 CLIENT/MASTER SIMULATOR DURING THE MG MODEL SIMULATION.

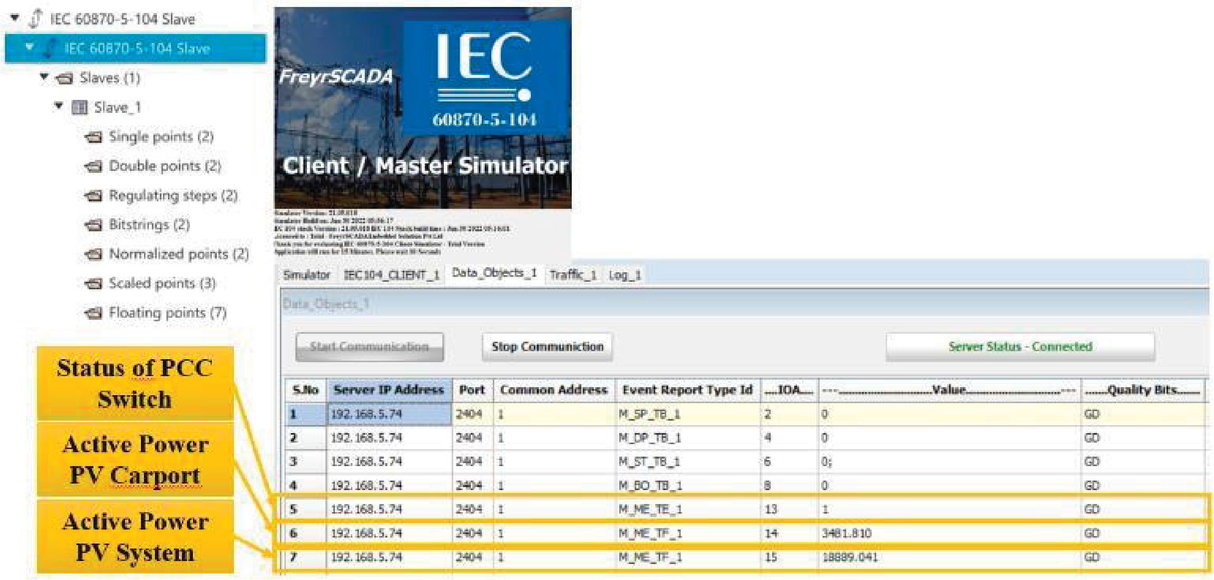

Source: The Author (2023)

6.4.2 MG islanding

Considering a contingency situation, where the supervisory system of the distributor requests the opening of the PCC switch (FIGURE 86) and the intentional islanding of the MG occurs, the battery inverters will assume the function of grid former, actuating as a reference for the system. The command for the MG islanding comes through the DSO, and in the current setup it is operated from the FreyrSCADA, being send through IEC-104 to the real-time simulation.

FIGURE 86 - PCC LOCATION AT THE BARIGUI PARK (AERIAL VIEW) AND ITS REPRESENTATION AT THE MODEL.

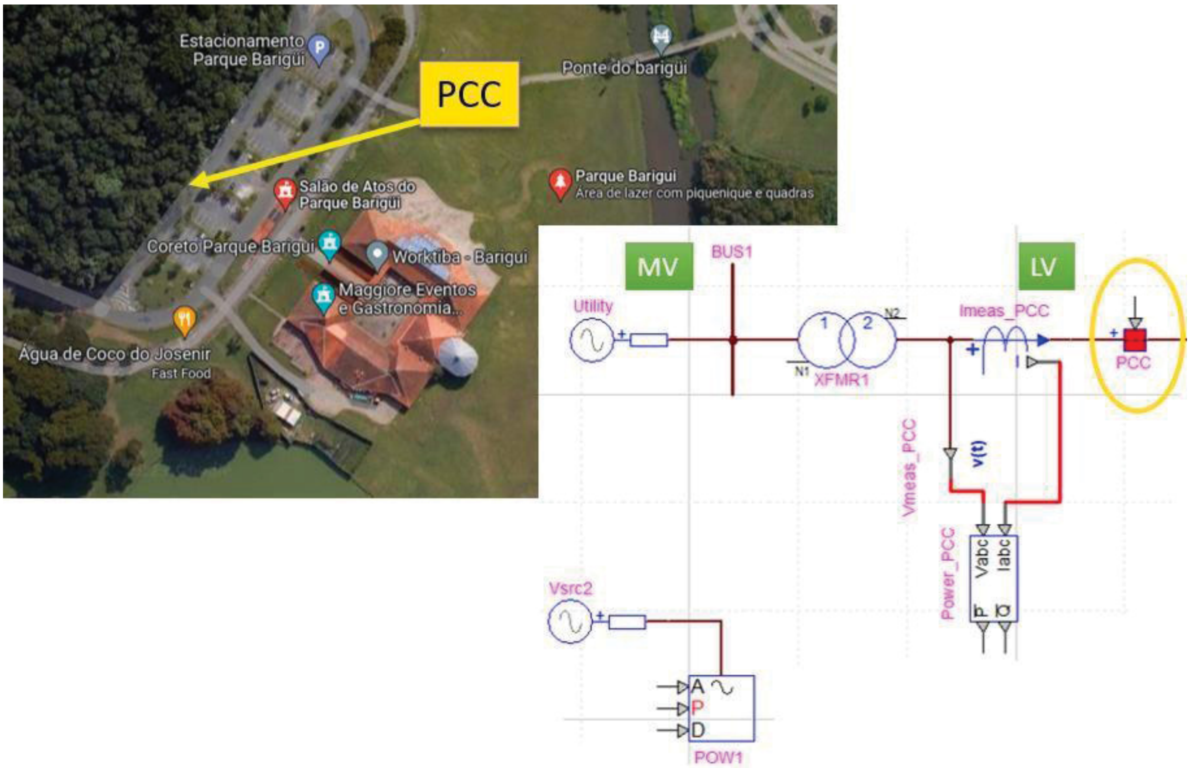

SOURCE: The Author (2023).

If the islanding occurs during the solar generation period, generation will be limited to meeting loads, activating the possibility of curtailment in solar systems, since it is not possible to export the surplus to the grid, and considering that the battery is already charged. In this scenario, it is possible to meet the controllable load without curtailment. It is also important to highlight that in the islanding period, the BESS will operate in grid forming mode.

FIGURE 87 and FIGURE 88 shows the behavior of power at different points on the grid during islanding, which occurs between 0.5 and 1.5s. In FIGURE 87 the MG exports power to the grid in the pre- and post-islanding periods, remaining equal to zero in the islanding period since there is no connection to the main grid. At FIGURE 88 it is shown the behavior of the uncontrolled load during islanding. The behavior remains the same, suffering only a transient when the PCC switch is thrown. It is also shown the behavior of the two photovoltaic systems, which also present fluctuation during the switching of the PCC switch.

FIGURE 87 - BEHAVIOR AT THE PCC, BEFORE, DURING AND AFTER THE ISLANDING

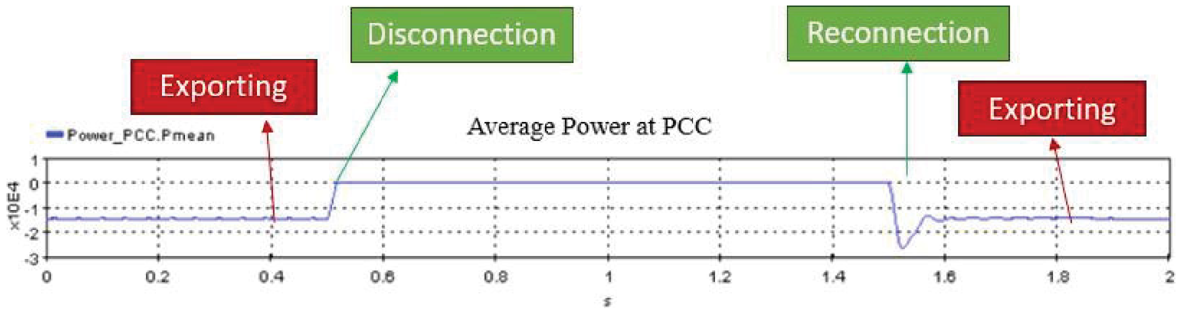

SOURCE: The Author (2023).

FIGURE 88 - BEHAVIOR AT PV SYSTEMS AND UNCONTROLLABLE LOADS BEFORE, DURING AND AFTER THE ISLANDING.

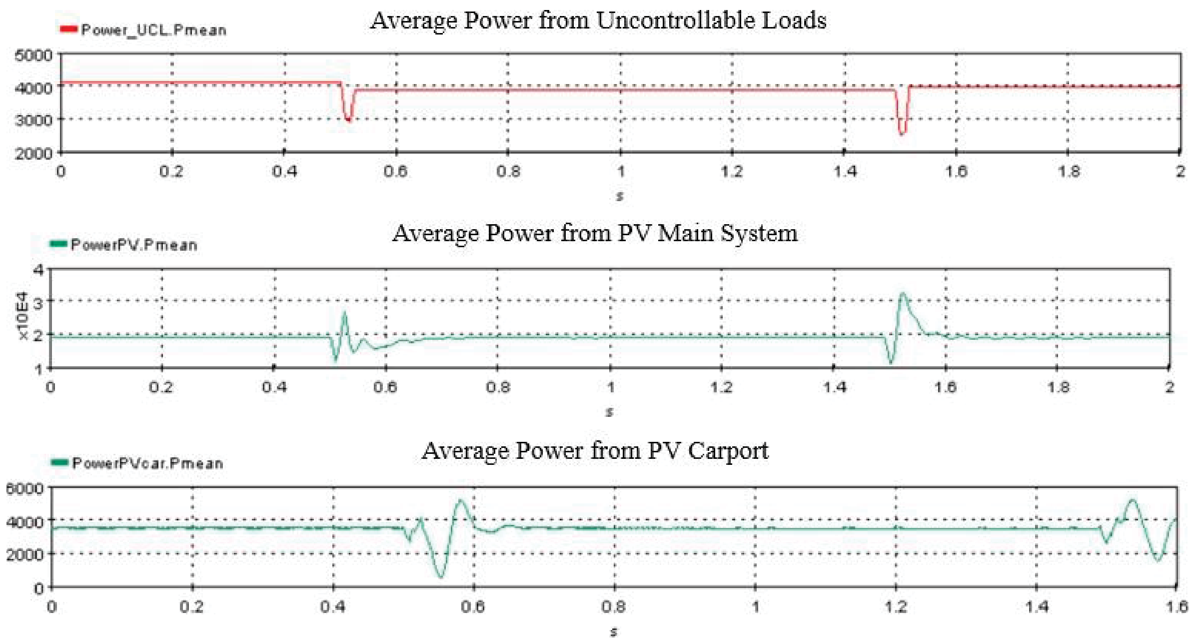

SOURCE: The Author (2023).

If there is no solar generation, the load service is done only for the uncontrolled load through battery discharge, as shown in FIGURE 89.

FIGURE 89 – BEHAVIOR OF THE MG BESS SYSTEM DURING AND AFTER THE ISLANDING, IN A SCENARIO WITH NO SOLAR GENERATION.

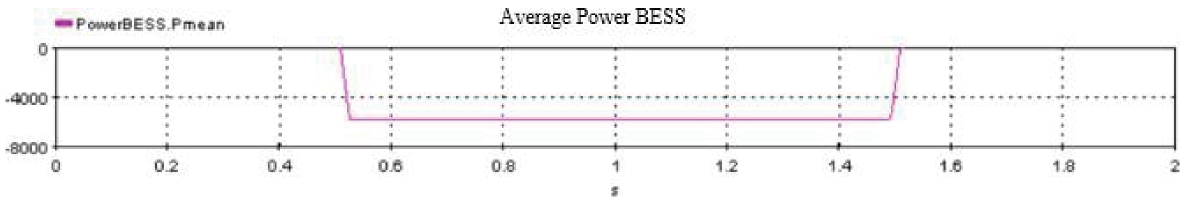

SOURCE: The Author (2023).

6.4.3 Fault application on the MG

Returning to the grid-connected scenario, a three-phase-to-ground fault is applied at bus 5, where the main PV system, BESS, and controllable loads are connected, as highlighted at FIGURE 90.

FIGURE 90 - HIGHLIGHT OF FAULT LOCATION AT THE MG MODEL.

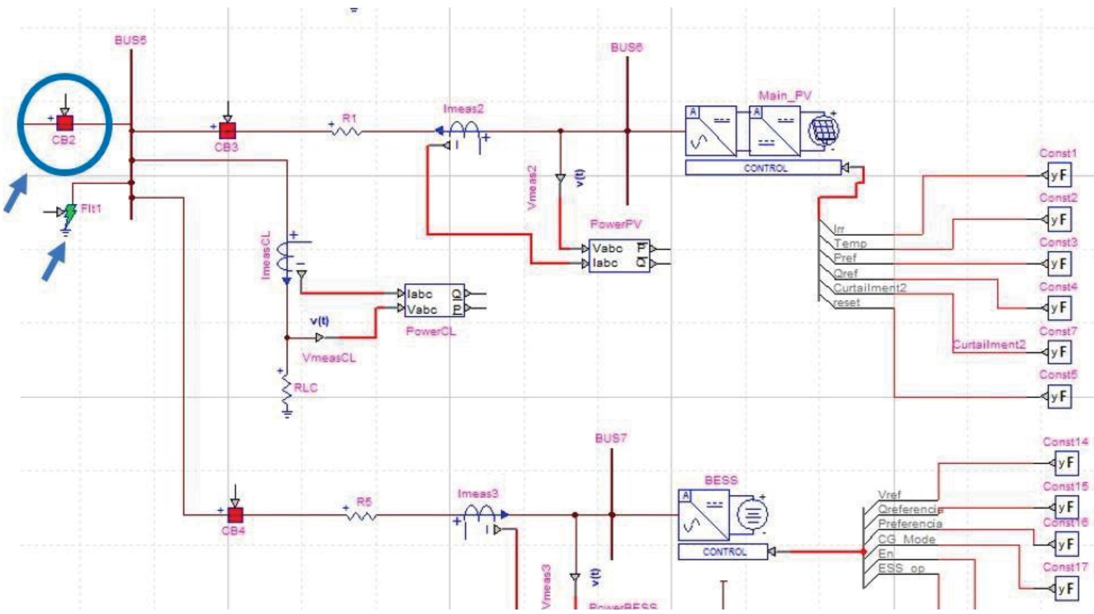

SOURCE: The Author (2023).

The fault is applied from 0.5 to 1.5 seconds. In this case, the storage system and the main generation system will be disconnected. However, in the PCC, if no protection operates, the short circuit propagates to the distribution grid, increasing the power demand of the network.

Thus, to prevent this from happening, the internal protection of the microgrid can be coordinated, in order that only the part of the MG which is under fault goes out of operation, isolating the fault and avoiding effects on the distribution network. In this case, the protection in switch CB2, located on bus 5 (FIGURE 90), where the fault is located, will actuate.

For this strategy, a time of 50 ms was considered for recognizing the fault and opening CB2. Then, from 0.5 to 0.55 s, the fault actuates on the entire circuit, bringing the voltage at bus 5 to zero. As soon as CB2 opens, the part of the MG that has the carport, as well as the uncontrolled loads, continues to operate normally, not being affected by the fault. FIGURE 91 shows the behavior of the voltage at bus 5 and the fault current applied to the bus. In 1.5 seconds, the fault is closed and the previously disconnected elements of the microgrid are reconnected, that is, the main solar generation, the BESS and the controllable loads.

FIGURE 91 - TOP: VOLTAGE ON BUS 5 BEFORE AND DURING THE FAULT. BOTTOM: THREE-PHASE FAULT CURRENT.

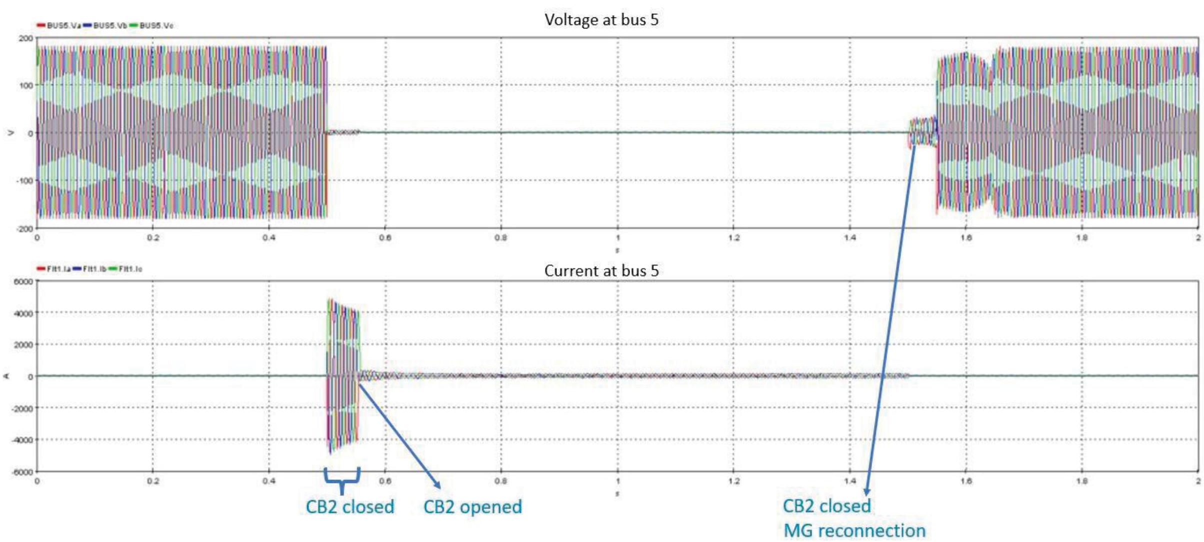

SOURCE: The Author (2023).

In FIGURE 92 it is possible to see the behavior of the different elements that remain connected to the network before, during and after the fault application. It is verified that two transients occur, the first in the period in which the switch has not yet recognized the fault (from 0.5 to 0.55 s) and later, when there is a reconnection of the systems to the MG.

For the elements that are not isolated from the MG after opening CB2, it is verified that the operation remains normal, and it is even possible to connect an EV for charging in the carport system, as shown in FIGURE 92. It can be noted that with the input from the EV, it is necessary to consume energy from the main grid, with 7.8 kW being supplied to complement the carport's solar generation and meet the uncontrolled load and the EV.

FIGURE 92 - AVERAGE POWER BEHAVIOR ON DIFFERENT ELEMENTS OF THE MG DURING THE FAULT SCENARIO AND ACTUATION OF CB2.

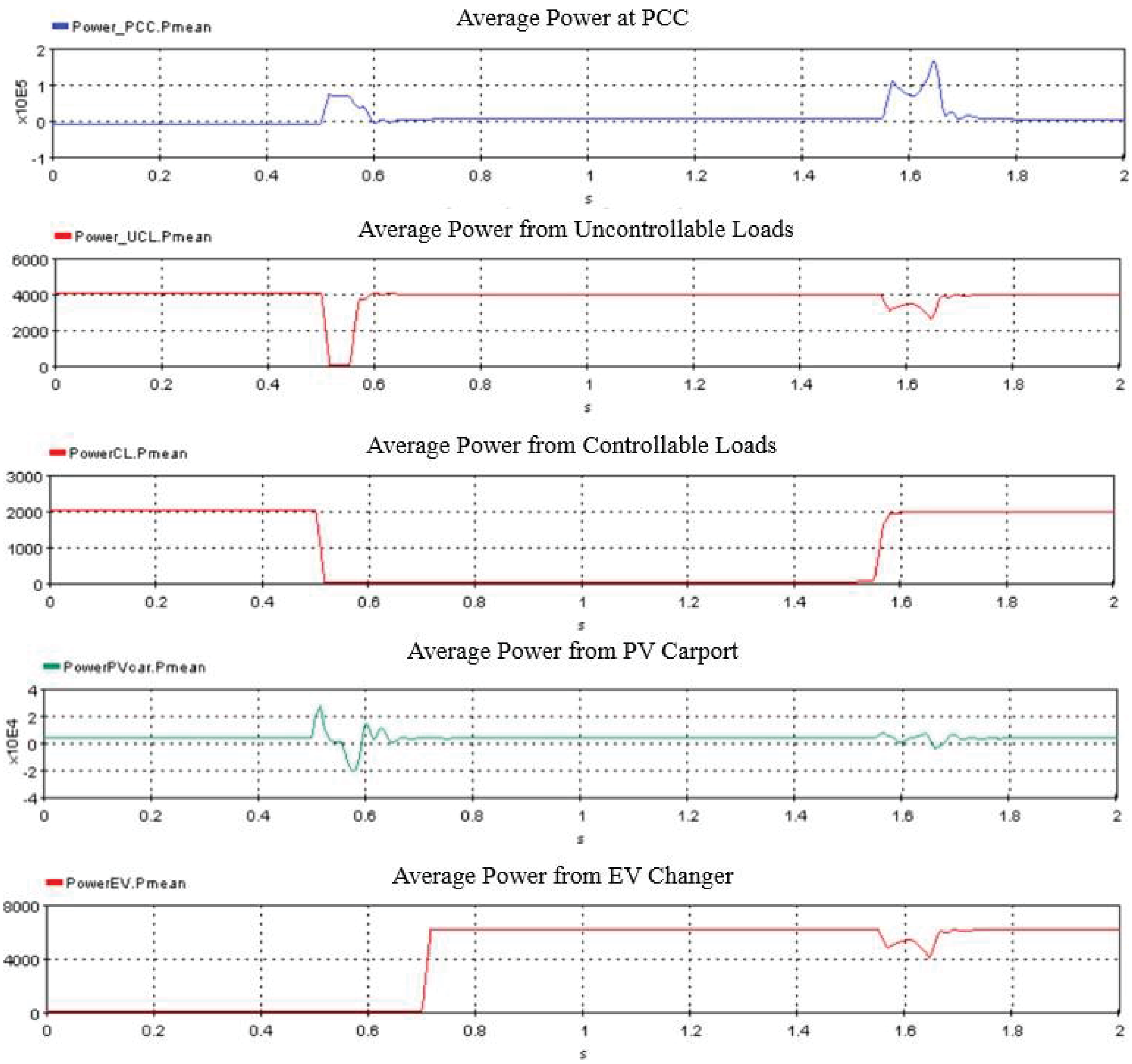

SOURCE: The Author (2023).

6.5 FINAL CONSIDERATIONS ABOUT THE DIGITAL-TWIN

A real microgrid was modeled, and its response under different operating situations was simulate in real time, as well as the communication layer with the utility's supervisory system.

One of the main advantages in obtaining the digital twin of the network, or part of the it, is being able to know the behavior and responses of the circuit in the same time order in which the real system would respond, thus allowing the evaluation of scenarios that in the field could lead to damage to equipment and damage to network operation.

Having this knowledge previously grants greater decision-making power to the distributor, contributing to improving the quality and continuity of the service. Additionally, it can contribute to the decision of provisioning of ancillary services, since a better understanding of the MG behavior happens. In this way the DSO can interact with the MG operation, receiving data from it, taking decisions and telecommanding some operations.

For the case of the studied microgrid, the effects visualized do not cause much impact on the distribution grid, neither on the microgrid operation itself. This is due to the low power and lower complexity of this MG. However, the study is relevant, since allows to see the dynamics of the system, being another approach that can be considered when MG starts to integrate the distribution network.

7 CONCLUSIONS AND FUTURE WORKS

The introduction of distributed energy resources and microgrids are growing day-after-day, all over the world. The economic forums and conferences emphasize the worries of governments for a sustainable future and changes in the energy matrices.

The impacts of these changes require multiple studies, considering different aspects. In this way, the present work proposes different approaches for microgrid integration at active distribution networks.

When different approaches are mentioned, it consists in different types of analysis, with different propositions, having in common the integration of distributed energy resources and microgrids on active distribution network.

The first approach presented on this thesis consists in the multiperiod optimum power flow for an active distribution network. In this case, the entire medium voltage distribution grid under analysis is modeled, considering different scenarios with the integration of different equipment, such as: photovoltaic generation, battery energy storage system, and D-FACTS. Moreover, the active and reactive dispatch of the equipment was considered in a day-ahead scenario.

For the optimum power flow analysis, the first scenario considered the test feeder of IEEE with 90 buses, where distributed generation, electric vehicles, BESS, flexible loads and microgrid were connected at once, allowing to evaluate the impacts and benefits of each technology on distribution grid dispatch. It is important to highlight that at this approach, the MG is modeled as an equivalent, corresponding to a bus capable of injecting or absorb power.

For this study case, the operational costs and equipment operation were evaluated, as well as the power flow and energy balance. In the sequency, the same approach was applied for a real distribution feeder from Curitiba, being the MV feeder modeled, as well as its loads behavior. As nowadays this feeder presents a classic behavior, just with loads connected on it, a future scenario where it becomes an active distribution network was also considered.

With the MPOPF approach was possible to consider the operation of an active distribution network under different scenarios, considering different combinations of equipment, and thus different complexity levels for the power grid dispatch.

A second approach was considered, being the hierarchical model, where the MPOPF was combined with the microgrid internal dispatch operation. Both methodologies are structured in a hierarchical way where the MPOPF corresponds to the master, and the MG dispatch to the slave. The day-ahead dispatch proposed by the MG is delivered to the distribution grid dispatch. With the updated values, the MPOPF can calculate the distribution grid operation and verify if no constraints are reached. If so, another dispatch from the MG is required, considering changes to the constraints. Then this new dispatch is proposed, allowing another MPOPF from the distribution grid. This process happens multiple times, allowing to find the best distribution grid dispatch considering the MG integration.

The hierarchical approach can be realized considering multiple MGs connection to the distribution grid, where each optimization will feed the distribution grid MPOPF. As many MGs are connected in the same network, more interactions between the master-slave hierarchical process must be required.

The third approach considered consists in the digital twin of a microgrid. In this case, the day-ahead scenario is not considered anymore, but the real-time operation of the MG. For this approach, the Barigui MG was modeled in Hypersim software up to the point of connection. In this case different MG operations were considered, as well as the telecommand from DSO SCADA through IEC 60870-5-104. For the digital twin the transients considering changes on the MG operation were evaluated. In this scenario, the impacts on distribution grid operation were not directly considered, being focused on the internal MG operation, as well as in the possibility to receive the data at the SCADA and consider, for example a contingency disconnection requested by the DSO.

Each approach studied in this thesis represents a different point of view of active distribution networks operations and microgrid integrations, corresponding to a complementary analysis of the future of distribution power grids.

Some suggestions of future works are:

- Based on MPOPF approach:
    - consider the integration of dispatchable generators, as biomass and biogass plants, and also wind power in the distribution feeder, and evaluate its impacts on the distribution grid dispatch;

  - increase the complexity of EV penetration, such as evaluation of different charging scenarios, also considering the connection of large charging station points.
- Considering the hierarchical approach:
  - Propose a market strategy to compensate the changes on MG optimum dispatch, based on distribution grid constraints requirements;
  - Evaluate the integration of multiple microgrids and load aggregators on the distribution grid, interacting with the main grid dispatch.
- For the digital-twin approach:
  - Consider cyber-physical attacks and communication failures on the communication link between MG and SCADA system;
  - Improve the control implemented for the MG, allowing to test different scenarios and the control autonomy.

REFERENCES

ABDEL-MOAMEN, M. A.; PADHY, N. P. **Optimal power flow incorporating FACTS devices - bibliography and survey**. 2003 IEEE PES Transmission and Distribution Conference and Exposition (IEEE Cat. No.03CH37495). **Anais**...IEEE, 2003Disponível em: <http://ieeexplore.ieee.org/document/1335357/>

ABDI, H.; BEIGVAND, S. D.; SCALA, M. LA. **A review of optimal power flow studies applied to smart grids and microgrids.** Renewable and Sustainable Energy Reviews, v. 71, n. December 2016, p. 742–766, 2017. Elsevier Ltd. Disponível em: <http://dx.doi.org/10.1016/j.rser.2016.12.102>

AEMO. **Guide to Ancillary Services in the National Electricity Market**. Disponível em: <https://aemo.com.au/-/media/files/electricity/nem/security_and_reliability/ancillary_services/guide-to-ancillary-services-in-the-national-electricity-market.pdf>.

AFZAL, M. J. et al. A review of DGs and FACTS in power distribution network: Methodologies and objectives. **2018 International …**, 2018.

AGUNDIS-TINAJERO, G.; DIAS,N.L.; LUNA, A.C.; SEGUNDO-RAMIREZ, J.; VISAIRO-CRUZ, N.; GUERRERO, J.M. Extended OPF-Based Hierarchical Control for Islanded AC Microgrids. IEEE Transaction on Power Electronics, 2018.

AIN, Q. U.; IQBAL, S.; JAVAID, N. **User Comfort Enhancement in Home Energy Management Systems using Fuzzy Logic**. [s.l.] National University of Science and Technology, 2019.

ANEEL. **Resolução Normativa 482/2012**, 2012. Disponível em: <http://www2.aneel.gov.br/cedoc/ren2012482.pdf>

ANEEL. **Microrredes**.

ANEEL. **Procedimentos de Distribuição de Energia Elétrica no Sistema Elétrico Nacional - PRODIST Módulo 8 - Qualidade de Energia Elétrica**. [s.l: s.n.]. Disponível em: <http://www.aneel.gov.br/documents/656827/14866914/Módulo_8-Revisão_10/2f7cb862-e9d7-3295-729a-b619ac6baab9>.

ANEEL. **Sistema de Informações de Geração da Aneel**. Disponível em: <https://www.aneel.gov.br/siga>.

ANEEL. **Geração Distribuída - Informações Compiladas e Mapa**. Disponível em: <https://app.powerbi.com/view?r=eyJrIjoiZjM4NjM0OWYtN2IwZS00YjViLTllMjItN2E5MzBkN2ZlMzVkIiwidCI6IjQwZDZmOWI4LWVjYTctNDZhMi05MmQ0LWVhNGU5YzA

xNzBlMSIsImMiOjR9>.

ANEEL. **ANEEL aprova Chamada Pública da Copel (PR) para criação de microrredes**. Disponível em: <https://www.aneel.gov.br/sala-de-imprensa/-/asset_publisher/zXQREz8EVlZ6/content/id/20848594>.

AOKI, A. R. et al. Evolução das Redes Ativas de Distribuição e Recursos Energéticos Distribuídos no Brasil. **Revista Eletroevolução**, v. 101, p. 21–35, 2020.

ARENA. **What are distributed energy resources and how do they work?** Disponível em: <https://arena.gov.au/blog/what-are-distributed-energy-resources/>.

BARAN JUNIOR, A. R.; PIAZZA FERNANDES, T. S.; BORBA, R. A. Voltage Regulation Planning for Distribution Networks Using Multi-Scenario Three-Phase Optimal Power Flow. **Energies**, v. 13, n. 1, p. 159, 29 dez. 2019.

BARAN, M. E.; WU, F. . Optimal capacitor placement on radial distribution systems. **IEEE Transactions on Power Delivery**, v. 4, n. 1, p. 725–734, 1989.

BASU, M. Optimal power flow with FACTS devices using differential evolution. **International Journal of Electrical Power & Energy Systems**, v. 30, n. 2, p. 150–156, fev. 2008.

BAZMOHAMMADI, N.; MADARY A.; VASQUEZ, J.C.; MOHAMMADI, H.B; KHAN, B.; WU, Y; GUERRERO, J.M. "Microgrid digital twins: Concepts, applications, and future trends." IEEE Access 10 (2021): 2284-2302. Disponível em: < https://ieeexplore.ieee.org/document/9663369/authors#authors >

BELANGER, J.; VENNE, P.; PAQUIN, J-N. The What, Where and Why of Real-Time Simulation. Planet RT. 2010. Disponível em: <https://blob.opal-rt.com/medias/L00161_0436.pdf>

BLASI, T.M. Análise Elétrica dos Impactos da Conexão de Sistemas Fotovoltaicos com Baterias na Rede de Distribuição. Trabalho de Conclusão de Curso. Departamento de Engenharia Elétrica. Universidade Federal do Paraná. 2017. Disponível em <https://www.eletrica.ufpr.br/p/arquivostccs/434.pdf>

BLASI, T. M. **PLANNING OF ACTIVE DISTRIBUTION SYSTEMS OPERATION WITH BATTERIES AND RENEWABLE ENERGY SOURCES**. [s.l.] Federal University of Paraná, 2020.

BLASI, T.M.; DE AQUINO, C.C.C.B.; PINTO, R.S.; DE LARA FILHO, M.O.; FERNANDES, T.S.P.; VILA, C.U.; AOKI, A.R.; DOS SANTOS, R.B.; TABARRO, F.H. Active Distribution Networks with Microgrid and Distributed Energy Resources Optimization Using Hierarchical Model. **Energies** 2022, 15, 3992. Disponível em:

<https://doi.org/10.3390/en15113992>

BORGES, S.; FERNANDES, T. S. P.; ALMEIDA, K. C. Pré-despacho hidrotérmico de potência ativa e reativa via Método dos Pontos Interiores e Coordenadas Retangulares. **Revista Controle & Automação**, v. 22, n. 5, p. 479–494, 2011.

BROSINSKY,C.; SONG X.; WESTERMANN, D. "Digital twin-concept of a continuously adaptive power system mirror." International ETG-Congress 2019; ETG Symposium. VDE, 2019

BUKHSH, W.A., ZHANG, C., PINSON, P. **An Integrated Multiperiod OPF Model With Demand Response and Renewable Generation Uncertainty**. IEEE Transactions on Smart Grid, 2015. Disponível em: 10.1109/TSG.2015.2502723

CARPENTIER, J. Contribution à l'Étude du Dispatching Économique. **Bulletin de la Societé Francaise des Electriciens**, v. 3 (Aug), p. 431–447, 1962.

CARVALHO, M. R. **Estudo Comparativo de Fluxo de Potência para Sistemas de Distribuição Radial**. [s.l.] Universidade de São Carlos, 2006.

CASTRO, M. A. L. **Propostas de Modelos Regulatórios para Inserção de Recursos Energéticos Distribuídos**, 2021.

CHANG, C.; MARTINEZ,S.; CORTES,J. Grid-Connected Microgrid Participation in Frequency-Regulation Markets via Hierarchical Coordination. IEEE 56th Annual Conference on Decision and Control (CDC), 2017.

CHE L.; SHAHIDEHPOUR M.; ALABDULWAHAB A.; AL-TURKI Y. Hierarchical Coordination of a Community Microgrid With AC and DC Microgrids. IEEE Transactions on Smart Grid, v.6, p. 3042-3051, 2015. Disponível em: <https://ieeexplore.ieee.org/document/7055892>

CIGRE. Technical Brochure 435 - Ancillary Services: an overview of International Practices. 2010.

CIGRE. **Working Group C6.11 Development and Operation of Active Distribution Networks**. [s.l: s.n.].

CIGRE. TB WG C6.22 - Microgrids 1: engineering, economics, and experience. Capabilities, Benefits, Business Opportunities, and Examples of Microgrids Evolution Roadmap. **Electra**, v. 283, p. 71–75, 2015a.

CIGRE. **Technical Brochure 635 - Microgrids 1: Engineering, Economics and Experience**. [s.l: s.n.].

COPEL. **NTC 905100 - Acesso de Geração Distribuída ao Sistema da Copel (com comercialização de energia)**, 2017.

COPEL. **Tarifa Branca**. Disponível em: <https://www.copel.com/hpcopel/root/nivel2.jsp?endereco=%2Fhpcopel%2Findustrial%2Fpagcopel2.nsf%2Fdocs%2FB0CA4C8DF4B62F98832581F00058CCF9>.

COPEL. **Geração Distribuída para Constituição de Microrredes**. Disponível em: <https://www.copel.com/hpcweb/microrredes/>.

D'ADAMO, C. et al. Active Distribution Networks: general features, present status of implementation and operation practices. **Electra**, v. 246, 2009.

DALL'ANESE, E., ZHU, H., GIANNAKIS, G.B. Distributed Optimum Power Flow for Smart Microgrids. **IEEE Transactions on Smar Grid**, 2013. Disponível em: < 10.1109/TSG.2013.2248175 >

DE CASTRO, N.; DANTAS, G. **Distributed Generation: International Experiences and Comparative Analyses**. Rio de Janeiro: [s.n.].

DIVYA, K. C.; OSTERGAARD, J. Battery Energy Storage Technology for Power Systems - An Overview. **Electric Power Systems Reseaarch**, v. 79, p. 511–520, 2009.

DOE. **How Microgrids Work**.

DOE. **Insights into Advanced Distribution Management Systems**. [s.l: s.n.]. Disponível em: <https://www.energy.gov/sites/prod/files/2015/02/f19/Voices of Experience - Advanced Distribution Management Systems February 2015.pdf>.

DOGAN, A. et al. **Impact of EV charging strategies on peak demand reduction and load factor improvement**. 2015 9th International Conference on Electrical and Electronics Engineering (ELECO). **Anais**...IEEE, nov. 2015 Disponível em: <http://ieeexplore.ieee.org/document/7394559/>

EBEED, M.; KAMEL, S.; JURADO, F. Optimal Power Flow Using Recent Optimization Techniques. In: **Classical and Recent Aspects of Power System Optimization**. [s.l.] Elsevier, 2018. p. 157–183.

ELECTRICITY ADVISORY COMMITTEE - DOE. **Enhancing Grid Resilience with integrated Storage from Electric Vehicles**. [s.l: s.n.]. Disponível em: <https://www.energy.gov/sites/prod/files/2018/06/f53/EAC_Enhancing Grid Resilience with Integrated Storage from EVs %28June 2018%29.pdf>.

ENSSLIN, L. et al. Processo de Seleção de Portifolio Bibliográfico. **Processo técnico com patente de registro pendente junto ao INPI**, 2010.

EPE. **Distributed Energy Resources: Impacts on Energy Planning Studies**. 2020. [s.l: s.n.]. Disponível em: <https://www.epe.gov.br/sites-en/sala-de-

imprensa/noticias/Documents/Discussion Paper - Distributed Energy Resources.pdf>.

Feng, F.; Zhang, P. Enhanced Microgrid Power Flow Incorporating Hierarchical Control. IEEE Trans. Power Syst. 2020, 35,
2463–2466. Disponível em: https://ieeexplore.ieee.org/document/8985431

EPE. **Brazilian Distributed Generation Dashboard.** 2024. Disponível em: <https://dashboard.epe.gov.br/apps/pdgd-eng/>

FERC. **Order Terminating Rulemaking Proceeding, Initiating New Proceeding, and Establishing Additional Procedures**. [s.l: s.n.].

FERNANDES, T. S. P. **An optimal power dispatch model for multi-user systems**. [s.l.] Federal University of Santa Catarina, 2004.

FREITAS, P. M. B. DE; PORTELINHA, R. K.; TORTELLI, O. D-SVC Controller Analysis in Active Distribution Systems Operation. **ISGTLA 2019**, 2019.

GABASH, A.; LI, P. On variable reverse power flow-part I: Active-Reactive optimal power flow with reactive power of wind stations. **Energies**, 2016.

GAYME, D.; TOPCU, U. Optimal power flow with large-scale storage integration. **IEEE Transactions on Power Systems**, 2012.

GEROSSIER, A.; GIRARD, R.; KARINIOTAKIS, G. Modeling and Forecasting Electric Vehicle Consumption Profiles. **Energies**, v. 12, n. 7, p. 1341, 8 abr. 2019.

GODOI.A.A.; AOKI, A. R.; FERNANDES, T. S. . Alocação ótima de bancos de capacitores em redes de distribuição de energia elétrica. **VIII Conferência Brasileira sobre Qualidade de Energia Elétrica**, 2009.

GOODENERGY. **What is Community Energy Aggregation?** 2023. Disponível em <https://goodenergy.com/community-energy-aggregation/>

GRANVILLE, S.; MELLO, F. C.; MELLO, A. C. G. Application of Interior Point Methods to Power Flow Unsolvability. **IEEE Transactions on Power Systems**, v. 11, n. 2, p. 1096–1103, 1996.

GREENER. **Strategic Market Research Distributed Generation (DG) - Photovoltaic (PV) Market. 1st half of 2021 - Brazil**. 2021. Disponível em <https://www.greener.com.br/estudo/strategic-report-distributed-generation-pv-market-brazil-1st-half-2021/>

GUERRERO, J.M.; CHANDORKAR, M.; LEE, T.L.; LOH, P.C Advanced Control Architectures for Intelligent Microgrids—Part I: Decentralized and Hierarchical Control. IEEE Trans. Ind. Electron. 2013, 60, 1254–1262. Disponível em: <https://ieeexplore.ieee.org/document/6184305>

HONG, Y.; APOLINARIO, G.F.D.G. "Ancillary Services and Risk Assessment of Networked Microgrids using Digital Twin." IEEE Transactions on Power Systems (2022)

IBM. “What is a Digital-Twin”. 2022. Available: <https://www.ibm.com/topics/what-is-a-digital- twin>

IEA. **Energy Storage**. Disponível em: <https://www.iea.org/reports/energy-storage>.

IEA. **Status of power System Transformation 2019**. [s.l: s.n.]. Disponível em: <https://www.iea.org/reports/status-of-power-system-transformation-2019>.

IEA. **Renewables 2020 Data Explorer**. Disponível em: <https://www.iea.org/articles/renewables-2020-data-explorer?mode=market&region=World&product=PV+by+segment>.

IEA. **Demand Response**. Disponível em: <https://www.iea.org/reports/demand-response>.

IEA. **Renewable Energy Progress Tracker**. 2024. Dispnível em: <https://www.iea.org/data-and-statistics/data-tools/renewable-energy-progress-tracker>

IEC. International Standard IEC 60870-5-104 Telecontrol equipment and systems - part 5-104: Transmission protocols – Network access for IEC 60870-5-101 using standard transport profiles. 2006. Disponível em: <https://webstore.iec.ch/preview/info_iec60870-5-104%7Bed2.0%7Den_d.pdf>

INPE. **Centro de Previsão de Tempo e Estudos Climáticos**. Disponível em: <https://www.cptec.inpe.br/glossario.shtml>. Acesso em: 6 jun. 2019.

IORGULESCU, M.; URSU, D. Chapter 6 - Reactive Power Control and Voltage Stability in Power Systems. In: **Reactive Power Control in AC Power Systems**. [s.l.] Springer, 2017.

IRENA. **Utility-Scale Batteries - Innivation ladscape brief**. [s.l: s.n.].

IRENA. **Innovation landscape for a renewable-powered future: Solutions to integrate variable renewables**. [s.l: s.n.]. Disponível em: <https://www.irena.org/-/media/Files/IRENA/Agency/Topics/Innovation-and-Technology/IRENA_Landscape_Solution_07.pdf?la=en&hash=57385C8E232455C58F845598879A9B8BFF55373B>.

JAYASEKARA, N.; MASOUM, M. A. S.; WOLFS, P. Optimal operation of distributed energy storage systems to improve distribution network load and generation hosting capability. **IEEE Transactions on …**, 2016.

KNEZOVIĆ, K.; MARINELLI, M. Phase-wise enhanced voltage support from electric vehicles in a Danish low-voltage distribution grid. **Electric Power Systems Research**, 2016.

LACHOVICZ, F. J. . **Planejamento de suporte de reativo para rede de distribuição com forte penetração de geração solar fotovoltaica.** [s.l.] Universidade Federal do Paraná, 2018.

LARA FILHO, M.; PINTO, R.; CAMPOS, A.; VILA, C.; TABARRO, F. Day-Ahead Robust Operation Planning of Microgrids Under Uncertainties Considering DERs and Demand Response. In Proceedings of the 2021 IEEE PES Innovative Smart Grid Technologies Conference— Latin America (ISGT Latin America), Lima, Peru, 15–17 September 2021; pp. 1–5.

LEVRON, Y., GUERRERO, J. M., & BECK, Y. Optimal power flow in microgrids with energy storage. **IEEE Transactions on Power Systems**. 2013. Disponível em : <http://ieeexplore.ieee.org/abstract/document/6469193/>

LILLEBO, M. et al. Impact of large-scale EV integration and fast chargers in a Norwegian LV grid. **The Journal of Engineering**, v. 2019, n. 18, p. 5104–5108, 21 jul. 2019.

LIU, S. et al. **Optimal power flow with Series Static Voltage Restorer (SSVR) in distribution systems considering PV integration**. 2016 IEEE PES Asia-Pacific Power and Energy Engineering Conference (APPEEC). **Anais**...IEEE, out. 2016 Disponível em: <http://ieeexplore.ieee.org/document/7779479/>

MARMARAS, C.; XYDAS, E.; CIPCIGAN, L. Simulation of electric vehicle driver behaviour in road transport and electric power networks. **Transportation Research Part C: Emerging Technologies**, v. 80, p. 239–256, jul. 2017.

MICROPOWER. **Estudos de Caso e Histórias**. Disponível em: <https://www.mpcenergy.com.br/pt/portfolio/>.

MORAES, E. E. C. et al. **The application of D-STATCOM in smart distribution grid with wind power plants**. 2012 10th IEEE/IAS International Conference on Industry Applications. **Anais**...IEEE, nov. 2012 Disponível em: <http://ieeexplore.ieee.org/document/6453881/>

NATIONAL ASSOCIATION OF REGULATORY UTILITY COMMISSIONERS - NARUC. **Advancing Electric System Resilience with Distributed Energy Resources: A Review of State Policies**. [s.l: s.n.]. Disponível em: <https://pubs.naruc.org/pub/ECD7FAA5-155D-0A36-3105-5CE60957C305>.

NGUYEN, N. T. A. et al. **Optimal power flow with energy storage systems: Singleperiod model vs. multi-period model.** 2015 IEEE Eindhoven …, 2015

NISSAN MOTOR CORPORATION. **Powering resilience: How EVs can help communities bounce back after a disaster**. Disponível em: <https://global.nissannews.com/en/releases/release-b8a1567ee6066d582c91ef8f1d0b47ad-190920-00-e>.

NREL. **Documenting a Decade of Cost Declines for PV Systems**. Disponível em: <https://www.nrel.gov/news/program/2021/documenting-a-decade-of-cost-declines-for-pv-systems.html>.

OPAL-RT. 3-phase Circuit Breaker. 2023. Disponível em: < https://opal-rt.atlassian.net/wiki/spaces/PDOCHS/pages/149621458/3-Phase+Circuit+Breaker>

ORTEGA, A.; MILANO, F. Frequency Control of Distributed Energy Resources in Distribution Networks. **IFAC-PapersOnLine**, p. 37–42, 2018.

PAIVA, R. R. **Fluxo de Potência Ótimo em Redes de Distribuição de Energia com a Presença de Geração Distribuída: Um Novo Algoritmo para Auxiliar a Análise do Perfil de Tensão**. [s.l.] Universidade Federal de Santa Catarina, 2006.

PALIZBAN, O.; KAUHANIEMI, K.; GUERRERO, J. M. Microgrids in active network management—Part I: Hierarchical control, energy storage, virtual power plants, and market participation. Renewable and Sustainable Energy, 2014.

PARHIZI, S. et al. State of the Art in Research on Microgrids: A Review. **IEEE Access**, v. 3, p. 890–925, 2015.

POLIMP. **Climate Polity Infor HUB.** 2015. Disponível em <https://climatepolicyinfohub.eu/>

REIHANI, E. et al. Energy management at the distribution grid using a Battery Energy Storage System (BESS). **Electrical Power and Energy Systems**, v. 77, p. 337–344, 2016.

RELIĆ, F. et al. Influence of FACTS Device Implementation on Performance of Distribution Network with Integrated Renewable Energy Sources. **Energies**, v. 13, n. 20, p. 5516, 21 out. 2020.

RIFFONNEAU, Y. et al. Optimal power flow management for grid connected PV systems with batteries. **IEEE Transactions on …**, 2011.

SALAH, F. et al. Impact of electric vehicles on distribution substations: A Swiss case study. **Applied Energy**, v. 137, p. 88–96, jan. 2015.

SANSEVERINO, E.R., QUANG, N.N., DI SILVESTRE, M.L., GUERRERO, J.M., LI,C.

Optimal power flow in three-phase islanded microgrids with inverter interfaced units. Electric Power Systems Research, 2015.

SMITH, J. **Current Utility Screening Practices, Technical Tools, Impact Studies, and Mitigation Strategies for Interconnecting PV on the Electric Distribution Systems**. [s.l: s.n.]. Disponível em: <https://www.epri.com/research/products/000000003002003277>.

SOUTH AUSTRALIAN POWER NETWORKS. **Trial aims to help support more solar**. [s.l: s.n.]. Disponível em: <https://www.sapowernetworks.com.au/data/308666/trial-aims-to-help-support-more-solar/>.

SUFYAN, M. et al. Sizing and applications of battery energy storage technologies in smart grid system: A review. **Journal of Renewable and Sustainable Energy**, v. 11, n. 1, p. 014105, jan. 2019.

TAPIA, F. Brasil já adicionou 2GW de Energia Solar em 2024. Canal Energia. 2024. Disponível em <https://canalsolar.com.br/brasil-ja-adicionou-2-gw-de-energia-solar-em-2024/>

TAZVINGA, H.; ZHU, B.; XIA, X. Optimal power flow management for distributed energy resources with batteries. **Energy Conversion and Management**, v. 102, p. 104–110, 2015.

UK POWER NETWORKS. **Invitation to Tender - Flaxibility Services Tender Round Jan-21 - Low Voltage Zones**, 2020.

USMAN, M.; CAPITANESCU, F. **A Stochastic Multi-period AC Optimal Power Flow for Provision of Flexibility Services in Smart Grids**. 2021 IEEE Madrid PowerTech. **Anais**...IEEE, 28 jun. 2021Disponível em: <https://ieeexplore.ieee.org/document/9495045/>

VANDARI, M. The Future of Distribution System Opertions and Planning. **IEEE power & energy magazine**, v. 18, p. 18–25, 2020.

WANG, C. et al. A probabilistic day-ahead scheduling with considering wind power curtailment. **… IEEE Conference on …**, 2017.

YAZDANIAN, M.; MEHRIZI-SANI, A. Distributed control techniques in microgrids. IEEE Trans. Smart Grid 2014, 5, 2901–2909. Disponível em <https://ieeexplore.ieee.org/document/6870484>

YI, J. et al. Modelling and simulation of a smartgrid architecture for a real distribution network in the UK. **The Journal of Engineering**, 2019.

ZHANG, L.; LI, Y. Optimal energy management of wind-battery hybrid power system with two-scale dynamic programming. **IEEE Transactions on sustainable energy**, 2013.

ZHAO, B.; WANG, X.; LIN, D.; CALVIN, M.; MORGAN, J.; QIN, R.; WANG, C. Energy management of multiple microgrids based on a system of systems architecture. **IEEE Transaction on Power Systems**. 2018, 33, 6410–6421. Disponível em: <https://ieeexplore.ieee.org/document/8364617>